

Deconvolution of Point Sources: A Sampling Theorem and Robustness Guarantees

Brett Bernstein* Carlos Fernandez-Granda*†

May 2018

Abstract

In this work we analyze a convex-programming method for estimating superpositions of point sources or spikes from nonuniform samples of their convolution with a known kernel. We consider a one-dimensional model where the kernel is either a Gaussian function or a Ricker wavelet, inspired by applications in geophysics and imaging. Our analysis establishes that minimizing a continuous counterpart of the ℓ_1 norm achieves exact recovery of the original spikes as long as (1) the signal support satisfies a minimum-separation condition and (2) there are at least two samples close to every spike. In addition, we derive theoretical guarantees on the robustness of the approach to both dense and sparse additive noise.

Keywords. Deconvolution, sampling theory, convex optimization, sparsity, super-resolution, dual certificate, nonuniform sampling, impulsive noise, Gaussian convolution, Ricker wavelet.

1 Introduction

The problem of deconvolution consists of estimating a signal μ from data y modeled as the convolution of μ with a kernel K sampled at a finite number of locations $s_1, s_2, \dots, s_n \in \mathbb{R}$

$$y_i := (K * \mu)(s_i), \quad i = 1, 2, \dots, n. \quad (1.1)$$

This problem arises in multiple domains of the applied sciences, including spectroscopy [20, 44], neuroscience [74], geophysics [50], ultrasound [1, 43], optics [11], where K is the point-spread function of the imaging system, and signal processing [49], where K is the impulse response of a linear system. In many of these applications, the signal μ is well modeled as a superposition of point sources or spikes, which could correspond to heat sources [47], fluorescent probes in microscopy [7, 40], celestial bodies in astronomy [56] or neural action potentials in neuroscience [60]. Mathematically, the spikes can be represented as a superposition of Dirac measures supported on a finite set $T \subseteq \mathbb{R}$

$$\mu := \sum_{t_j \in T} a_j \delta_{t_j}, \quad (1.2)$$

*Courant Institute of Mathematical Sciences, New York University

†Center for Data Science, New York University

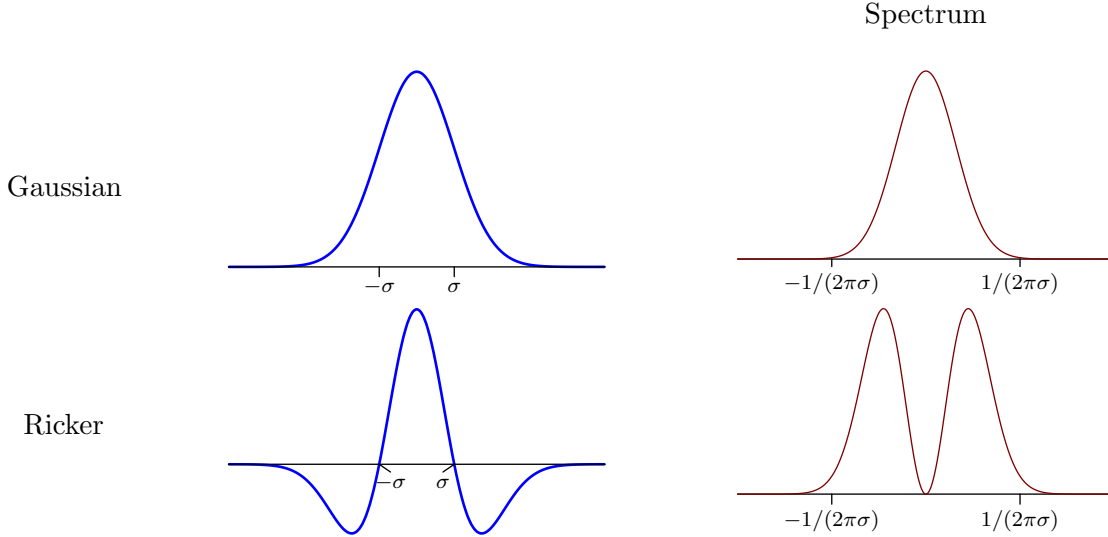


Figure 1: The Gaussian and Ricker kernels with their respective spectra.

with amplitudes $a_1, a_2, \dots \in \mathbb{R}$. For such signals, the data correspond to samples from a linear combination of shifted and scaled copies of the convolution kernel

$$y_i = \sum_{t_j \in T} a_j K(s_i - t_j), \quad i = 1, 2, \dots, n. \quad (1.3)$$

To make our analysis concrete, we focus on two specific convolution kernels, depicted in Figure 1, that are particularly popular in deconvolution applications: the Gaussian kernel,

$$K^{\mathcal{G}}(t) := \exp\left(-\frac{t^2}{2\sigma^2}\right), \quad (1.4)$$

and the Ricker wavelet

$$K^{\mathcal{R}}(t) := \left(1 - \frac{t^2}{\sigma^2}\right) \exp\left(-\frac{t^2}{2\sigma^2}\right), \quad (1.5)$$

which equals the second derivative of the Gaussian kernel up to a multiplicative constant. In both cases $\sigma > 0$ is a real-valued parameter that determines the spread of the kernel. Figure 2 illustrates the measurement model described by equation (1.3) for the Gaussian and Ricker kernels. Gaussian kernels are used to model the point-spread function of diffraction-limited imaging systems such as microscopes [7, 75] and telescopes [3], blurring operators in computer vision [42] and the Green's function of systems governed by the diffusion equation [47, 52]. The Ricker kernel is relevant to reflection seismology, a technique to estimate properties of the subsurface of the Earth by transmitting a short pulse into the ground and then measuring the reflected signal [66]. Processing these measurements can be reduced to a one-dimensional deconvolution problem of the form (1.3) [55], where the signal μ represents the reflection coefficients at the interface between adjacent underground layers and the convolution kernel corresponds to the pulse, which can be modeled using a Ricker wavelet [59].

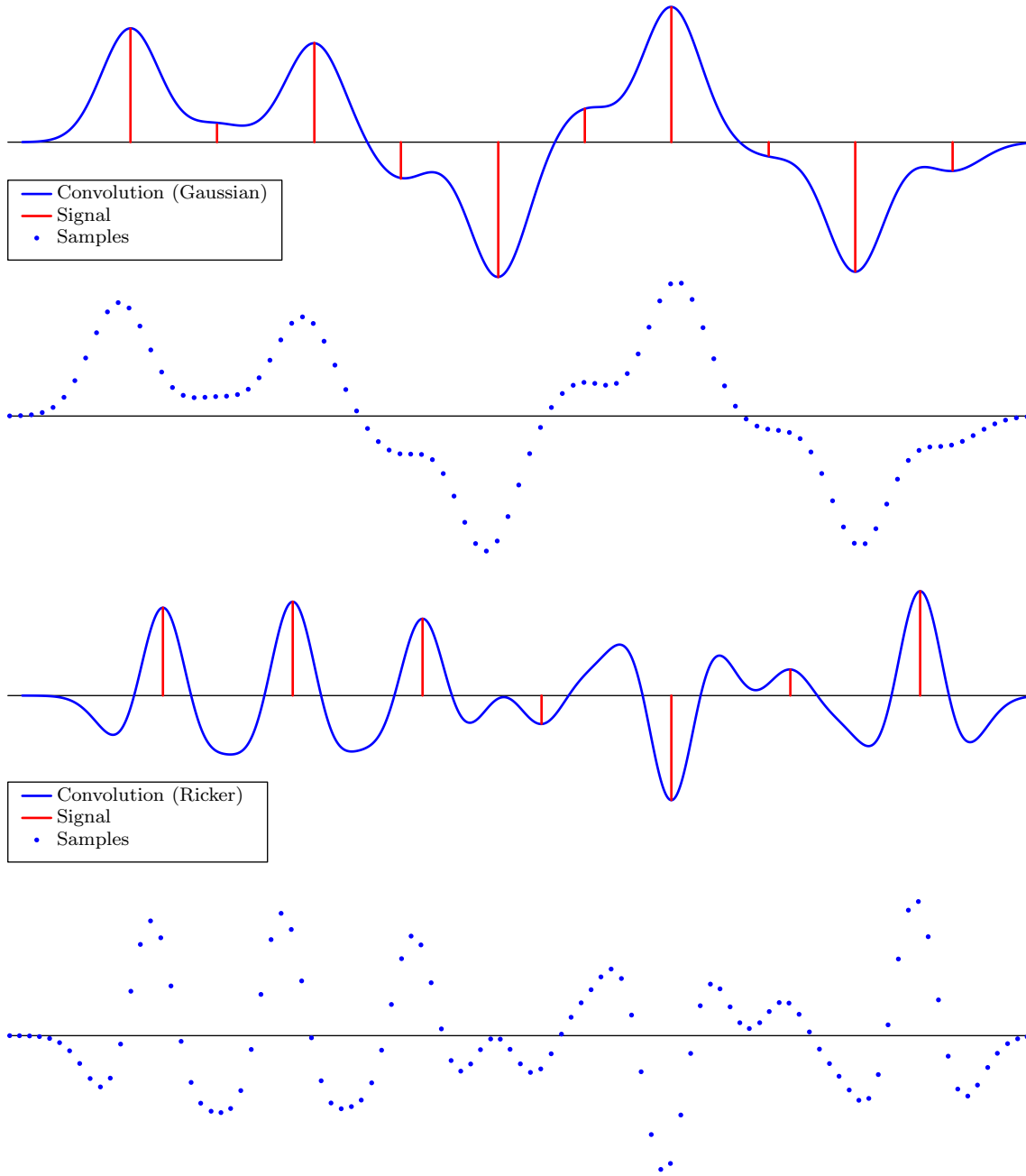


Figure 2: Measurement model where a superposition of spikes is convolved with a Gaussian (top) or Ricker (bottom) kernel and then sampled to produce the data.

In the 1970s and 1980s, geophysicists working on reflection seismology proposed to tackle the spike-deconvolution problem by solving a regularized least-squares problem incorporating an ℓ_1 -norm penalty to promote sparse solutions [22, 26, 45, 63, 70]. Empirically, the method often recovers the spikes exactly from noiseless data—this is the case for instance for the data shown in Figure 2—and produces robust estimates when the data are perturbed by noise. This optimization-based approach has also been successfully applied to deconvolution problems arising in other domains such as processing of marine seismic data [21], signal processing [29], ultrasound imaging [5, 53] and estimation of initial conditions for systems governed by the heat equation [47].

In this paper we provide a theoretical framework to analyze deconvolution via ℓ_1 -norm minimization when the sampling pattern is nonuniform. In order to make our analysis independent of the discretization of the signal support, we consider a continuous counterpart of the ℓ_1 norm, called the total-variation (TV) norm [36, Section 3.1], which should not be interpreted as the total variation of a piecewise-constant function [62], but rather as the analog of the ℓ_1 norm for atomic measures. In fact, the TV norm of an atomic measure of the form $\sum_{i=1}^n b_i \delta_{t_i}$, $b_1, \dots, b_n \in \mathbb{R}$, equals the ℓ_1 norm of the coefficients $\sum_{i=1}^n |b_i|$. Our goal is to characterize under what conditions minimizing the TV norm subject to measurement constraints is an accurate and robust deconvolution method. In the noiseless case, we consider the solution to the problem

$$\begin{aligned} & \underset{\tilde{\mu}}{\text{minimize}} && \|\tilde{\mu}\|_{\text{TV}} \\ & \text{subject to} && (K * \tilde{\mu})(s_i) = y_i, \quad i = 1, \dots, n. \end{aligned} \tag{1.6}$$

Our main result is a sampling theorem for deconvolution via convex programming. We prove that solving Problem (1.6) achieves exact recovery as long as the signal support is not too clustered—a condition which is necessary for the problem to be well posed—and the set of samples contains at least two samples that are close to each spike. Our analysis holds for any nonuniform sampling pattern satisfying this condition, except for some pathological cases described in Section 2.1.2. In addition, the method is shown to be robust to dense additive noise in terms of support estimation. Finally, we illustrate the potential of this framework for incorporating additional assumptions by providing exact-recovery guarantees when the data are corrupted by impulsive perturbations.

The paper is organized as follows: In Section 2 we describe our main results and discuss related work. Section 3 is devoted to the proof of the deconvolution sampling theorem, which is based on a novel dual-certificate construction that is our main technical contribution. Sections 4 and 5 establish robustness to dense and sparse noise respectively. In Section 6 we report the results of several experiments illustrating the numerical performance of our methods. We conclude the paper in Section 7, where we discuss several future research directions. Code implementing all the algorithms discussed in this work is available online¹.

2 Main Results

2.1 Conditions on the Signal Support and the Sample Locations

In this section we introduce conditions to characterize the class of signals and sampling patterns that we consider in our analysis of the point-source deconvolution problem.

¹http://www.cims.nyu.edu/~cfgranda/scripts/deconvolution_simulations.zip

2.1.1 Minimum Separation

A remarkable insight that underlies compressed-sensing theory is that randomized linear measurements preserve the energy of most sparse signals (more technically, they satisfy conditions such as the restricted isometry property [19]). As a result, it is possible to robustly recover arbitrary sparse signals from such measurements, even if the problem is underdetermined [18, 28]. Unfortunately, this is not the case for the deconvolution problem, unless the convolution kernel is random [39, 61]. For smooth deterministic kernels, the data corresponding to different sparse signals can be almost identical, even if we have access to their full convolution with the kernel. Figure 3 shows an example of this phenomenon, where a pair of distinct sparse signals become essentially indistinguishable after they are convolved with a Gaussian kernel (the same happens if we use a Ricker kernel instead). No algorithm would be able to tell the two signals apart from noisy samples of the convolution even at very high signal-to-noise ratios. The reason why the data are so similar becomes apparent in the frequency domain: most of the energy of the convolution kernel is concentrated in a low-pass band, whereas the energy of the difference between the signals is concentrated in the high end of the spectrum. Since convolution is equivalent to pointwise multiplication in frequency, the difference is suppressed by the measurement process.

In order to restrict our attention to a class of signals for which deconvolution is a well-posed problem for our convolution kernels of interest, we constrain the support to have a certain minimum separation.

Definition 2.1 (Minimum Separation). *The minimum separation of the support $T = \{t_1, \dots, t_m\}$ of a signal is*

$$\Delta(T) = \min_{i \neq i'} |t_i - t_{i'}|. \quad (2.1)$$

This quantity was introduced in [14] in the context of super-resolution of point sources from low-pass measurements (see also [27]). In that case, the minimum separation necessary to ensure that two signals do not produce very similar measurements can be characterized theoretically by applying Slepian’s seminal work on prolate spheroidal sequences [67] (see also [51] and Section 3.2 in [14]). In Section 6.1 we report numerical experiments indicating that for Gaussian and Ricker convolution kernels the minimum separation must be at least around σ to avoid situations like the one in Figure 3.

2.1.2 Sample Proximity

In order to estimate a signal of the form (1.2) we need to determine two uncoupled parameters for each spike: its location and its amplitude. As a result, at least two samples per spike are necessary to deconvolve the signal from data given by (1.3). In addition, the amplitude of our convolution kernels of interest decay quite sharply away from the origin, so most of the energy in the convolved signal corresponding to a particular spike is concentrated around that location. We therefore need two samples that are near each spike to estimate the signal effectively. To quantify to what extent this is the case for a fixed sampling pattern S and signal support T we define the *sample proximity* of S and T . In words, S and T have sample proximity $\gamma(S, T)$ if for each spike in T there are at least two samples that are $\gamma(S, T)$ close to it.

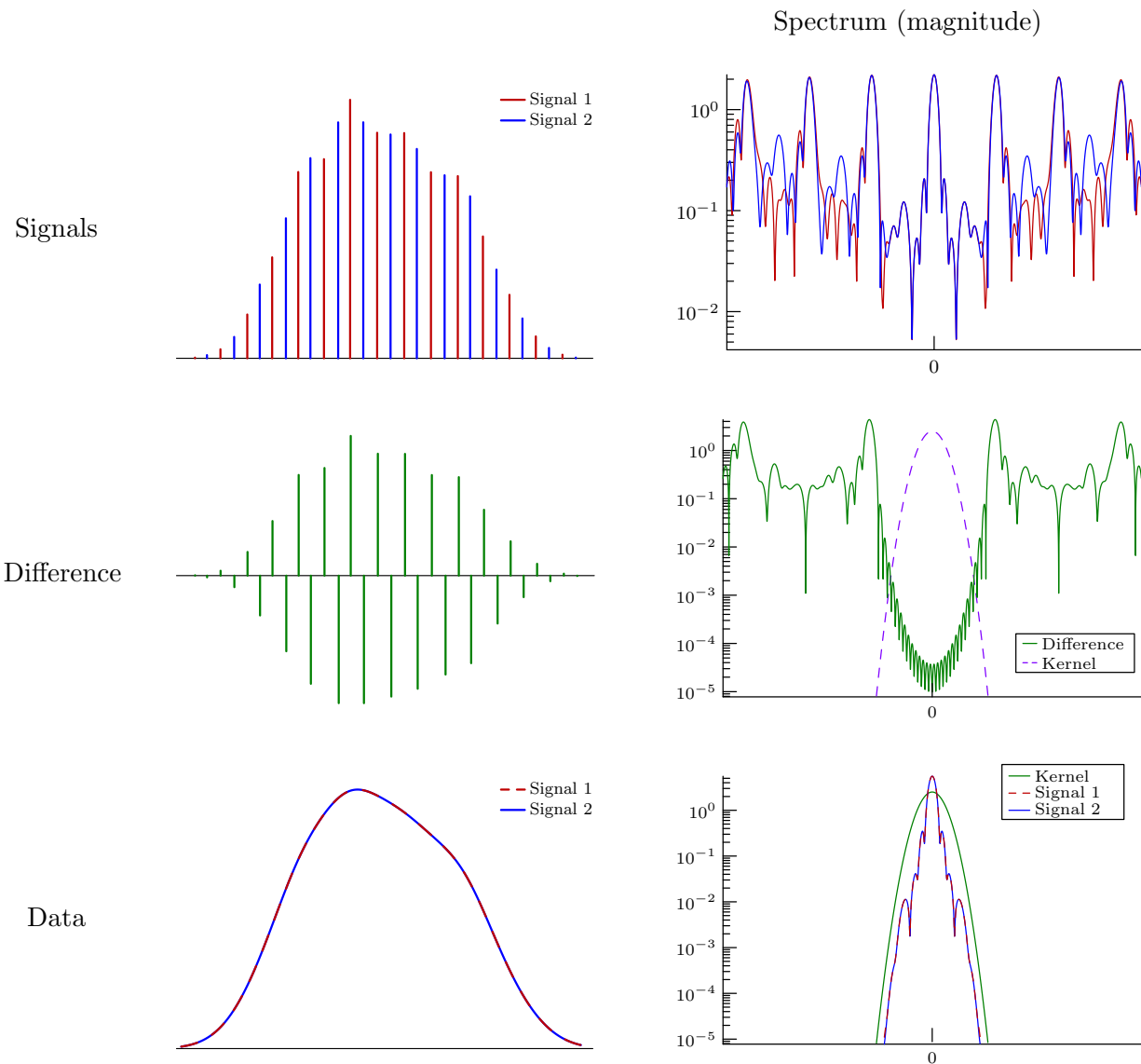


Figure 3: The top row shows two signals with a minimum separation of σ which have disjoint supports (no two spikes are closer than $\sigma/2$), but are very similar in the low-pass band of the spectrum. The difference between them is approximately high pass, which is problematic if the convolution kernel is approximately low pass (center row). The bottom row shows that the convolution of both signals with a Gaussian kernel are almost identical.

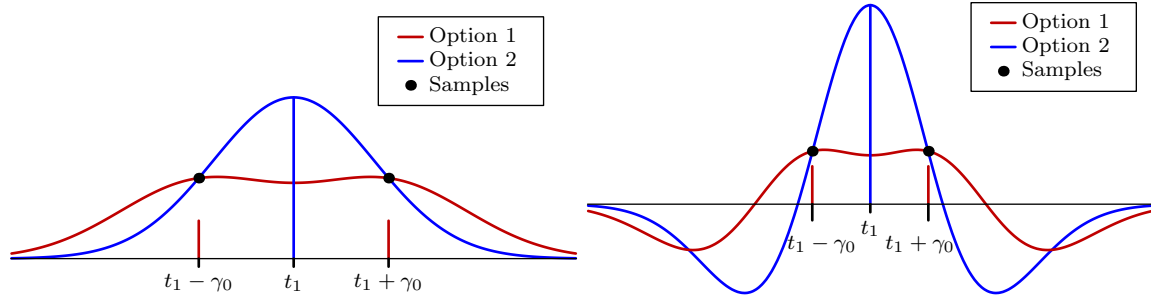


Figure 4: The two measurements in this example can be interpreted as samples from one spike situated at t_1 or two spikes situated at $t_1 - \gamma_0$ and $t_1 + \gamma_0$. When γ_0 is larger than $\sqrt{2 \log 2} \sigma$ for the Gaussian kernel (left) and 0.7811σ for the Ricker wavelet (right), the two-spike option has a smaller TV norm.

Definition 2.2 (Sample Proximity). *Fix a set of sample locations S and a signal support T . Then S has sample proximity $\gamma(S, T) > 0$ if for every spike location $t_i \in T$ there exist two distinct sample locations $s, s' \in S$ such that*

$$|t_i - s| \leq \gamma(S, T) \quad \text{and} \quad |t_i - s'| \leq \gamma(S, T). \quad (2.2)$$

To derive an upper bound on the sample proximity necessary for TV-norm minimization to identify a spike we consider a signal consisting of a single spike, $T := \{t_1\}$, and a sampling pattern with two samples $S := \{s_1, s_2\}$, where $s_1 := t_1 - \gamma_0$ and $s_2 := t_1 + \gamma_0$. Figure 4 shows two alternative explanations for these data: a single spike at t_1 or two spikes at s_1 and s_2 . For the Gaussian kernel, minimizing the TV norm chooses the two-spike option when $\gamma_0 > \sqrt{2 \log 2} \sigma \approx 1.18\sigma$. For the Ricker wavelet, minimizing the TV norm chooses the two-spike option when $\gamma_0 > 0.7811\sigma$.

If we describe a sampling pattern only through its sample proximity, we allow for the following situation: there could be *only* two samples close to a spike which also happen to be very close to each other. We cannot expect to derive robust-deconvolution guarantees for such patterns: a small perturbation in the measurements can have a dramatic effect on the estimated spike location *for any recovery method* due to the local smoothness of the convolution kernels of interest. This is illustrated in Figure 5. The good news is that this situation is pathological and would never arise in practice: placing the samples in this way requires knowing the location of the spikes beforehand! In order to rule out these patterns in our analysis, we define the sample separation associated to a given sample proximity and fix it to a small value.

Definition 2.3 (Sample Separation). *Fix a set of samples S and a signal support T with sample proximity $\gamma(S, T)$. S and T have sample separation $\kappa(S, T)$ for every spike location $t_i \in T$ there exist at least two samples locations s and s' such that*

$$|t_i - s| \leq \gamma(S, T), \quad |t_i - s'| \leq \gamma(S, T), \quad \text{and} \quad |s - s'| \geq \kappa(S, T). \quad (2.3)$$

2.2 Sampling Theorem for Exact Recovery

Our main result is a sampling theorem for deconvolution via convex optimization from nonuniform samples. We show that solving problem (1.6) achieves exact recovery for the Gaussian and Ricker

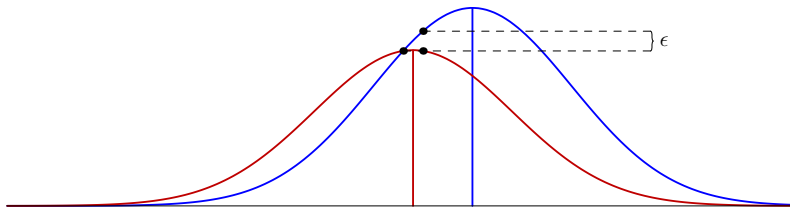


Figure 5: A small sample separation may make it impossible to estimate the spike location robustly. In this example the original signal is shown in blue. A small perturbation of ϵ on one of the samples makes the red spike more plausible, producing a large error in the estimate of the support.

kernels under minimum-separation and sample-proximity conditions on the support and sample locations.

Theorem 2.4. *Let μ be a signal defined by (1.2) and assume that the data are of the form (1.3), where K is the Gaussian kernel or the Ricker wavelet. Then μ is the unique solution to problem (1.6), as long as the signal support T and the sampling pattern S have a minimum separation $\Delta(T)$ and a sample proximity $\gamma(S, T)$ lying in the orange region depicted in the corresponding plot of Figure 6, and the sample separation $\kappa(S, T)$ is greater than $\sigma/20$.*

As explained in Section 2.1.2, we fix a small sample separation to rule out pathological sampling patterns. Except for such cases, the result holds for *any nonuniform sampling pattern* satisfying the sample-proximity condition: among the samples there must be two close to each spike, but the rest can be situated at any arbitrary location. The proof of the theorem, presented in Section 3, relies on a novel construction of a dual certificate, which is our main technical contribution and can be applied to derive recovery guarantees for other convolution kernels.

In order to evaluate the accuracy of our theoretical analysis, we compare our results to the numerical performance of the method for a sampling pattern containing only two samples close to each spike placed at different sample proximities. This sampling pattern is not realistic, because placing only two samples close to every spike requires knowing the support of the signal. How-

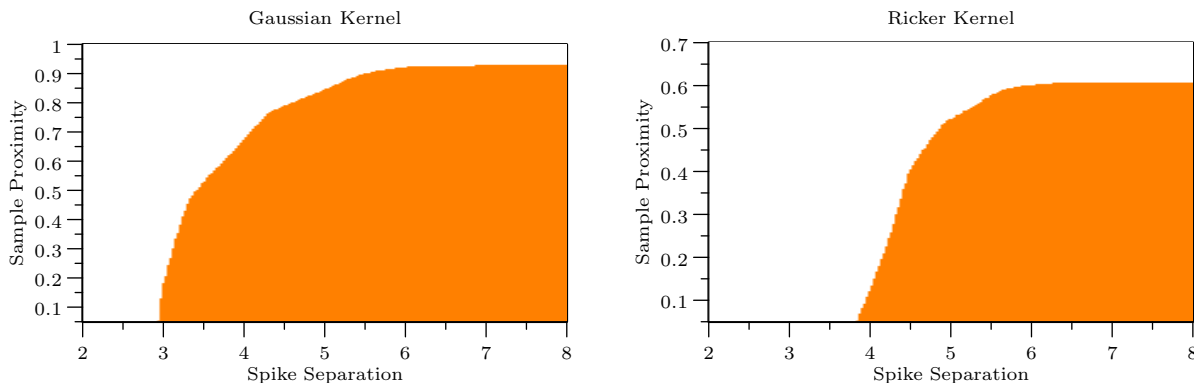


Figure 6: We prove exact recovery for the region marked in orange. The sample-proximity and minimum-separation samples are in units of σ .

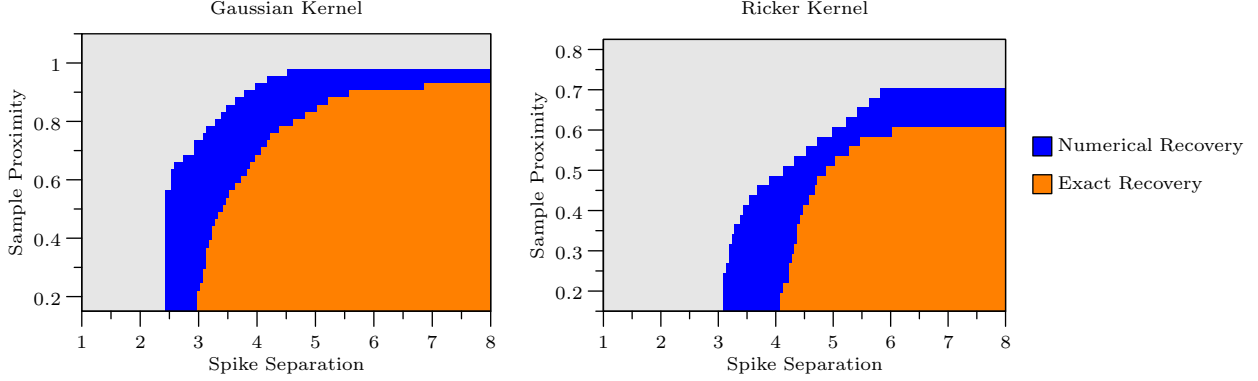


Figure 7: Comparison of the region where we prove exact recovery (orange) with the region where we observe exact recovery in the numerical experiment using 60 spikes described in Figure 23 (blue). Every blue point indicates that exact recovery occurs for all larger minimum separations and smaller sample proximities.

ever, it provides a worst-case characterization of the method for a given sample proximity, since incorporating additional samples can only increase the chances of achieving exact recovery. The simulation, described in more detail in Section 6.2, confirms that the method succeeds as long as the minimum separation is not too small and the sample proximity is not too large. Figure 7 shows that the numerical exact-recovery region contains the theoretical exact-recovery region established by Theorem 2.4.

Our analysis focuses on the continuous TV-norm minimization problem. In practice, this can be implemented by discretizing the domain and then minimizing the ℓ_1 -norm of the discretized estimate. Theorem 2.4 implies that this procedure succeeds if the original signal is supported on the discretization grid. As we explain at the end of Section 2.3 the techniques we present to derive robustness guarantees provide some control over the error incurred if the signal is not supported on the grid. Performing a more detailed analysis of discretization error is an interesting direction for future research.

Corollary 2.5. *Assume that the support of the measure μ in equation (1.2) lies on a known discretized grid $G \subset \mathbb{R}$. Then as long as its support T and the set of samples S satisfy the conditions of Theorem 2.4, the true coefficients $a_1, \dots, a_{|G|}$ are the unique solution to the ℓ_1 -norm minimization problem*

$$\begin{aligned}
 & \underset{\tilde{a} \in \mathbb{R}^{|G|}}{\text{minimize}} && \|\tilde{a}\|_1 \\
 & \text{subject to} && \sum_{t_j \in T} \tilde{a}_j K(s_i - t_j) = y_i, \quad i = 1, \dots, n.
 \end{aligned} \tag{2.4}$$

Proof. Problem (2.4) is equivalent to problem (1.6) restricted to measures supported on G . As a result, any respective solutions \hat{a} and $\hat{\mu}$ must satisfy $\|\hat{a}\|_1 \geq \|\hat{\mu}\|_{\text{TV}}$. By Theorem 2.4, (1.6) is uniquely minimized by μ . Since μ is supported on T , a is the unique solution of (2.4). \square

When the original spike does not lie exactly on the grid the approximation error can be controlled to some extent using the results on additive dense noise in the following section. A more specific

analysis of the effect of discretization in the spirit of [32] is an interesting topic for future research.

2.3 Robustness to dense noise

In this section we consider the deconvolution problem when additive noise perturbs the data,

$$y_i := (K * \mu)(s_i) + z_i, \quad i = 1, 2, \dots, n. \quad (2.5)$$

Our only assumption on the perturbation $z \in \mathbb{R}^n$ is that it has bounded ℓ_2 norm, i.e. $\|z\|_2 < \xi$ for some noise level ξ . Otherwise, the error is arbitrary and can be adversarial. To adapt the TV-norm minimization problem (1.6) to this scenario we relax the data-consistency constraint from an equality to an inequality involving a known upper bound on the noise level $\bar{\xi} \geq \xi$,

$$\begin{aligned} & \underset{\tilde{\mu}}{\text{minimize}} && \|\tilde{\mu}\|_{\text{TV}} \\ & \text{subject to} && \sum_{i=1}^n (y_i - (K * \tilde{\mu})(s_i))^2 \leq \bar{\xi}^2. \end{aligned} \quad (2.6)$$

For real analytic kernels that decay at infinity, which includes the Gaussian kernel and the Ricker wavelet, the solution to this problem is atomic.

Lemma 2.6 (Proof in Appendix E). *Assume y satisfies (2.5) with $\|z\|_2 < \bar{\xi}$. If K is real analytic with $K(t) \rightarrow 0$ as $t \rightarrow \infty$ then the solution $\hat{\mu}$ to problem (2.6) is an atomic measure with finite support $\hat{T} \subseteq \mathbb{R}$ of the form*

$$\hat{\mu} = \sum_{\hat{t}_k \in \hat{T}} \hat{a}_k \delta_{\hat{t}_k}, \quad \hat{a}_1, \dots, \hat{a}_{|\hat{T}|} \in \mathbb{R}. \quad (2.7)$$

Empirically, we observe that the estimated support is an accurate estimate of the true support when the noise is not too high, as illustrated in Figure 8. The following theorem shows that this is guaranteed to be the case under the assumptions of Theorem 2.4.

Theorem 2.7 (Proof in Section 4). *Let μ be a signal defined by (1.2) and assume that the data are of the form (2.5), where K is the Gaussian kernel or the Ricker wavelet and $\|z\|_2 < \xi$. If the sample separation $\kappa(S)$ is at least $\sigma/20$ and the minimum separation and sample proximity lie in the exact-recovery regions depicted in Figure 6, the solution*

$$\hat{\mu} := \sum_{\hat{t}_k \in \hat{T}} \hat{a}_k \delta_{\hat{t}_k} \quad (2.8)$$

to problem (2.6) has the following properties:

$$\left| a_j - \sum_{\{\hat{t}_l \in \hat{T}: |\hat{t}_l - t_j| \leq \eta\sigma\}} \hat{a}_l \right| \leq C_1 \bar{\xi} \sqrt{|T|} \quad \text{for all } t_j \in T, \quad (2.9)$$

$$\sum_{\{\hat{t}_l \in \hat{T}, t_j \in T: |\hat{t}_l - t_j| \leq \eta\sigma\}} |\hat{a}_l| (\hat{t}_l - t_j)^2 \leq C_2 \bar{\xi} \sqrt{|T|}, \quad (2.10)$$

$$\sum_{\{\hat{t}_l \in \hat{T}: |\hat{t}_l - t_j| > \eta\sigma, \forall t_j \in T\}} |\hat{a}_l| \leq C_3 \bar{\xi} \sqrt{|T|}, \quad (2.11)$$

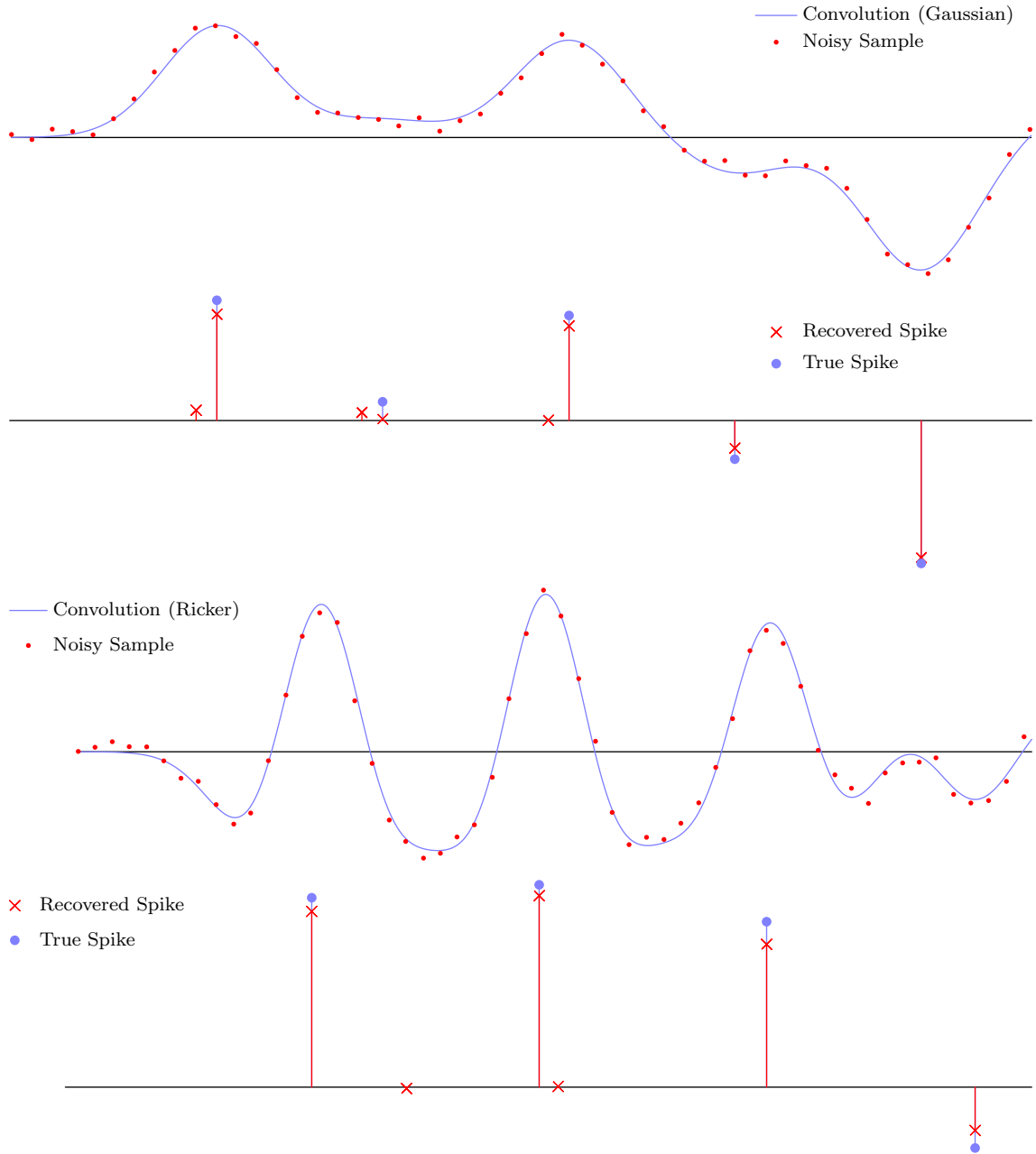


Figure 8: Deconvolution from noisy samples (in red) with a signal-to-noise ratio of 21.6 dB for the Gaussian kernel (top) and 20.7 dB for the Ricker wavelet (bottom). The noise is iid Gaussian. The recovered signals are obtained by solving equation (2.6) on a fine grid which contains the location of the original spikes. Here we set $\bar{\xi} := 1.25\xi$.

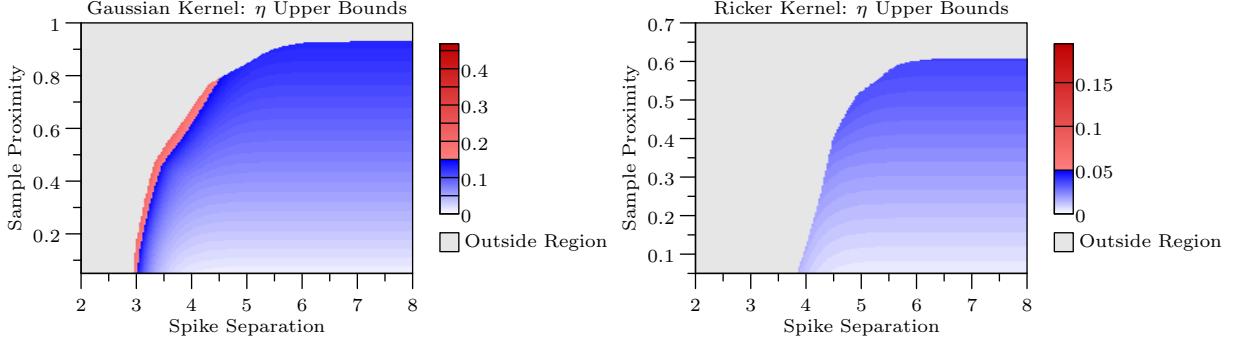


Figure 9: Upper bound on the values of η in Theorem 2.7 for the corresponding values of the sample proximity and minimum separation. Sample proximity and spike separation are given in units of σ .

where $\eta, C_1, C_2, C_3 > 0$ depend only on $\Delta(T)$, $\gamma(S, T)$, and $\kappa(S)$. Upper bounds on the values of η are given in Figure 9.

Property (2.9) implies that the amplitude of each spike is well approximated by the sum of the estimated spikes close to it, where *close* means in a radius of $\eta\sigma < \Delta(T)/2$. η is smaller than 0.15 for the Gaussian kernel and 0.05 for the Ricker kernel for most values of the minimum separation and sample proximity for which exact recovery occurs, as shown in Figure 9. Property (2.10) implies that the estimated support clusters around the support of the true signal. Property (2.11) shows that spurious spikes detected away from the support have small magnitude. An interesting consequence of the theorem is that the error incurred by the method at each spike can be bounded by a quantity that does not depend on the amplitude of other spikes.

Corollary 2.8. *Under the conditions of Theorem 2.7, for any element t_i in the support of μ such that $|a_i| > C_1\bar{\xi}\sqrt{|T|}$ there exists an element \hat{t}_i in the support of the estimate $\hat{\mu}$ satisfying*

$$|t_i - \hat{t}_i| \leq \sqrt{\frac{C_2\bar{\xi}\sqrt{|T|}}{|a_i| - C_1\bar{\xi}\sqrt{|T|}}}. \quad (2.12)$$

These guarantees demonstrate that the method is robust in a small-noise regime: the error tends to zero as the noise decreases. This occurs under the same conditions that we require for exact recovery. In particular, we only assume that the sampling pattern has two samples close to each spike, but we do not account for the rest of the samples. Characterizing how additional samples improve the estimation accuracy of the algorithm in the presence of noise is an interesting problem for future research.

The results of this section allow us to control the error of our recovered signal when the measurements are corrupted by noise. Another source of measurement error is due to discretization. As mentioned earlier, in practice we often solve the continuous TV-norm minimization problem by discretizing and solving an ℓ_1 -norm minimization problem. In general the true signal does not necessarily lie on the grid, which means the model is not completely accurate. We can account for

this by solving the following discretized version of problem (2.6)

$$\begin{aligned} & \underset{\tilde{a} \in \mathbb{R}^{|G|}}{\text{minimize}} && \|\tilde{a}\|_1 \\ & \text{subject to} && \sum_{i=1}^n \left(y_i - \sum_{g_j \in G} \tilde{a}_j K(s_i - g_j) \right)^2 \leq \bar{\xi}^2, \end{aligned} \quad (2.13)$$

where G is some fixed discretization grid. By bounding the effect of shifting the true measure μ onto G we can obtain results analogous to Theorem 2.7 and Corollary 2.8 for $\bar{\xi} \geq L\eta \|\mu\|_{\text{TV}} \sqrt{|S|}$. Here η is the grid separation and L is the Lipschitz constant of the kernel. Improving these somewhat crude error bounds is an interesting direction for future work.

2.4 Sparse Noise

In this section we consider data contaminated by outliers, where some of the samples are completely corrupted by impulsive noise,

$$y_i := (K * \mu)(s_i) + w_i \quad i = 1, 2, \dots, n. \quad (2.14)$$

Here $w \in \mathbb{R}^n$ is a sparse vector with arbitrary amplitudes. In order to account for the presence of the sparse perturbation, we incorporate an additional variable to Problem (2.6) and add a corresponding sparsity-inducing penalty term to the cost function:

$$\begin{aligned} & \underset{\tilde{\mu}, \tilde{w}}{\text{minimize}} && \|\tilde{\mu}\|_{\text{TV}} + \lambda \|\tilde{w}\|_1 \\ & \text{subject to} && (K * \tilde{\mu})(s_i) + \tilde{w}_i = y_i, \quad i = 1, \dots, n, \end{aligned} \quad (2.15)$$

where $\lambda > 0$ is a regularization parameter. An equivalent approach was previously proposed in [37] without theoretical guarantees. In [35] an analogous formulation is applied to spectral super-resolution in the presence of outliers, where the impulsive noise occurs in the spectral domain and is consequently very incoherent with the signal. In our case, the sparse noise and the clean samples are much less incoherent: most of the energy corresponding to a given spike in the signal is concentrated in a few samples around it, which could be mistaken for sparse noise. For the Gaussian and Ricker kernels, we observe that solving problem (2.15) is effective as long as there are not too many contiguous noisy samples. Figure 10 shows an example where the solution to the optimization problem estimates both the signal and the sparse corruptions exactly.

The following theorem provides exact-recovery guarantees in the presence of sparse noise. For simplicity, we assume that the samples lie on a regular grid with step size τ , so that $S := \{s_1, \dots, s_n\}$ where $s_{i+1} = s_i + \tau$, instead of requiring a sample-proximity condition. In addition, we impose a minimum-separation condition on the support of the signal, as well as on the set of noise locations $\mathcal{N} \subseteq S$ to preclude it from being too clustered. Finally, we require that the samples surrounding the spikes and the sparse noise, denoted by

$$\mathcal{I} := \{s_i \in S \setminus \mathcal{N} \mid \exists t_j \in T, s_i \leq t_j < s_{i+1}\} \cup \{s_{i+1} \in S \setminus \mathcal{N} \mid \exists t_j \in T, s_i \leq t_j < s_{i+1}\}, \quad (2.16)$$

$$\mathcal{C} := \{s_{i-1} \in S \setminus \mathcal{N} \mid s_i \in \mathcal{N}\} \cup \{s_{i+1} \in S \setminus \mathcal{N} \mid s_i \in \mathcal{N}\}, \quad (2.17)$$

respectively, be unaffected by the noise and non-overlapping (so that there are at least two clean samples between every corruption and every spike).

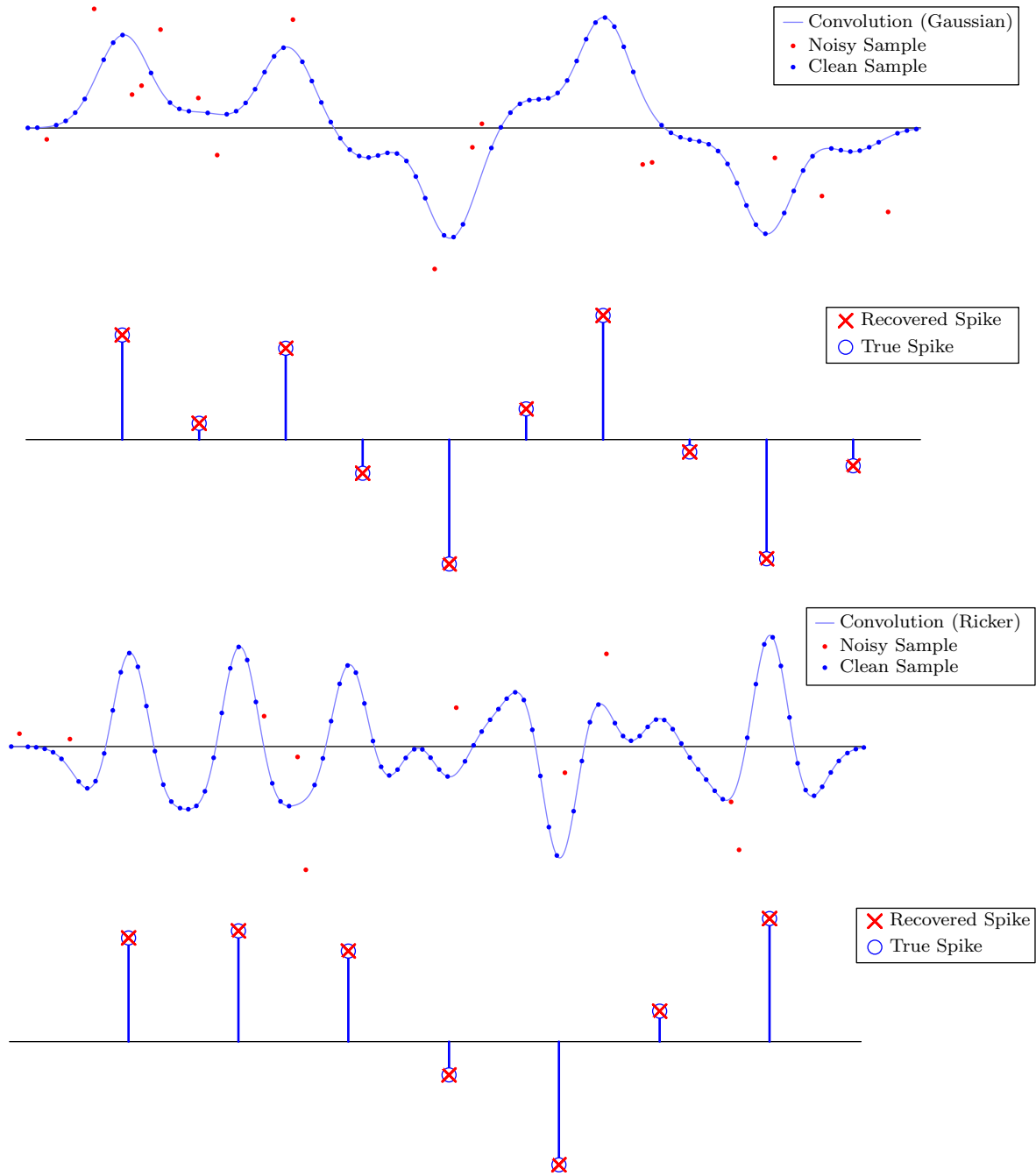


Figure 10: Deconvolution from convolution samples (blue) corrupted by large-amplitude impulsive noise (red) for the Gaussian kernel (top) and the Ricker wavelet (bottom). The recovered signals are obtained by solving equation (2.15) on a fine grid, which achieves exact recovery.

Theorem 2.9 (Proof in Section 5). *Let μ be a signal defined by (1.2) and y be data of the form (2.14), where K is the Gaussian kernel and the samples lie on a grid with step size $\tau \in [0.065\sigma, 0.2375\sigma]$. Assume the spikes and samples are both surrounded by clean samples, so that:*

$$|\mathcal{I}| = 2|T|, \quad |\mathcal{C}| = 2|\mathcal{N}|, \quad \text{and} \quad \mathcal{C} \cap \mathcal{I} = \emptyset. \quad (2.18)$$

If μ has minimum separation $\Delta(T) \geq 3.751\sigma$, and the noise locations \mathcal{N} have minimum separation $\Delta(\mathcal{N}) \geq 3.751\sigma$ then solving problem (2.15) with parameter $\lambda := 2$ recovers μ and w exactly.

Theorem 2.10 (Proof in Section 5). *Let μ be a signal defined by (1.2) and y be data of the form (2.14), where K is the Ricker wavelet and the samples lie on a grid with step size $\tau \in [0.0775\sigma, 0.165\sigma]$. If (2.18) holds, μ has minimum separation $\Delta(T) \geq 5.056\sigma$, and the noise locations \mathcal{N} have minimum separation $\Delta(\mathcal{N}) \geq 5.056\sigma$ then solving problem (2.15) with parameter $\lambda := 2$ recovers μ and w exactly.*

Section 6.3 reports the results of several numerical experiments showing that the method achieves exact recovery under weaker assumptions than those in Theorems 2.9 and 2.10. Characterizing the performance of the method more generally is an interesting research problem. These experiments also suggest that the approach is quite robust to the choice of the regularization parameter λ . The following lemma, which is based on Theorem 2.2 in [16], provides some theoretical justification: it establishes that if the method recovers a signal and a sparse noise realization for a certain value of λ , then it also achieves exact recovery for data corresponding to any trimmed versions of the signal or the noise for that same value of λ . Note that Ω denotes the nonzero entries of w , as opposed to \mathcal{N} which denotes the corresponding sample locations.

Lemma 2.11 (Proof in Appendix H). *Let w be a vector with support Ω and let μ be an arbitrary measure such that*

$$y_i = (K * \mu)(s_i) + w_i, \quad (2.19)$$

for $i = 1, \dots, n$. Assume that the pair (μ, w) is the unique solution to Problem (2.15) for the data y , and consider the data

$$y'_i = (K * \mu')(s_i) + w'_i, \quad (2.20)$$

for $i = 1, \dots, n$. Here μ' is a trimmed version of μ : it is equal to μ on a subset $T' \subseteq T$ of its support. Similarly, the support Ω' of w' satisfies $\Omega' \subseteq \Omega$. For any choice of T' and Ω' , the pair (μ', w') is the unique solution to Problem (2.15) if we set the data vector to equal y' for the same value of λ .

2.5 Related work

There are two previous works that derive exact recovery guarantees for the Gaussian kernel in one dimension. In [64] the authors prove exact deconvolution of k spikes from samples at $2k + 1$ arbitrary locations using a weighted version of the TV norm that avoids having to impose a sample proximity condition. The result only holds for positive spikes, but does not require a minimum-separation condition. In [73] the authors prove exact recovery of k spikes from $2k$ samples lying on a uniform grid, also without a minimum-separation condition. The method can be interpreted as an extension of Prony's method [25]. In both cases, no robustness guarantees are provided (such guarantees would require conditions on the support of the signal, as explained in Section 2.1.1).

As mentioned in the introduction, to the best of our knowledge ℓ_1 -norm minimization for deconvolution was originally proposed by researchers in geophysics from the 1970s [22, 26, 45, 63, 70]. Initial theoretical works focused on analyzing random convolution kernels [39, 61] using techniques from compressed sensing [19, 28]. A series of recent papers analyze TV-norm minimization for recovering point sources from low-pass measurements [14, 23, 34] and derive stability guarantees [4, 15, 31, 33, 46, 69]. This framework has been extended to obtain both exact-recovery and robustness guarantees for deconvolution via convex programming for bump-like kernels including the Gaussian in [5, 6] and specifically Ricker kernels in [55] under the assumption that the complete convolution between a train of spikes and the kernel of interest is known (i.e. without sampling).

When the convolution kernel is a low-pass function, as is approximately the case for the Gaussian kernel, one can reformulate the spike deconvolution as a super-resolution problem. First, the spectrum of the convolved signal is estimated from the data. Then the low-frequency component of the spikes is approximated by dividing the result by the spectrum of the convolution kernel. Finally, the spikes are recovered from the estimate of their low-pass spectrum using spectral super-resolution techniques based on convex programming [14] or on Prony’s method [25, 68], as in the finite-rate-of-innovation (FRI) framework [30, 73]. This framework can also be applied to arbitrary non-bandlimited convolution kernels [71] and nonuniform sampling patterns [54], but without exact-recovery guarantees.

3 Proof of Exact Recovery (Theorem 2.4)

In the proof of Theorem 2.4 we use standardized versions of our kernels where $\sigma = 1$:

$$K^{\mathcal{G}}(t) := \exp\left(-\frac{t^2}{2}\right) \quad \text{and} \quad K^{\mathcal{R}}(t) := (1 - t^2) \exp\left(-\frac{t^2}{2}\right) = -(K^{\mathcal{G}})^{(2)}(t), \quad (3.1)$$

without loss of generality. This is equivalent to expressing t in units of σ . Auxiliary Mathematica code to perform the computations needed for the proof is available online².

3.1 Dual Certificate

We prove Theorem 2.4 by establishing the existence of a *certificate* that guarantees exact recovery.

Proposition 3.1 (Proof in Appendix A). *Let $T \subseteq \mathbb{R}$ be the nonzero support of a signal μ of the form (1.2). If for any sign pattern $\rho \in \{-1, 1\}^{|T|}$ there exists a function of the form*

$$Q(t) := \sum_{i=1}^n q_i K(s_i - t) \quad (3.2)$$

satisfying

$$Q(t_j) = \rho_j, \quad \forall t_j \in T, \quad (3.3)$$

$$|Q(t)| < 1, \quad \forall t \in T^c, \quad (3.4)$$

then the unique solution to Problem (1.6) is μ .

²http://www.cims.nyu.edu/~cfgranda/scripts/deconvolution_proof.zip

In words, to prove exact recovery we need to show that it is possible to interpolate the sign of the amplitudes of any superposition of spikes, which we denote ρ , on the support of the spikes using scaled copies of the convolution kernel centered at the location of the samples.

The vector q is known as a *dual certificate* in the literature [19] because it certifies recovery and is a solution to the Lagrange dual of Problem (1.6):

$$\begin{aligned} & \underset{q}{\text{maximize}} && q^T y \\ & \text{subject to} && \sup_t \left| \sum_{i=1}^n q_i K(s_i - t) \right| \leq 1. \end{aligned} \tag{3.5}$$

Dual certificates have mostly been used to derive guarantees for inverse problems involving random measurements, including compressed sensing [17,19], matrix completion [12] and phase retrieval [13]. In such cases, the construction relies on concentration bounds and other tools from probability theory [72]. In contrast, our setting is completely deterministic.

Our techniques are inspired by the deterministic certificate used to establish exact recovery of an atomic measure from low-pass measurements in [14]. In that case, the certificate corresponds to a low-pass trigonometric polynomial which also interpolates an arbitrary sign pattern on the support of the atomic measure that represents the signal. This polynomial is constructed via interpolation using a low-pass interpolation kernel with fast decay. The crucial difference with our setting is that in [14] the interpolating function just needs to be low-pass, which makes it possible to center the shifted copies of the interpolation kernel at the elements of the signal support (T in our notation). Similarly, if the whole convolution $K * \mu$ is assumed to be known, as in [5,6,55], a certificate can be built by interpolating the sign pattern with the convolution kernel in the same way. In contrast, if we incorporate sampling into the measurement process, we are constrained to use shifted kernels *centered at the sample locations* s_1, \dots, s_n . This requires a new method for constructing the dual certificate, which is our main technical contribution.

By the sample proximity and separation conditions (Definition 2.2), we can associate each spike location in T with two nearby samples that are not too close to each other. This allows us to form a subset $\tilde{S} \subseteq S$ of size $2|T|$ that contains pairs of samples separated by $\kappa(S, T)$ that are $\gamma(S, T)$ -close to each spike location in the support T . We construct the *dual combination* Q using kernels centered at the elements of \tilde{S} ,

$$Q(t) := \sum_{\tilde{s}_i \in \tilde{S}} q_i K(\tilde{s}_i - t). \tag{3.6}$$

In order to satisfy condition (3.3), Q must interpolate the sign pattern ρ on T . To satisfy condition (3.4), Q must have a local extremum at each element of T . Otherwise the construction will violate condition (3.4) close to the support of the signal as shown in Figure 12. To favor local extrema on T , we constrain the derivative of Q to vanish at those points. The sign-interpolation and zero-derivative constraints yield a system of $2|T|$ equations,

$$\begin{aligned} Q(t_i) &= \rho_i, \\ Q'(t_i) &= 0, \quad \text{for all } t_i \in T. \end{aligned} \tag{3.7}$$

The main insight underlying our proof is that the solution to this system is amenable to analysis once Q is reparametrized appropriately. The reparametrization, described in the next section, allows us to prove that the system is invertible and to control the amplitude of Q on T^c .

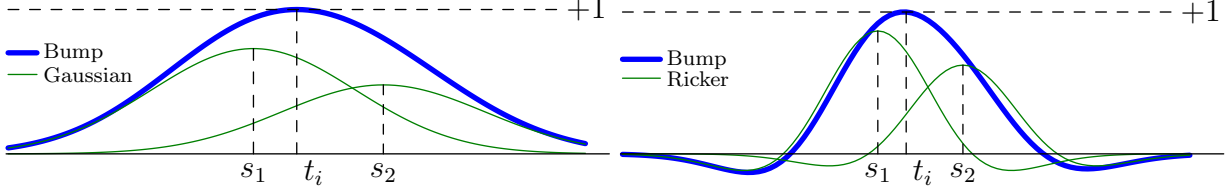


Figure 11: The bump interpolation function $B_{t_i}(t, s_1, s_2)$ is a linear combination of kernels centered at s_1, s_2 . The figure shows examples for the Gaussian kernel (left) and the Ricker wavelet (right).

3.2 Interpolation With Bumps and Waves

We construct the dual combination Q defined in Proposition 3.1 by interpolating an arbitrary sign pattern ρ using modified interpolation kernels, which are linear combinations of shifted copies of K . The construction is a reparametrization of (3.6) of the form

$$Q(t) = \sum_{t_i \in T} \alpha_i B_{t_i}(t, \tilde{s}_{i,1}, \tilde{s}_{i,2}) + \beta_i W_{t_i}(t, \tilde{s}_{i,1}, \tilde{s}_{i,2}), \quad (3.8)$$

where for each $t_i \in T$ we define a pair of modified kernels B_{t_i} and W_{t_i} . The motivation is that controlling the coefficients α_i and β_i is considerably simpler than controlling $q_1, \dots, q_{|\tilde{S}|}$ directly.

We call the first interpolation kernel B_{t_i} a *bump*, defined as

$$B_{t_i}(t, \tilde{s}_{i,1}, \tilde{s}_{i,2}) := b_{i,1}K(\tilde{s}_{i,1} - t) + b_{i,2}K(\tilde{s}_{i,2} - t), \quad (3.9)$$

where $\tilde{s}_{i,1}$ and $\tilde{s}_{i,2}$ are the two elements of \tilde{S} that are closest to t_i . The coefficients $b_{i,1}$ and $b_{i,2}$ are adjusted so that B_{t_i} has a local extremum equal to one at t_i :

$$B_{t_i}(t_i, \tilde{s}_{i,1}, \tilde{s}_{i,2}) = 1, \quad (3.10)$$

$$\frac{\partial}{\partial t} B_{t_i}(t_i, \tilde{s}_{i,1}, \tilde{s}_{i,2}) = 0. \quad (3.11)$$

If $\tilde{s}_{i,1}$ and $\tilde{s}_{i,2}$ are close enough to t_i , the extremum is a maximum and B_{t_i} is indeed a bump-like kernel centered at t_i . Figure 11 shows examples of bumps when K is the Gaussian kernel and the Ricker wavelet.

The bumps are linear combinations of shifted copies of the interpolation kernel K centered at the samples, so we can construct a dual combination Q of the form (3.2) interpolating an arbitrary sign pattern ρ by weighting them appropriately. The problem is that the resulting construction does not satisfy the zero-derivative condition in (3.7) and therefore tends to violate condition (3.3) close to the elements of T , as shown in Figure 12. This is the reason why our dual-combination candidate (3.8) contains an additional interpolation kernel, which we call a *wave*,

$$W_{t_i}(t, \tilde{s}_{i,1}, \tilde{s}_{i,2}) = w_{i,1}K(\tilde{s}_{i,1} - t) + w_{i,2}K(\tilde{s}_{i,2} - t). \quad (3.12)$$

In this case, the coefficients are adjusted so that

$$W_{t_i}(t_i, \tilde{s}_{i,1}, \tilde{s}_{i,2}) = 0, \quad (3.13)$$

$$\frac{\partial}{\partial t} W_{t_i}(t_i, \tilde{s}_{i,1}, \tilde{s}_{i,2}) = 1. \quad (3.14)$$

Each W_{t_i} is a wave-shaped function centered at t_i . Figure 13 shows examples of waves when K is the Gaussian kernel and the Ricker wavelet. The additional degrees of freedom in (3.8) allow us to enforce the zero-derivative condition and obtain a valid dual combination. The role of the wave in our analysis is analogous to the role of the derivative of the interpolation kernel in the dual-certificate construction for super-resolution from low-pass data [14]. Note that here we cannot use the derivative of the bumps or of K , as the resulting construction would not be a linear combination of shifted copies of K .

The following lemma provides a closed-form expression for the coefficients used to build the bump and the wave. In addition, it shows that the bump and wave always exist for the Gaussian kernel and the Ricker wavelet under mild assumptions on the sample proximity and the sample separation.

Lemma 3.2 (Proof in Appendix B.2). *For a fixed kernel K , the bump B_{t_i} and wave W_{t_i} exist with coefficients given by*

$$\begin{bmatrix} b_{i,1} & w_{i,1} \\ b_{i,2} & w_{i,2} \end{bmatrix} = \frac{1}{K(\tilde{s}_{i,2} - t_i)K^{(1)}(\tilde{s}_{i,1} - t_i) - K^{(1)}(\tilde{s}_{i,2} - t_i)K(\tilde{s}_{i,1} - t_i)} \begin{bmatrix} -K^{(1)}(\tilde{s}_{i,2} - t_i) & -K(\tilde{s}_{i,2} - t_i) \\ K^{(1)}(\tilde{s}_{i,1} - t_i) & K(\tilde{s}_{i,1} - t_i) \end{bmatrix}$$

when the expression in the denominator is nonzero. The Gaussian kernel has nonzero denominator for $\tilde{s}_{i,1} \neq \tilde{s}_{i,2}$. The Ricker wavelet has nonzero denominator when $\tilde{s}_{i,1} \neq \tilde{s}_{i,2}$ and $|\tilde{s}_{i,1}|, |\tilde{s}_{i,2}| < 1$.

The condition $|\tilde{s}_{i,1}|, |\tilde{s}_{i,2}| < 1$ is natural for the Ricker wavelet, since it has roots at ± 1 .

We would like to emphasize that the bumps and waves are just a tool for analyzing the dual certificate obtained by solving the system of equations (3.7). Under the conditions of Theorem 2.4, which ensure that the support of the signal is not too clustered and that there are two samples close to each spike, we show that each coefficient α_i is close to the sign of the spike and β_i is small, so that

$$Q(t) = \sum_{t_i \in T} \alpha_i B_{t_i}(t, \tilde{s}_{i,1}, \tilde{s}_{i,2}) + \beta_i W_{t_i}(t, \tilde{s}_{i,1}, \tilde{s}_{i,2}) \quad (3.15)$$

$$\approx \sum_{t_i \in T} \rho_i B_{t_i}(t, \tilde{s}_{i,1}, \tilde{s}_{i,2}). \quad (3.16)$$

This allows us to control Q and show that it is a valid dual combination. In contrast, characterizing the coefficients $q_1, \dots, q_{|\tilde{S}|}$ directly is much more challenging, as illustrated in Figure 14.

The following two lemmas formalize this intuition. The first establishes that the system of equations (3.7) is invertible. The second shows that the amplitude of Q is bounded on T^c . Together

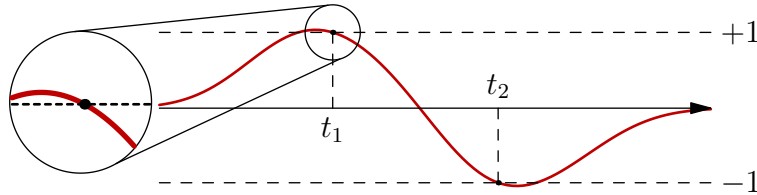


Figure 12: A linear combination of two bumps interpolating the signs $+1$ at t_1 and -1 at t_2 . Since there are no constraints on its derivative, the red curve does not have local extrema at t_1, t_2 . The construction is not a valid certificate because its magnitude is not bounded by one.

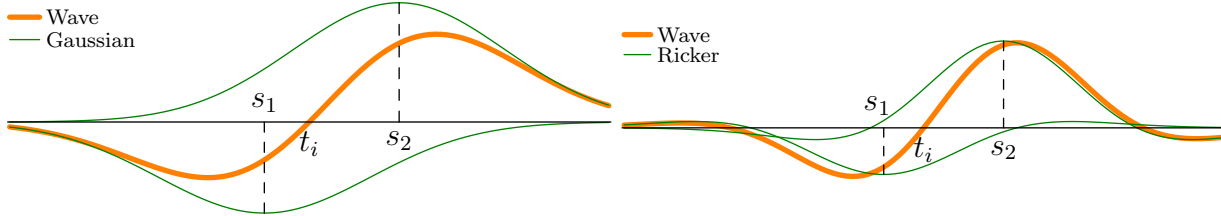


Figure 13: The wave interpolation function $W_{t_i}(t, s_1, s_2)$ is a linear combination of kernels centered at s_1, s_2 . The figure shows examples for the Gaussian kernel (left) and the Ricker wavelet (right).

with Proposition 3.1 they yield a proof of Theorem 2.4. Both of their proofs rely heavily on bounds controlling the bumps and waves and their derivatives, which are compiled in Section 3.3.

Lemma 3.3 (Proof in Section 3.4). *Under the assumptions of Theorem 2.4, the system of equations (3.7) has a unique solution.*

Lemma 3.4 (Proof in Section 3.5). *Under the assumptions of Theorem 2.4, the dual combination corresponding to the solution system (3.7) satisfies $|Q(t)| < 1$ for all $t \in T^c$.*

We now illustrate the proof technique described in this section using a simple example. Consider an atomic measure μ consisting of 3 point masses:

$$\mu := a_1\delta_{t_1} + a_2\delta_{t_2} + a_3\delta_{t_3}. \quad (3.17)$$

Here $T = \{t_1, t_2, t_3\} \subset \mathbb{R}$. Let S denote a set of sample locations, and let $\tilde{S} \subseteq S$ be defined by

$$\tilde{S} = \{\tilde{s}_{1,1}, \tilde{s}_{1,2}, \tilde{s}_{2,1}, \tilde{s}_{2,2}, \tilde{s}_{3,1}, \tilde{s}_{3,2}\}, \quad (3.18)$$

where $\tilde{s}_{i,1}$ and $\tilde{s}_{i,2}$ are close to t_i for $i = 1, 2, 3$. We fix a sign pattern $\rho = (1, -1, 1)$. Using kernels centered at the elements of \tilde{S} we construct a dual combination $Q(t)$ of the form in (3.6) that satisfies the interpolation equations in (3.7). The resulting dual combination $Q(t)$ can be seen in the first and third plots of Figure 14. The amplitudes of the kernels centered at the samples are difficult to control. We then reparametrize $Q(t)$ into the form given in (3.8) by writing it as a linear combination of 3 bumps and 3 waves. This reparametrization is shown in the second and fourth plots of Figure 14. As can be seen in the figure, the bump coefficients roughly match the values of ρ and the wave coefficients are very small, making them amenable to analysis.

3.3 Bounding Bumps and Waves

In this section we establish bounds on the bumps and waves and their derivatives, which are used in Sections 3.4 and 3.5 to establish exact recovery. To simplify notation, without loss of generality we consider a bump and a wave centered at the origin and set

$$B(t, \tilde{s}_{i,1}, \tilde{s}_{i,2}) := B_0(t, \tilde{s}_{i,1}, \tilde{s}_{i,2}), \quad (3.19)$$

$$W(t, \tilde{s}_{i,1}, \tilde{s}_{i,2}) := W_0(t, \tilde{s}_{i,1}, \tilde{s}_{i,2}). \quad (3.20)$$

We begin with a simplifying observation. For even kernels like the Gaussian and Ricker, the bumps and waves exhibit a form of symmetry.

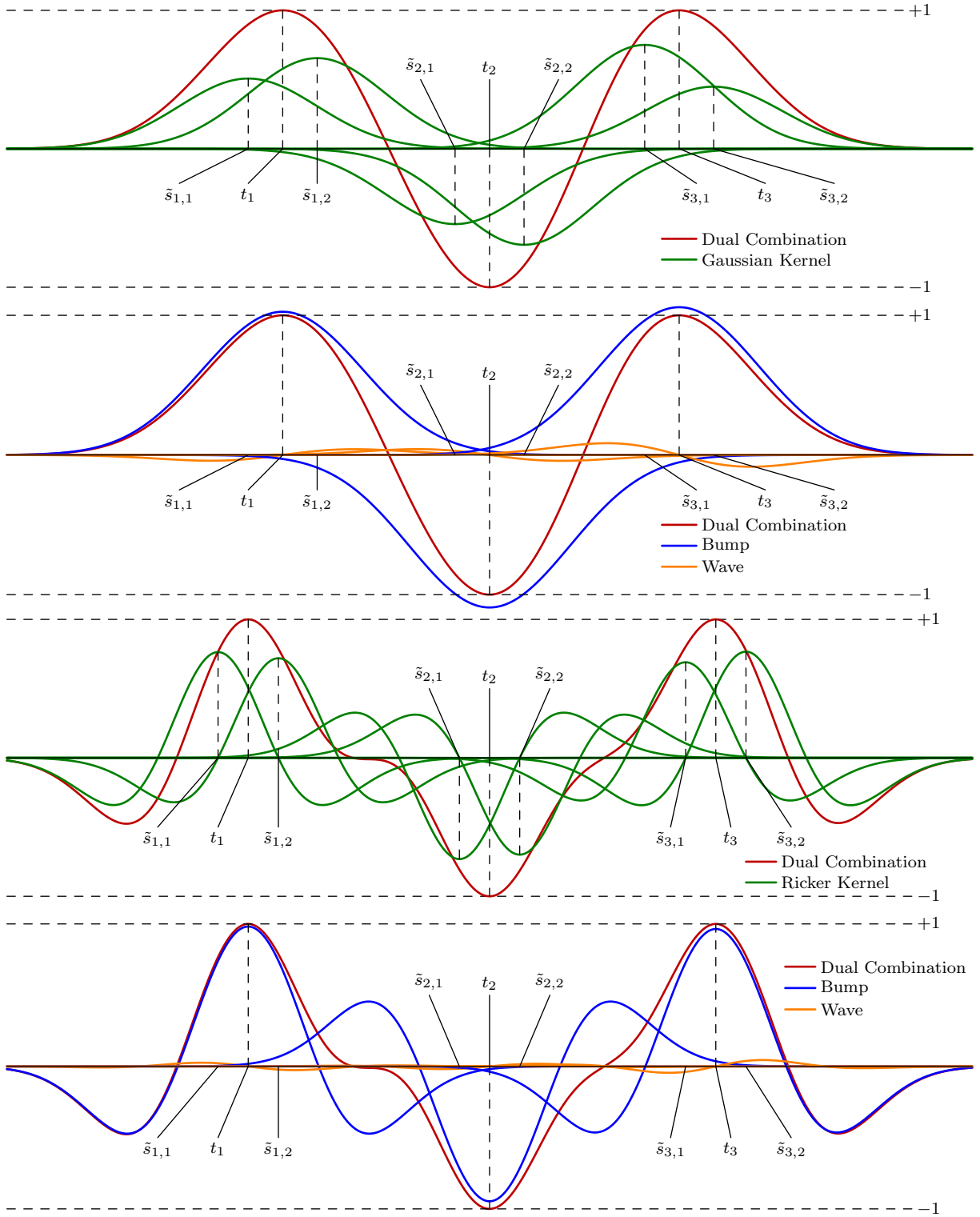


Figure 14: Effect of the proposed reparametrization for the Gaussian (top) and Ricker kernels (bottom). The dual combination Q (red) is a sum of scaled shifted kernels with varying amplitudes (green). When we decompose the same function Q into bumps (blue) and waves (orange), the amplitudes of the bumps all approximately equal the signs of the corresponding spikes, whereas the waves are very small.

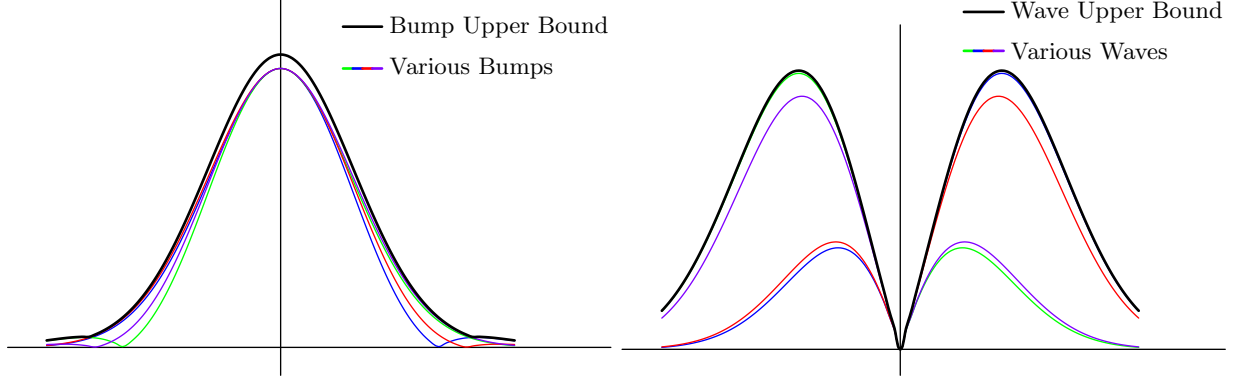


Figure 15: Sample-independent bounds on the absolute bump $|B|_\infty(t)$ (left) and absolute wave $|W|_\infty(t)$ (right) for the Gaussian kernel under a sample proximity $\gamma(S, T) = 0.5$ and sample separation $\kappa(S) = 0.05$

Lemma 3.5 (Proof in Appendix B.3). *Let K be a kernel with corresponding bump B and wave W . If the kernel satisfies $K(t) = K(-t)$ for all $t \in \mathbb{R}$ then*

$$B(t, s_1, s_2) = B(-t, -s_1, -s_2) \quad \text{and} \quad W(t, s_1, s_2) = -W(-t, -s_1, -s_2), \quad (3.21)$$

for all $s_1, s_2, t \in \mathbb{R}$.

The shape of each bump and wave depends on where its corresponding samples are located. In order to account for all possible sample locations satisfying the sample-proximity and sample-separation conditions in Definition 2.2, we define sample-independent upper bounds of the form

$$|B^{(i)}|_\infty(t) := \sup_{\substack{|s_1|, |s_2| \leq \gamma(S, T) \\ |s_1 - s_2| \geq \kappa(S)}} |B^{(i)}(t, s_1, s_2)|, \quad (3.22)$$

$$|W^{(i)}|_\infty(t) := \sup_{\substack{|s_1|, |s_2| \leq \gamma(S, T) \\ |s_1 - s_2| \geq \kappa(S)}} |W^{(i)}(t, s_1, s_2)|, \quad (3.23)$$

$$B_\infty^{(i)}(t) := \sup_{\substack{|s_1|, |s_2| \leq \gamma(S, T) \\ |s_1 - s_2| \geq \kappa(S)}} B^{(i)}(t, s_1, s_2), \quad (3.24)$$

for $i = 0, 1, 2$. By Lemma 3.5, these functions are all even. The bounds are depicted in Figure 15.

To simplify our analysis, we define monotonized versions of the absolute bounds above for $i \in \{0, 1, 2\}$:

$$|B^{(i)}|_\infty^\downarrow(t) := \sup\{|B^{(i)}|_\infty(u) \mid u \geq |t|\}, \quad (3.25)$$

$$|W^{(i)}|_\infty^\downarrow(t) := \sup\{|W^{(i)}|_\infty(u) \mid u \geq |t|\}. \quad (3.26)$$

The decay properties of the Gaussian and Ricker kernels translate to fast-decaying bumps and waves. The following lemma formalizes this, by controlling the tails of our monotonic bounds.

Lemma 3.6 (Proof in Appendix B.4). *For the Gaussian and Ricker kernels we have*

$$\sum_{j=6}^{\infty} |B^{(i)}|_{\infty}^{\downarrow}((j-1/2)\Delta) \leq \frac{10^{-12}}{\kappa(S)}, \quad \sum_{j=6}^{\infty} |W^{(i)}|_{\infty}^{\downarrow}((j-1/2)\Delta) \leq \frac{10^{-12}}{\kappa(S)}, \quad (3.27)$$

$$|B^{(i)}|_{\infty}^{\downarrow}(t) \leq \frac{10^{-12}}{\kappa(S)}, \quad |W^{(i)}|_{\infty}^{\downarrow}(t) \leq \frac{10^{-12}}{\kappa(S)}, \quad (3.28)$$

for $i = 0, 1, 2$, $t \geq 10$, and $\Delta \geq 2$.

When applying the lemma, Δ corresponds to the minimum separation $\Delta(T)$ of the signal support. There is nothing special about the constants above (i.e. $j = 6$, $t \geq 10$, $\Delta \geq 2$); they are simply chosen for definiteness and other values would also work (see Appendix B.4 for more details).

Lemma 3.6 shows that the bumps, waves, and their derivatives are small for $t \geq 10$. The following lemma provides piecewise constant bounds for $t \in [0, 10)$.

Lemma 3.7 (Proof in Appendix B.5). *Fix $\gamma(S, T)$ and $\kappa(S)$ and let $N_1 \in \mathbb{Z}_{>0}$. Partition the interval $[0, 10)$ into N_1 intervals of the form*

$$\mathcal{U}_j := \left[\frac{10(j-1)}{N_1}, \frac{10j}{N_1} \right), \quad (3.29)$$

and $j = 1, \dots, N_1$. For the Gaussian and Ricker kernels, there exist functions $|\widetilde{B}^{(i)}|$, $|\widetilde{W}^{(i)}|$, $\widetilde{B}^{(i)}$, such that for all $t \in \mathcal{U}_j$ and $i = 0, 1, 2$

$$|B^{(i)}|_{\infty}(t) \leq |\widetilde{B}^{(i)}|(j), \quad (3.30)$$

$$|W^{(i)}|_{\infty}(t) \leq |\widetilde{W}^{(i)}|(j), \quad (3.31)$$

$$B_{\infty}^{(i)}(t) \leq \widetilde{B}^{(i)}(j). \quad (3.32)$$

These bounds depend on $\gamma(S, T)$, $\kappa(S)$ and an additional parameter N_2 , satisfying $\kappa(S) > 2\gamma(S, T)/N_2$ as explained in Appendix B.5.

Lemma 3.6 can be used to extend the bounds of Lemma 3.7 to the monotonized bumps, waves, and their derivatives.

Corollary 3.8. *Assuming the conditions and definitions in Lemmas 3.6 and 3.7 we have, for $i = 0, 1, 2$ and $t \in \mathcal{U}_j$*

$$|B^{(i)}|_{\infty}^{\downarrow}(t) \leq \max \left(\max_{k:j \leq k \leq N_1} |\widetilde{B}^{(i)}|(k), \epsilon \right), \quad (3.33)$$

$$|W^{(i)}|_{\infty}^{\downarrow}(t) \leq \max \left(\max_{k:j \leq k \leq N_1} |\widetilde{W}^{(i)}|(k), \epsilon \right), \quad (3.34)$$

where $\epsilon := 10^{-12}/\kappa(S)$.

Lemma 3.7 and Corollary 3.8 provide upper bounds on the bumps, waves, and their derivatives that are symmetric, sample-independent and, in the case of Corollary 3.8, monotonic.

3.4 Proof of Lemma 3.3: Invertibility of the Interpolation Equations

In this section we prove Lemma 3.3, establishing the invertibility of the interpolation equations (3.7). As a by-product, we also obtain bounds on the interpolation coefficients α, β in (3.8). For simplicity we use the following abbreviated notation for the bumps and waves:

$$B_i(t) := B_{t_i}(t, \tilde{s}_{i,1}, \tilde{s}_{i,2}), \quad (3.35)$$

$$W_i(t) := W_{t_i}(t, \tilde{s}_{i,1}, \tilde{s}_{i,2}). \quad (3.36)$$

To begin, we express equations (3.7) in terms of bumps and waves:

$$\sum_{j=1}^n \alpha_j B_j(t_i) + \beta_j W_j(t_i) = \rho_i, \quad (3.37)$$

$$\sum_{j=1}^n \alpha_j B_j^{(1)}(t_i) + \beta_j W_j^{(1)}(t_i) = 0, \quad \text{for all } t_i \in T. \quad (3.38)$$

Define the $n \times n$ matrices $\mathcal{B}, \mathcal{W}, \mathcal{B}^{(1)}, \mathcal{W}^{(1)}$ by

$$\begin{aligned} (\mathcal{B})_{ij} &:= B_j(t_i), \\ (\mathcal{W})_{ij} &:= W_j(t_i), \\ (\mathcal{B}^{(1)})_{ij} &:= B_j^{(1)}(t_i), \\ (\mathcal{W}^{(1)})_{ij} &:= W_j^{(1)}(t_i). \end{aligned} \quad (3.39)$$

This allows us to express the reparametrized interpolation equations in block-matrix form:

$$\begin{bmatrix} \mathcal{B} & \mathcal{W} \\ \mathcal{B}^{(1)} & \mathcal{W}^{(1)} \end{bmatrix} \begin{bmatrix} \alpha \\ \beta \end{bmatrix} = \begin{bmatrix} \rho \\ 0 \end{bmatrix}. \quad (3.40)$$

If $\Delta(T)$ is sufficiently large we can exploit the decay of the bumps and waves to prove that this matrix is close to the identity. This is formalized in the following linear-algebra result, which shows how to convert norm bounds on these blocks into bounds on α, β , and gives conditions under which the system is invertible. Throughout, for an $n \times n$ matrix A , we write $\|A\|_\infty$ to denote the matrix norm

$$\|A\|_\infty = \sup_{\|x\|_\infty \leq 1} \|Ax\|_\infty. \quad (3.41)$$

Lemma 3.9. *Suppose $\|\mathcal{I} - \mathcal{W}^{(1)}\|_\infty < 1$, and $\|\mathcal{I} - \mathcal{C}\|_\infty < 1$ where*

$$\mathcal{C} = \mathcal{B} - \mathcal{W}(\mathcal{W}^{(1)})^{-1}(\mathcal{B}^{(1)})$$

is the Schur complement of $\mathcal{W}^{(1)}$, and \mathcal{I} is the identity matrix. Then

$$\begin{bmatrix} \mathcal{B} & \mathcal{W} \\ \mathcal{B}^{(1)} & \mathcal{W}^{(1)} \end{bmatrix} \begin{bmatrix} \alpha \\ \beta \end{bmatrix} = \begin{bmatrix} \rho \\ 0 \end{bmatrix} \quad (3.42)$$

has a unique solution. Furthermore, we have

$$\|\alpha\|_\infty \leq \|\mathcal{C}^{-1}\|_\infty, \quad (3.43)$$

$$\|\beta\|_\infty \leq \|(\mathcal{W}^{(1)})^{-1}\|_\infty \|\mathcal{B}^{(1)}\|_\infty \|\mathcal{C}^{-1}\|_\infty, \quad (3.44)$$

$$\|\alpha - \rho\|_\infty \leq \|\mathcal{I} - \mathcal{C}\|_\infty \|\mathcal{C}^{-1}\|_\infty, \quad (3.45)$$

where

$$\|\mathcal{I} - \mathcal{C}\|_\infty \leq \|\mathcal{I} - \mathcal{B}\|_\infty + \|\mathcal{W}\|_\infty \|(\mathcal{W}^{(1)})^{-1}\|_\infty \|\mathcal{B}^{(1)}\|_\infty, \quad (3.46)$$

$$\|\mathcal{C}^{-1}\|_\infty \leq \frac{1}{1 - \|\mathcal{I} - \mathcal{C}\|_\infty}, \quad (3.47)$$

$$\|(\mathcal{W}^{(1)})^{-1}\|_\infty \leq \frac{1}{1 - \|\mathcal{I} - \mathcal{W}^{(1)}\|_\infty}. \quad (3.48)$$

Proof. Follows as a special case of Lemma I.4. \square

To apply Lemma 3.9 we require bounds on $\|\mathcal{I} - \mathcal{B}\|_\infty$, $\|\mathcal{W}\|_\infty$, $\|\mathcal{B}^{(1)}\|_\infty$, and $\|\mathcal{I} - \mathcal{W}^{(1)}\|_\infty$. We compute these using the bounds in Section 3.3. We have

$$\|\mathcal{I} - \mathcal{B}\|_\infty = \max_{t_i \in T} \sum_{\substack{t_j \in T \\ t_j \neq t_i}} |B_j(t_i)| \leq 2 \sum_{j=1}^{\infty} |B|_\infty^\downarrow(j\Delta(T)), \quad (3.49)$$

$$\|\mathcal{W}\|_\infty = \max_{t_i \in T} \sum_{t_j \in T} |W_j(t_i)| \leq 2 \sum_{j=1}^{\infty} |W|_\infty^\downarrow(j\Delta(T)), \quad (3.50)$$

$$\|\mathcal{B}^{(1)}\|_\infty = \max_{t_i \in T} \sum_{t_j \in T} |B_j^{(1)}(t_i)| \leq 2 \sum_{j=1}^{\infty} |B^{(1)}|_\infty^\downarrow(j\Delta(T)), \quad (3.51)$$

$$\|\mathcal{I} - \mathcal{W}^{(1)}\|_\infty = \max_{t_i \in T} \sum_{\substack{t_j \in T \\ t_j \neq t_i}} |W_j^{(1)}(t_i)| \leq 2 \sum_{j=1}^{\infty} |W^{(1)}|_\infty^\downarrow(j\Delta(T)), \quad (3.52)$$

where the monotonicity of the bounds allows us to assume that the spacing between adjacent spikes equals the minimum separation. All sums start at $j = 1$ because $W_j(t_j) = B_j^{(1)}(t_j) = 0$ and $W_j^{(1)}(t_j) = B_j(t_j) = 1$ by construction.

Applying Lemma 3.6 we obtain, for $\Delta(T) \geq 2$ and $\epsilon := 10^{-12}/\kappa(S)$,

$$\|\mathcal{I} - \mathcal{B}\|_\infty \leq 2 \sum_{j=1}^5 |B|_\infty^\downarrow(j\Delta(T)) + 2\epsilon \quad (3.53)$$

$$\|\mathcal{W}\|_\infty \leq 2 \sum_{j=1}^5 |W|_\infty^\downarrow(j\Delta(T)) + 2\epsilon \quad (3.54)$$

$$\|\mathcal{B}^{(1)}\|_\infty \leq 2 \sum_{j=1}^5 |B^{(1)}|_\infty^\downarrow(j\Delta(T)) + 2\epsilon \quad (3.55)$$

$$\|\mathcal{I} - \mathcal{W}^{(1)}\|_\infty \leq 2 \sum_{j=1}^5 |W^{(1)}|_\infty^\downarrow(j\Delta(T)) + 2\epsilon. \quad (3.56)$$

If we fix values for $\Delta(T)$, $\gamma(S, T)$, $\kappa(S)$, and the parameters N_1 and N_2 from Lemma 3.7, we can use Corollary 3.8 to compute the above bounds numerically. This allows us to check whether the

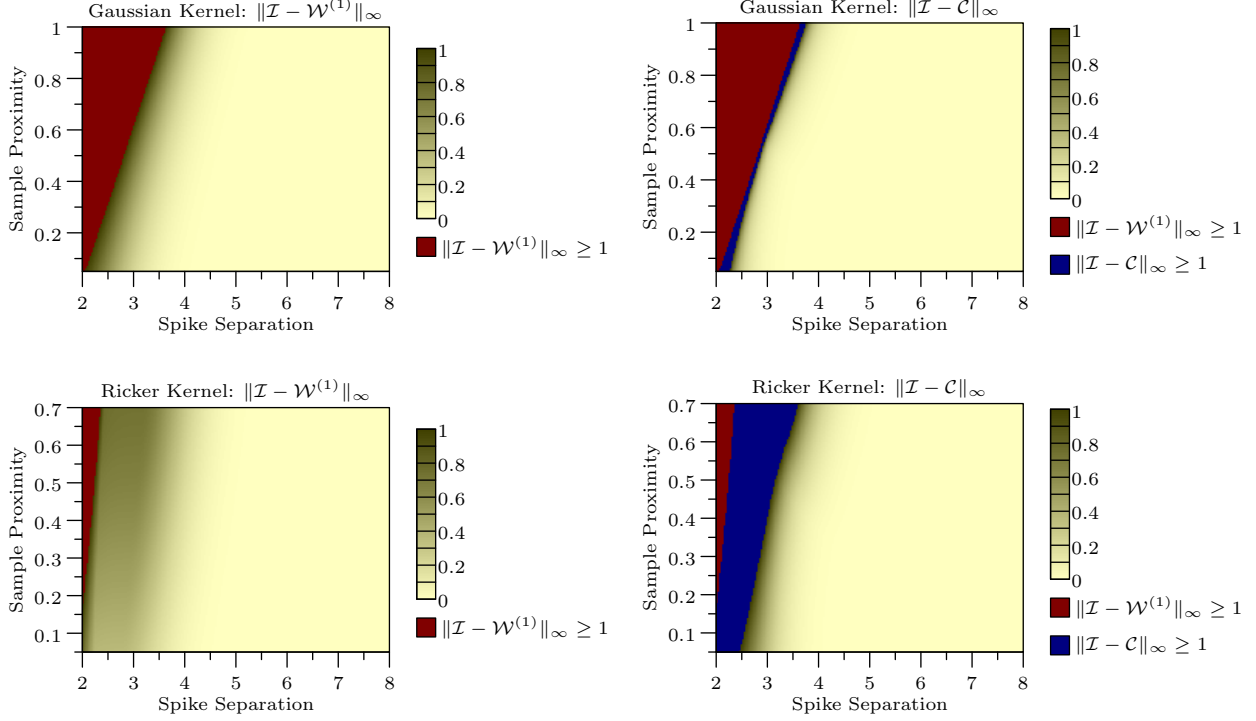


Figure 16: Upper bounds on $\|\mathcal{I} - \mathcal{W}^{(1)}\|_\infty$ and $\|\mathcal{I} - \mathcal{C}\|_\infty$ for different values of the minimum separation and the sample proximity.

interpolation equations are invertible for a specific triple $(\Delta(T), \gamma(S, T), \kappa(S))$ by Lemma 3.9. The upper bounds in equations (3.53) to (3.56) decrease as $\Delta(T)$ increases due to monotonicity. By combining this fact with the definitions of $\gamma(S, T)$ and $\kappa(S)$, we see that invertibility for a fixed triple (a, b, c) implies invertibility for all triples in the set

$$\{(\Delta(T), \gamma(S, T), \kappa(S)) \mid \Delta(T) \geq a, \gamma(S, T) \leq b, \kappa(S) \geq c\}. \quad (3.57)$$

This allows us to compute the above bounds for a finite set of triples and obtain an infinite continuous region on which invertibility occurs.

In Figure 16 we compute bounds on $\|\mathcal{I} - \mathcal{W}^{(1)}\|_\infty$ and $\|\mathcal{I} - \mathcal{C}\|_\infty$ for $\kappa(S) = 0.05$. The values of $\gamma(S, T)$ are sampled at 200 equally-spaced points in the interval $[0.05, 1]$ for the Gaussian and $[0.05, 0.7]$ for the Ricker. The values of $\Delta(T)$ are sampled at 200 equally-spaced points in the interval $[2, 8]$ for both kernels. For fixed $\gamma(S, T)$ the value of N_1 is chosen to satisfy $\gamma(S, T)/N_1 = 1/500$ for the Gaussian and $\gamma(S, T)/N_1 = 0.7/500$ for the Ricker. For fixed $\Delta(T)$ the value of N_2 is chosen to satisfy $\Delta(T)/N_2 = 8/700$ for both kernels. In other words, we use a fixed partition width in all upper bound computations (see Lemma 3.7 and Appendix B.5 for the definitions of N_1 and N_2). The plots show that invertibility is achieved over the required region.

3.5 Proof of Lemma 3.4: Bounding the Dual Combination

In this section, we prove that the dual combination Q satisfies the condition $|Q(t)| < 1$ for $t \in T^c$. Without loss of generality, we assume that there is a spike at the origin with sign $+1$ and we restrict our analysis to the region between this spike and the next one. The same argument can be applied to the interval between any two other spikes. For clarity, we again use the shorthand notation (3.35) and (3.36) for the bumps and waves.

We begin by decomposing Q as the sum of two terms that account for the contribution of the bumps and waves separately: $Q(t) = \mathcal{B}(t) + \mathcal{W}(t)$, where

$$\mathcal{B}(t) := \sum_{j=1}^n \alpha_j B_j(t) \quad \text{and} \quad \mathcal{W}(t) := \sum_{j=1}^n \beta_j W_j(t). \quad (3.58)$$

In the following lemma we bound these functions by applying the triangle inequality, Lemma 3.9, and Lemma 3.6.

Lemma 3.10 (Proof in Appendix C). *Fix our kernel to be the Gaussian kernel or the Ricker wavelet. Assume the conditions of Lemmas 3.6 and 3.9 hold, and that there is a spike at the origin with sign $+1$. Let h denote half the distance from the origin to the spike with smallest positive location, or ∞ if no such spike exists. Then, for $0 < t \leq h$ (or $t > 0$ if $h = \infty$) and $\epsilon := 10^{-12}/\kappa(S)$,*

$$|\mathcal{B}^{(p)}(t)| \leq \|\alpha\|_\infty \left(|B^{(p)}|_\infty^\downarrow(v) + 2\epsilon + \sum_{j=1}^5 |B^{(p)}|_\infty^\downarrow(v + j\Delta(T)) + |B^{(p)}|_\infty^\downarrow(j\Delta(T) - v) \right) \quad (3.59)$$

$$|\mathcal{W}^{(p)}(t)| \leq \|\beta\|_\infty \left(|W^{(p)}|_\infty^\downarrow(v) + 2\epsilon + \sum_{j=1}^5 |W^{(p)}|_\infty^\downarrow(v + j\Delta(T)) + |W^{(p)}|_\infty^\downarrow(j\Delta(T) - v) \right), \quad (3.60)$$

for $p = 0, 1, 2$ and $v = \min(t, \Delta(T)/2)$. For $q = 1, 2$

$$\mathcal{B}^{(q)}(t) \leq \alpha_{\text{LB}} B_\infty^{(q)}(t) + \|\alpha\|_\infty \left(2\epsilon + \sum_{j=1}^5 |B^{(q)}|_\infty^\downarrow(v + j\Delta(T)) + |B^{(q)}|_\infty^\downarrow(j\Delta(T) - v) \right), \quad (3.61)$$

as long as $B_\infty^{(q)}(t) \leq 0$, where $\alpha_{\text{LB}} := 1 - \|\alpha - \rho\|_\infty \geq 0$.

The following lemma provides three conditions under which Q is strictly bounded by one on the interval $(0, h]$. We omit the proof, which follows from basic calculus and the fact that $Q(0) = 1$ and $Q^{(1)}(0) = 0$ by Lemma 3.3.

Lemma 3.11. *Assume the conditions of Lemma 3.10. Suppose there are $u_1, u_2 \in (0, h]$ such that*

1. (Neighboring) $Q^{(2)}(t) < 0$ on $[0, u_1]$,
2. (Near) $Q^{(1)}(t) < 0$ on $[u_1, u_2]$,
3. (Far) $|Q(t)| < 1$ on $[u_2, h]$,

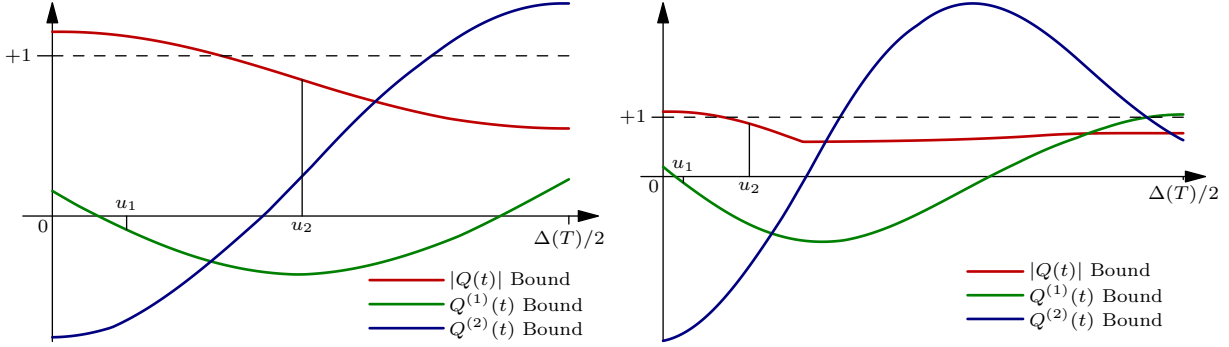


Figure 17: Bounds on the magnitude and the first and second derivatives of the dual combination Q for a fixed value of the minimum separation and sample proximity. The left figure uses the Gaussian kernel with $\Delta(T) = 3.5$. The right figure uses the Ricker kernel with $\Delta(T) = 4.7$. Both figures have $\gamma(S, T) = 0.3$ and $\kappa(S) = 0.05$.

Then $|Q(t)| < 1$ for $t \in (0, h]$.

With Lemma 3.11 in place, we outline a procedure for establishing exact recovery for fixed values of $\Delta(T)$, $\gamma(S, T)$, $\kappa(S)$ and the parameters N_1 and N_2 from Lemma 3.7.

1. Apply Corollary 3.8 and Lemma 3.9 to check that the interpolation equations are invertible.
2. Using Lemma 3.7 and Corollary 3.8, compute piecewise-constant upper bounds for $|B^{(q)}|_{\infty}^{\downarrow}(t)$, $|W^{(q)}|_{\infty}^{\downarrow}(t)$, and $B_{\infty}^p(t)$ for $q = 0, 1, 2$, $p = 1, 2$, and $t \in [0, \Delta/2]$. These piecewise-constant functions are all defined on the same partition (see Lemma 3.7). By Lemma 3.10, we obtain bounds on $|Q(t)|$ for $t \in (0, h]$, and on $Q^{(1)}(t), Q^{(2)}(t)$ for $t \in (0, \Delta(T)/2]$.
3. By iterating over the partition, test whether the conditions of Lemma 3.11 are satisfied. If they are, Q is a valid dual combination and exact recovery is proven.

As all of the upper bounds in Lemma 3.10 decrease as $\Delta(T)$ increases, we again obtain that recovery for a single triple (a, b, c) implies recovery for all triples in

$$\{(\Delta(T), \gamma(S, T), \kappa(S)) \mid \Delta(T) \geq a, \gamma(S, T) \leq b, \kappa(S) \geq c\}. \quad (3.62)$$

Using the same parameters as described in Section 3.4 to compute Figure 16 we verify that exact recovery holds for the entire region specified in Theorem 2.4. In Figure 17 we show an example for the Gaussian and Ricker kernels where our bounds on $|Q|$, $Q^{(1)}$ and $Q^{(2)}$ meet the criteria of Lemma 3.11. In Figure 18 we plot the region where exact recovery is proven, and show upper bounds on the value of u_1 .

4 Proof of Robustness to Dense Noise (Theorem 2.7)

The proof of Theorem 2.7 is based on the proof of support-detection guarantees for super-resolution from low-pass data in [33]. The proofs in [33] assume the existence of a dual certificate for the super-resolution problem, provided in [14]. Here, we use similar arguments to derive robustness guarantees

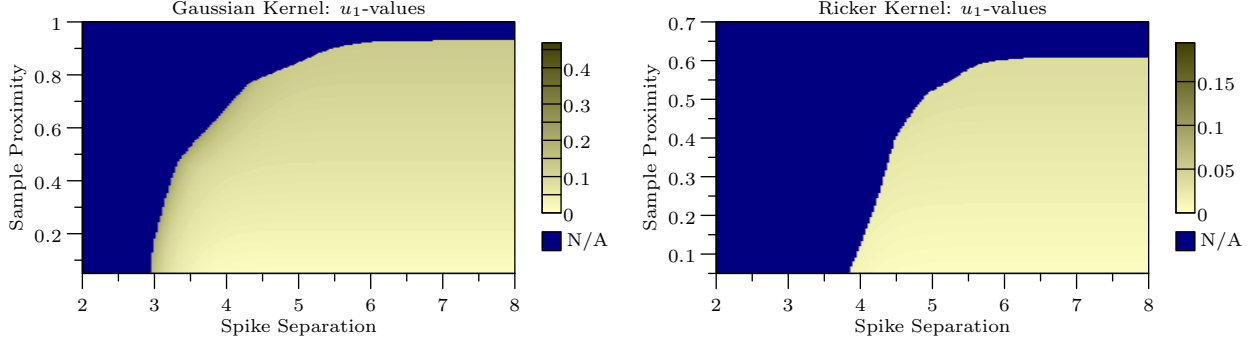


Figure 18: Upper bounds on the values of u_1 in the range of values of the minimum separation and the sample proximity for which we establish exact recovery.

for the deconvolution problem using the dual-certificate construction presented in Section 3. We again assume, without loss of generality, that $\sigma = 1$. Auxiliary Mathematica code to perform the computations needed for the proof is available online³.

4.1 Proof of Theorem 2.7, Inequalities (2.10) and (2.11)

To prove (2.10) and (2.11), we exploit some properties of the dual certificate from Section 3, which are established in the following lemma.

Lemma 4.1 (Proof in Appendix F.1). *Under the assumptions of Theorem 2.7, there exists a function Q of the form*

$$Q(t) := \sum_{s_i \in S} q_i K(s_i - t), \quad (4.1)$$

for some $q \in \mathbb{R}^n$ that satisfies:

1. $Q(t_j) = \text{sign}(a_j)$ for all $t_j \in T$,
2. $|Q(t)| < 1$ for all $t \in T^c$,
3. $|Q(t)| \leq 1 - C_1(t - t_j)^2$ if $|t - t_j| \leq \eta$ for some $t_j \in T$,
4. $|Q(t)| \leq 1 - C_2$ if $|t - t_j| > \eta$ for all $t_j \in T$,
5. $\|q\|_\infty \leq C_3$.

The values $\eta, C_1, C_2, C_3 > 0$ depend only on $\Delta(T)$, $\gamma(S, T)$, and $\kappa(S)$.

By combining Lemma 4.1 with the fact that $\|\hat{\mu}\|_{\text{TV}} \leq \|\mu\|_{\text{TV}}$ we obtain two useful bounds. Below we use $d(\hat{t}_k, T)$ to denote the distance from \hat{t}_k to the set T :

$$d(\hat{t}_k, T) := \min_{t \in T} |\hat{t}_k - t|. \quad (4.2)$$

³http://www.cims.nyu.edu/~cfgranda/scripts/deconvolution_proof.zip

Corollary 4.2 (Proof in Appendix F.2). *Under the assumptions of Lemma 4.1*

$$\int Q(t) d\hat{\mu}(t) \geq \|\hat{\mu}\|_{\text{TV}} - 2\|q\|_{\infty} \bar{\xi} \sqrt{|T|}, \quad (4.3)$$

$$\int Q(t) d\hat{\mu}(t) \leq \sum_{\hat{t}_k \in \hat{T}: d(\hat{t}_k, T) \leq \eta} (1 - C_1 d(\hat{t}_k, T)^2) |\hat{a}_k| + \sum_{\hat{t}_k \in \hat{T}: d(\hat{t}_k, T) > \eta} (1 - C_2) |\hat{a}_k|. \quad (4.4)$$

The proof of inequality (4.3) differs from the analogous result in [33] because we cannot use Plancherel's theorem. As a result, a factor of $\|q\|_{\infty} \sqrt{|T|}$ appears in the bound (see Appendix F.2 for more details).

Applying (4.3) and (4.4) we obtain

$$\sum_{\hat{t}_k \in \hat{T}: d(\hat{t}_k, T) \leq \eta} (1 - C_1 d(\hat{t}_k, T)^2) |\hat{a}_k| + \sum_{\hat{t}_k \in \hat{T}: d(\hat{t}_k, T) > \eta} (1 - C_2) |\hat{a}_k| \geq \int Q(t) d\hat{\mu}(t) \quad (4.5)$$

$$\geq \|\hat{\mu}\|_{\text{TV}} - 2\|q\|_{\infty} \bar{\xi} \sqrt{|T|} \quad (4.6)$$

$$= \sum_{\hat{t}_k \in \hat{T}} |\hat{a}_k| - 2\|q\|_{\infty} \bar{\xi} \sqrt{|T|}. \quad (4.7)$$

Rearranging terms gives

$$\sum_{\hat{t}_k \in \hat{T}: d(\hat{t}_k, T) \leq \eta} C_1 d(\hat{t}_k, T)^2 |\hat{a}_k| + \sum_{\hat{t}_k \in \hat{T}: d(\hat{t}_k, T) > \eta} C_2 |\hat{a}_k| \leq 2\|q\|_{\infty} \bar{\xi} \sqrt{|T|}. \quad (4.8)$$

By Property 5 in Lemma 4.1 we obtain (2.10) and (2.11).

4.2 Proof of Theorem 2.7, Inequality (2.9)

The main technical contribution of [33] is a method to isolate the error incurred by TV-norm minimization for each particular spike by constructing a low-pass trigonometric polynomial that is equal to one at the location of the spike and zero on the rest of the signal support. The following lemma provides an analogous object, which we construct using the techniques described in Section 3.

Lemma 4.3 (Proof in Appendix F.3). *Assume the conditions of Lemma 4.1. Then for any $t_j \in T$ there exists a function Q_j of the form*

$$Q_j(t) = \sum_{s_i \in S} q(j)_i K(s_i - t), \quad (4.9)$$

where $q(j) \in \mathbb{R}^n$, such that:

1. $Q_j(t_j) = 1$ and $Q_j(t_l) = 0$ for $t_l \in T \setminus \{t_j\}$,
2. $|Q_j(t)| < 1$ for $t \in T^c$,
3. $|1 - Q_j(t)| \leq C'_1 (t - t_j)^2$ for $|t - t_j| \leq \eta$,

4. $|Q_j(t)| \leq C'_1(t - t_l)^2$ for $|t - t_l| \leq \eta$, $l \neq j$,
5. $|Q_j(t)| \leq C'_2$ for $\min_{t_l \in T} |t - t_l| > \eta$,
6. $\|q(j)\|_\infty \leq C'_3$.

Here the values $C'_1, C'_2, C'_3 > 0$ only depend on $\Delta(T)$, $\gamma(S, T)$ and $\kappa(S)$. The constant η is the same as in Lemma 4.1.

Lemma 4.3 yields two inequalities that allow us to control the estimation error for the spike at t_j .

Corollary 4.4 (Proof in Appendix F.4). *Under the conditions of Lemma 4.3*

$$\left| \int Q_j(t) d(\mu - \hat{\mu})(t) \right| \leq 2 \|q(j)\|_\infty \bar{\xi} \sqrt{|T|}, \quad (4.10)$$

$$\left| \int Q_j(t) d\hat{\mu}(t) - \sum_{\hat{t}_k \in \hat{T}: |\hat{t}_k - t_j| \leq \eta} \hat{a}_k \right| \leq C' \bar{\xi} \sqrt{|T|}, \quad (4.11)$$

for some $C' > 0$ that only depends on $\Delta(T)$, $\gamma(S, T)$, and $\kappa(S)$.

Applying Corollary 4.4 we have

$$\left| a_j - \sum_{\hat{t}_k \in \hat{T}: |\hat{t}_k - t_j| \leq \eta} \hat{a}_k \right| = \left| \int Q_j(t) d(\mu - \hat{\mu})(t) + \int Q_j(t) d\hat{\mu}(t) - \sum_{\hat{t}_k \in \hat{T}: |\hat{t}_k - t_j| \leq \eta} \hat{a}_k \right| \quad (4.12)$$

$$\leq 2 \|q(j)\|_\infty \bar{\xi} \sqrt{|T|} + C' \bar{\xi} \sqrt{|T|} \quad (4.13)$$

$$\leq C \bar{\xi} \sqrt{|T|}, \quad (4.14)$$

for some $C > 0$ by Property 6 in Lemma 4.3. This concludes the proof.

5 Proof of Exact Recovery with Sparse Noise (Theorems 2.9 and 2.10)

We again assume, without loss of generality, that $\sigma = 1$. Auxiliary Mathematica code to perform the computations needed for the proof is available online⁴.

5.1 Dual Certificate

The proof is based on the construction of a dual certificate that guarantees exact recovery of the signal μ and of the sparse noise component z .

⁴http://www.cims.nyu.edu/~cfgranda/scripts/deconvolution_proof.zip

Proposition 5.1 (Proof in Appendix G). *Let $T \subseteq \mathbb{R}$ be the nonzero support of μ and $\mathcal{N} \subseteq S$ be the nonzero support of w . If for any sign patterns $\rho \in \{-1, 1\}^{|T|}$ and $\rho' \in \{-1, 1\}^n$ there exists a dual combination Q of the form*

$$Q(t) := \sum_{i=1}^n q_i K(s_i - t) \quad (5.1)$$

satisfying

$$Q(t_j) = \rho_j, \quad \forall t_j \in T \quad (5.2)$$

$$|Q(t)| < 1, \quad \forall t \in T^c, \quad (5.3)$$

$$q_l = \lambda \rho'_l, \quad \forall s_l \in \mathcal{N}, \quad (5.4)$$

$$|q_l| < \lambda, \quad \forall s_l \in \mathcal{N}^c, \quad (5.5)$$

then (μ, w) is the unique solution to problem (2.15). Here $\mathcal{N}^c := S \setminus \mathcal{N}$.

The form of this dual certificate comes from the Lagrange dual to problem (2.15) given below:

$$\begin{aligned} & \underset{q}{\text{maximize}} && q^T y \\ & \text{subject to} && \sup_t \left| \sum_{i=1}^n q_i K(s_i - t) \right| \leq 1, \\ & && \|q\|_\infty \leq \lambda. \end{aligned} \quad (5.6)$$

Condition (5.4) implies that any valid dual combination is of the form $Q(t) = Q_{\text{aux}}(t) + R(t)$ where

$$Q_{\text{aux}}(t) := \sum_{s_i \in \mathcal{N}^c} q_i K(s_i - t), \quad (5.7)$$

$$R(t) := \lambda \sum_{s_i \in \mathcal{N}} \rho'_i K(s_i - t), \quad (5.8)$$

To obtain a valid certificate, we must construct Q_{aux} so that it interpolates $\rho_i - R(t_i)$ for every $t_i \in T$, while ensuring that (5.3) and (5.5) hold. This is reminiscent of the certificate constructed in [35] to provide exact recovery guarantees for spectral super-resolution in the presence of sparse corruptions. The crucial difference is that in [35] R is a combination of sinusoids with random signs. As a result, its magnitude is quite small and the certificate can be constructed by choosing the coefficients of Q_{aux} so that $Q_{\text{aux}}(t_i) = \rho_i - R(t_i)$ and $Q_{\text{aux}}(t_i) = -R^{(1)}(t_i)$ for all $t_i \in T$. In our case, such a construction satisfies condition (5.2), but violates either (5.3) or (5.5). More concretely, suppose we let $\lambda \geq 1$. Then (5.3) does not hold at samples that are distant from any spike. If we instead choose $\lambda < 1$, it is usually not possible to satisfy (5.2) and (5.5) simultaneously at samples that are close to a spike. In order to construct a valid certificate it is necessary to cancel the effect of R on T^c , as well as on T . This requires a new proof technique described in the following section.

5.2 Interpolation with Cancellations

Under the assumptions of Theorem 2.9, the grid of samples contains two disjoint subsets \mathcal{I} and \mathcal{C} which do not overlap with \mathcal{N} , such that \mathcal{I} contains the two samples that are closest to each element

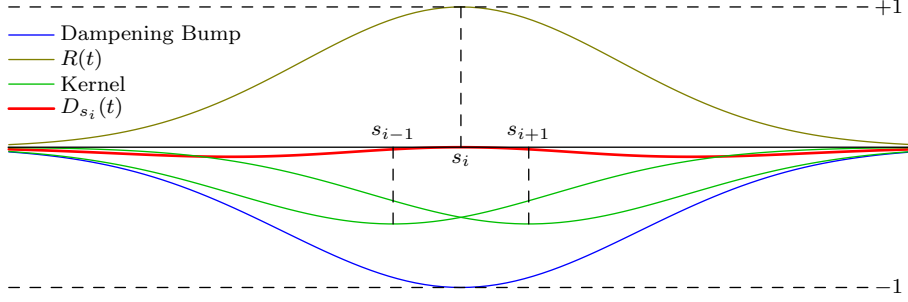


Figure 19: Example of dampened kernel D_{s_i} when the convolution kernel K is Gaussian. A shifted copy of K at s_i is dampened by subtracting a bump formed using shifted copies of K centered at two adjacent clean sample locations s_{i-1} and s_{i+1} .

in the support T and \mathcal{C} contains the two samples that are immediately adjacent to each corrupted sample. We decompose Q_{aux} into two terms $Q_{\text{aux}} := Q_{\mathcal{I}} + Q_{\mathcal{C}}$, where

$$Q_{\mathcal{I}}(t) := \sum_{s_i \in \mathcal{I}} q_i K(s_i - t), \quad (5.9)$$

$$Q_{\mathcal{C}}(t) := \sum_{s_i \in \mathcal{C}} q_i K(s_i - t). \quad (5.10)$$

The role of $Q_{\mathcal{C}}$ is to cancel out R so that condition (5.3) is not violated, whereas the role of $Q_{\mathcal{I}}$ is to ensure that (5.2) holds after the cancellation. We build $Q_{\mathcal{C}}$ as a superposition of shifted copies of the bump defined by equation (3.9), each of which neutralize one term of R :

$$Q_{\mathcal{C}}(t) := -\lambda \sum_{s_i \in \mathcal{N}} \rho'_i B_{s_i}(t, s_{i-1}, s_{i+1}). \quad (5.11)$$

As a result, $Q_{\mathcal{C}} + R$ can be decomposed into a sum of *dampened kernels* defined by

$$D_{s_i}(t, \lambda, \rho'_i) := \lambda \rho'_i (K(s_i - t) - B_{s_i}(t, s_{i-1}, s_{i+1})). \quad (5.12)$$

D_{s_i} is depicted in Figure 19. Let us define $R_{\mathcal{C}} := Q_{\mathcal{C}} + R$, the sum of all dampened kernels,

$$R_{\mathcal{C}}(t) = \sum_{s_i \in \mathcal{N}} D_{s_i}(t, \lambda, \rho'_i). \quad (5.13)$$

We choose the coefficients of $Q_{\mathcal{I}}$ so that Q interpolates the sign pattern ρ and has zero derivative on T , analogously to the system (3.7):

$$\begin{aligned} Q_{\mathcal{I}}(t_i) &= \rho_i - R_{\mathcal{C}}(t_i), \\ Q_{\mathcal{I}}^{(1)}(t_i) &= -R_{\mathcal{C}}^{(1)}(t_i), \quad \text{for all } t_i \in T. \end{aligned} \quad (5.14)$$

This construction is depicted in Figure 20. The same techniques used in Section 3.4 to prove invertibility apply here, giving the following lemma.

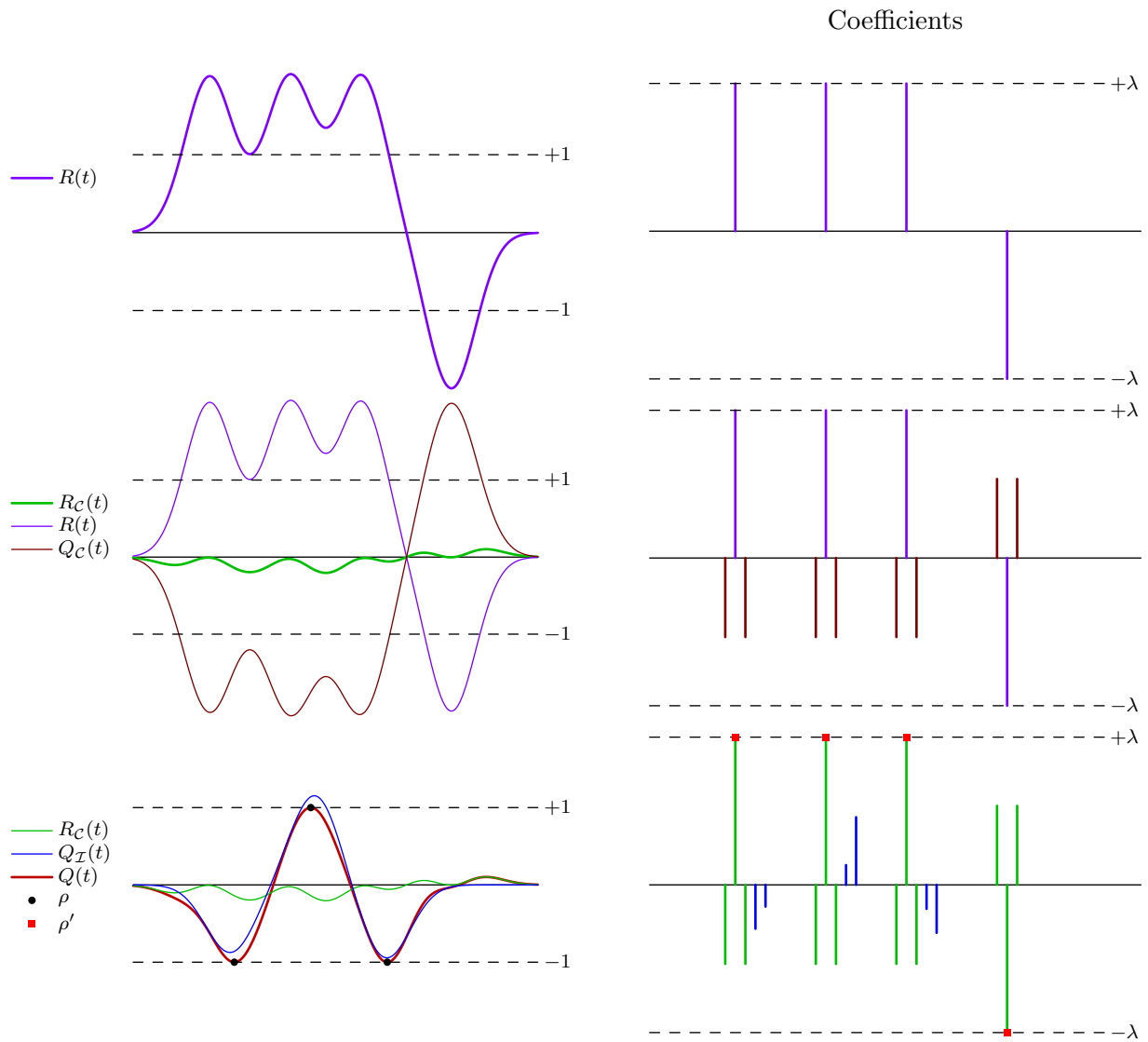


Figure 20: Construction of the certificate to prove exact recovery in the presence of sparse noise. The top row illustrates the term in the dual combination that is fixed by the sparse noise. The second row shows how this term can be cancelled by forming dampened kernels using the adjacent clean samples. Finally on the third row two additional samples surrounding the spike are used to ensure that the construction interpolates the sign pattern of the spikes and has zero derivative on their support. This produces a valid certificate.

Lemma 5.2 (Proof in Appendix I.2). *Under the assumptions of Theorem 2.9 for the Gaussian kernel, and Theorem 2.10 for the Ricker wavelet, the system of equations defined in (5.14) has a unique solution.*

Once $Q_{\mathcal{I}}$ is uniquely determined, the two lemmas below can be used to show conditions (5.3) and (5.5) hold. To show $|Q|$ is bounded, we write $Q(t) = Q_{\mathcal{I}}(t) + R_C(t)$ and combine bounds on R_C with the techniques used in the proof of noiseless exact recovery to obtain Lemma 5.3. Having proven $|Q(t)| < 1$ for $t \in T^c$, we then use this fact to prove a bound on q_i for $s_i \in \mathcal{I}$. We defer the details to the appendix.

Lemma 5.3 (Proof in Appendix I.3). *Under the assumptions of Theorem 2.9 for the Gaussian kernel, and Theorem 2.10 for the Ricker wavelet, the dual combination corresponding to the solution of (5.14) satisfies $|Q(t)| < 1$ for all $t \in T^c$.*

Lemma 5.4 (Proof in Appendix I.4). *Under the assumptions of Theorem 2.9 for the Gaussian kernel, and Theorem 2.10 for the Ricker wavelet, the dual combination corresponding to the solution of (5.14) satisfies $|q_l| < \lambda$ for all $l \in \mathcal{N}^c$.*

6 Numerical experiments

6.1 Conditioning of Convolution Measurements with a Fixed Support

Figure 3 shows an example of two signals with substantially different supports that produce almost the same measurements when convolved with a Gaussian or Ricker kernel. In this section we investigate this phenomenon. We fix a set of points $T_D := \{t_1, t_2, \dots, t_m\} \subseteq \mathbb{R}$ with minimum separation $\Delta_0/2$. This represents the support of the difference between two signals with minimum separation Δ_0 , the first corresponding to the odd locations t_1, t_3, t_5, \dots and the second to the even locations t_2, t_4, t_6, \dots as in the example in Figure 3. We denote the amplitudes of the difference by $\tilde{a} \in \mathbb{R}^m$, which is normalized so that $\|\tilde{a}\|_2 = 1$. The difference between the convolutions of the two signals at a fixed sample s_i is given by $\sum_{t_j \in T_D} \tilde{a}_j K(s_i - t_j)$.

Our aim is to determine for what values of Δ_0 these samples have negligible energy in the worst case and on average for a fixed set of sample locations s_1, s_2, \dots, s_n . This requires choosing a worst-case and average-case value for the amplitudes, which can be achieved by computing the singular-value decomposition of a matrix with entries given by $K(s_i - t_j)$ for $t_j \in T_D$ and $1 \leq i \leq n$. The smallest singular value corresponds to the smallest possible ℓ_2 norm of the samples, whereas the middle singular value can be interpreted as an average value of their ℓ_2 norm. In Figure 21 we plot the smallest and the middle singular value for a range of values of the number of spikes m and the minimum separation Δ_0 using a uniform grid of $n := 10m$ samples. For both convolution kernels of interest there is a phase transition at a value of the minimum separation that does not seem to depend on the number of spikes, as long as they are not very few. This phase transition occurs around $\Delta_0 = \sigma$ (smallest singular value) and $\Delta_0 = 0.5\sigma$ (middle singular value) for both kernels⁵. These results are not affected by the choice of step size for the sampling grid, as shown in Figure 22, where we fix the number of spikes to 50 and repeat the experiment for different step sizes.

⁵The experiment is carried out for $\sigma = 1$, but the results apply to any σ by a simple change of variable.

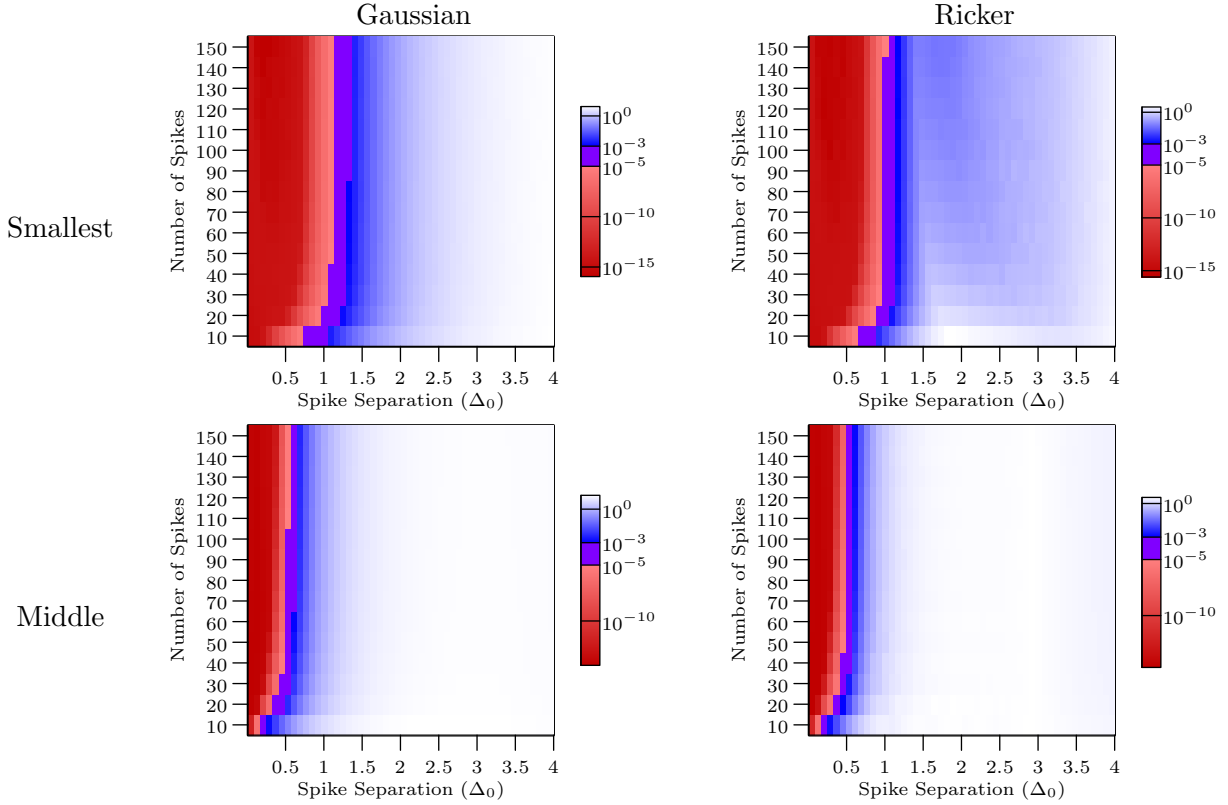


Figure 21: The smallest and middle singular values of the measurement operator as a function of spike separation and number of spikes. Each plotted value is an average over 5 runs. The spike locations are perturbed randomly so that their separation varies up to 2.5% of the given Δ_0 value. The spike separation is expressed in units of σ .

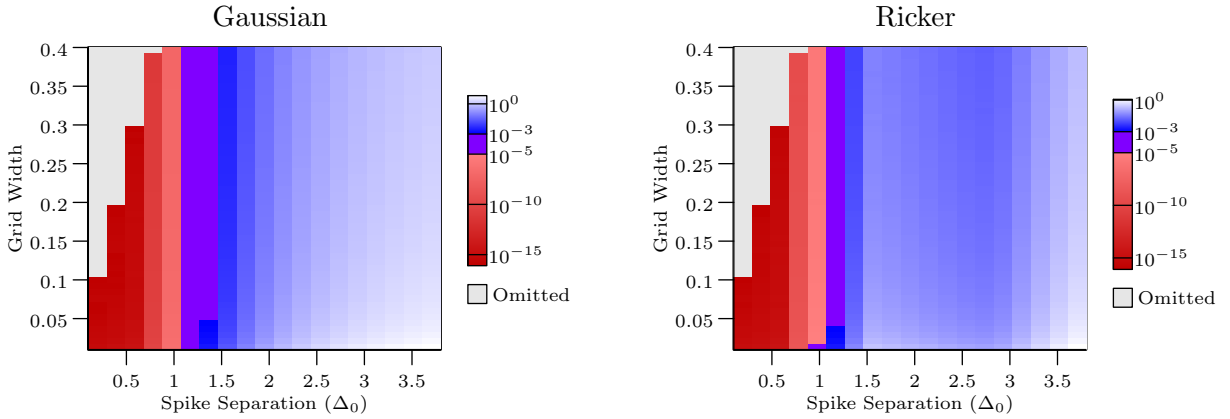


Figure 22: The smallest singular value of the measurement operator as a function of spike separation and sampling grid width. The number of spikes is fixed at 50. Grid widths and spike separations are in units of σ . Points with grid width larger than $\Delta_0/2$ are omitted.

6.2 Exact Recovery

In this section we evaluate our optimization-based deconvolution method for different values of the minimum separation and the sample separation. In our experiments, we restrict the signal to lie on a uniform grid with $5 \cdot 10^4$ points and solve problem (2.4) using CVX [38]. We choose the sample locations so that there are just two samples per spike which are as far as possible from the spike location, with some random jitter ($\pm 1\%$ of the sample proximity). In our experience, this yields a *worst-case* nonuniform sampling pattern for a fixed sample proximity. The spike locations are also worst case in the sense that the spikes are separated as much as possible, with some random jitter ($\pm 1\%$ of the minimum separation). We consider that the method achieves exact recovery if the relative error of the recovered amplitudes is below 10^{-4} . We observe that when the minimum separation is small, the chances of achieving exact recovery may be higher for larger sample proximities. In those cases, there are four samples close to any given spike (its own two and two more from the neighboring spikes), which may be better than having two samples that are closer. In order to correct for this effect in Figure 7 we *monotonize* the results to show when we observe exact recovery for all larger minimum separations and smaller sample proximities.

In addition, we evaluate the method for a uniform sampling pattern, varying the grid step size and the minimum separation between spikes. Figure 24 shows the results. The method recovers the signal perfectly up until a grid step size that is approximately double the largest sample proximity at which exact recovery occurs in Figure 23. The reason may be that there are spikes that are right in between two samples, so we can interpret the grid as imposing an effective sample separation that is half the grid step size (note however that this is not completely accurate because every spike has a neighboring sample that is closer and another that is farther than this separation).

6.3 Robustness to Sparse Noise

In this section, we investigate the performance of the optimization-based approach for deconvolution in the presence of outliers described in Section 2.4. As in Section 6.2, we discretize Problem (2.15) by restricting the spikes in the measure to lie on a uniform grid with $5 \cdot 10^4$ points and solve the resulting convex program using CVX [38]. We consider that the method achieves exact recovery if the relative error is 10^{-3} (we use a larger tolerance because we found the solutions to be less precise than in Section 6.2). Our experiments evaluate the effect of the following parameters:

- *Number of spikes and minimum separation:* Adjacent spike locations have separation Δ with a random jitter of $\pm 1\%$. The amplitudes are drawn iid from a standard normal distribution.
- *Number of corruptions:* We divide the unit interval into segments of length Δ and corrupt c samples per segment selected at random by drawing their amplitudes iid from a standard normal distribution. This allows c to be interpreted as the number of corruptions per spike, and prevents the corruptions from becoming too clustered.
- The *regularization parameter* λ .

For all experiment the samples are uniformly distributed in the unit interval on a grid of width 0.2σ . Figure 25 shows that the performance of the method is quite robust to λ , as suggested by Lemma 2.11. Figure 26 shows that for a fixed number of corruptions (two per spike in this case)

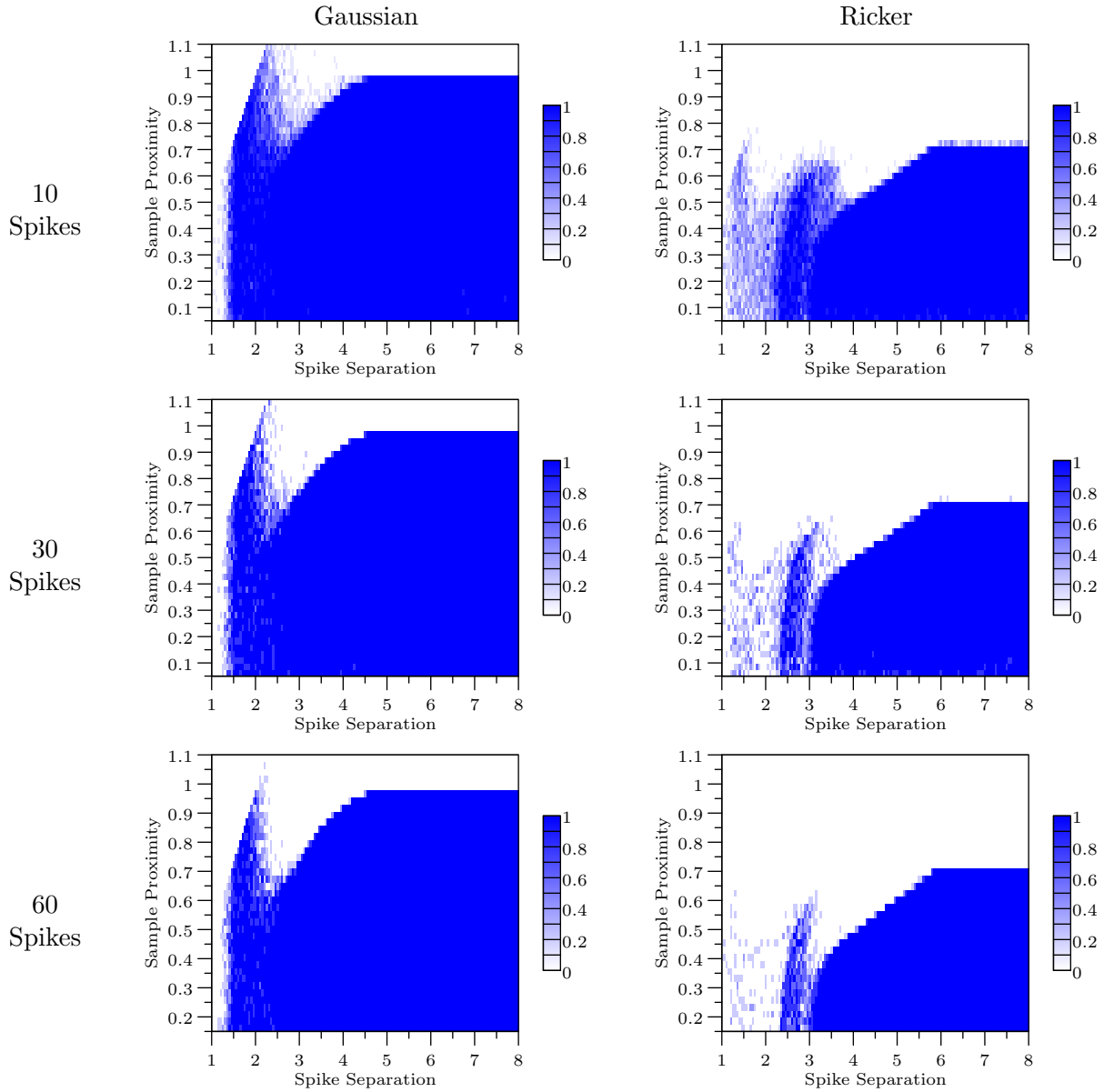


Figure 23: Fraction of 5 runs yielding exact recovery for varying values of the spike minimum separation, sample proximity, and numbers of spikes in the signal. Spike separations and sample proximities are given in units of σ (the experiments are carried out for $\sigma := 0.003$).

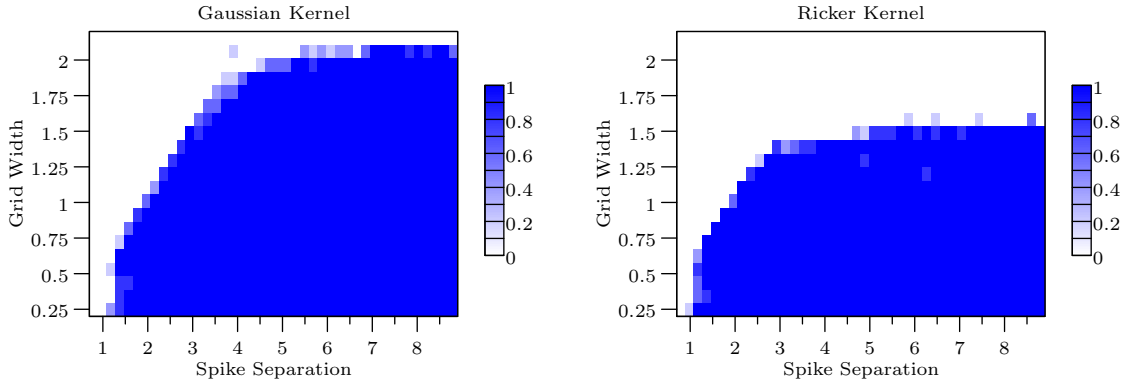


Figure 24: Fraction of 5 runs yielding exact recovery for varying spike separations and grid widths when the sampling pattern is uniform. Spike separations and sampling grid widths are given in units of σ .

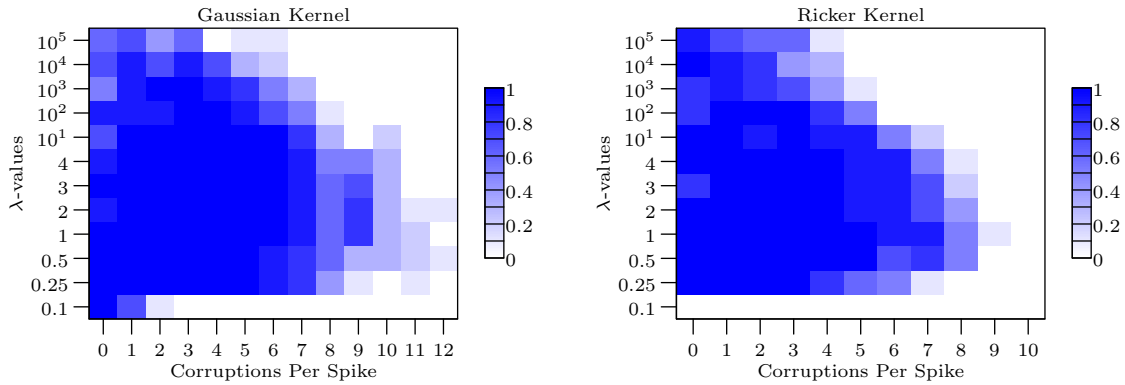


Figure 25: Fraction of 10 instances yielding exact recovery for varying values of λ and number of corruptions per spike. We fix $\sigma = 0.02$, 10 spikes and a spike separation of 4.5σ .

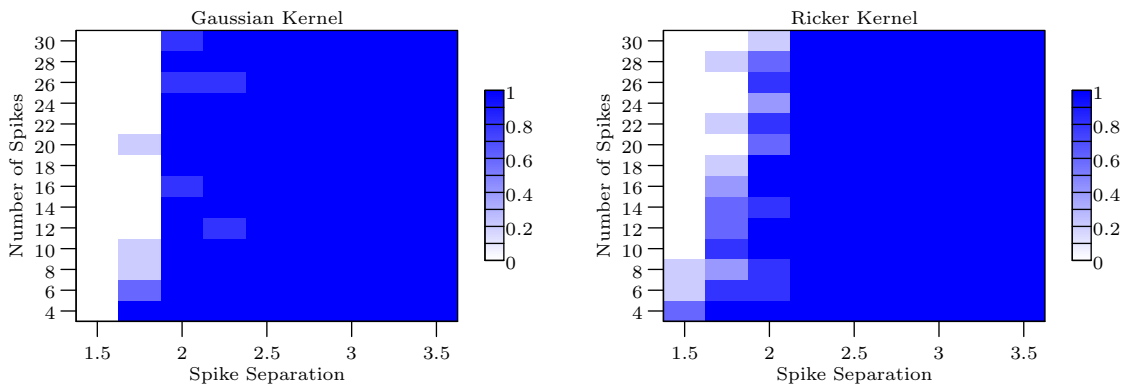


Figure 26: Fraction of 5 instances yielding exact recovery with 2 corruptions per spike for varying numbers of spikes, and values of the spike separation. We fix $\sigma = 0.004$, $\lambda = 2$, and a sampling grid width of 0.2σ . Spike separations are given in units of σ .

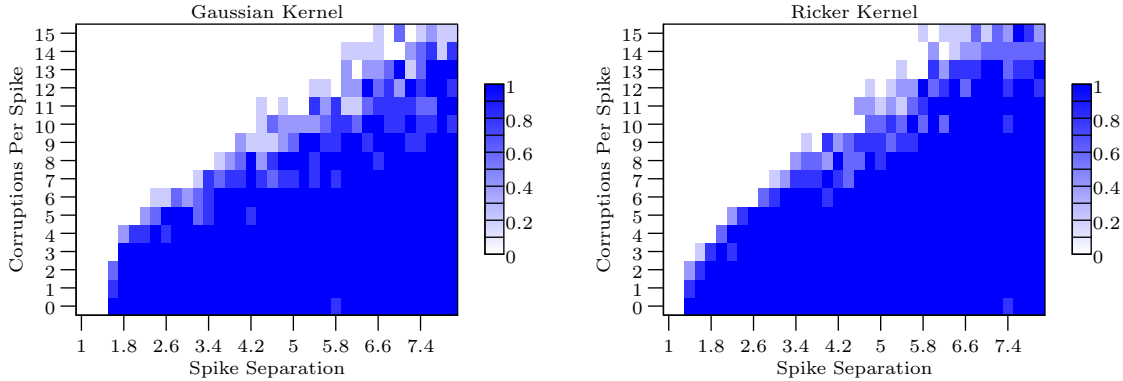


Figure 27: Fraction of 5 runs yielding exact recovery with 10 spikes for varying spike separation and corruptions per spike. We fix $\sigma = 0.01$ and $\lambda = 2$. Spike separations are given in units of σ .

the method succeeds as long as the minimum separation is large enough, and that this minimum separation does not vary much for different numbers of spikes (especially in the case of the Gaussian kernel). Figure 27 shows that a larger minimum separation between spikes allows the method to achieve exact recovery in the presence of more corruptions.

7 Conclusions and Directions for Future Research

In this work we establish that minimizing a continuous counterpart of the ℓ_1 norm achieves exact recovery of signals satisfying a minimum-separation condition from samples of their convolution with a Gaussian or Ricker kernel, under the assumption that there are at least two samples that are close to each spike. Our theoretical analysis is based on a dual-certificate construction that is not specific to these convolution kernels and can be adapted to study other deconvolution problems. In addition, we show that the optimization-based deconvolution approach is robust to dense and sparse noise. Some interesting research directions are:

- Investigating the effect of additional samples (beyond two per spike) on the minimum separation at which exact recovery is achieved, as well as on robustness to noise.
- Quantifying the discretization error incurred by solving ℓ_1 -norm minimization on a fine grid instead of solving the continuous TV-norm minimization problem, in the spirit of [32].
- Developing algorithms for TV-norm minimization on a continuous domain, see [8, 10, 57] for some recent work in this direction.
- Extending our proof techniques to analyze deconvolution in multiple dimensions.
- Characterizing robustness to sparse noise under weaker conditions.
- Extending the method to handle unknown noise levels as in [9], which studies super-resolution of point sources.
- Studying blind deconvolution, i.e. joint estimation of the convolution kernel and the signal, for deterministic kernels. Recent works in this direction focus on randomized measurements [2, 48] and alternating optimization [58].

Acknowledgements

C.F. is generously supported by NSF award DMS-1616340. C.F. thanks Waheed Bajwa for useful comments and Stan Osher for introducing him to the problem of heat-source localization via deconvolution.

References

- [1] U. R. Abeyratne, A. P. Petropulu, and J. M. Reid. Higher order spectra based deconvolution of ultrasound images. *IEEE Transactions on Ultrasonics, Ferroelectrics, and Frequency Control*, 42(6):1064–1075, 1995.
- [2] A. Ahmed, B. Recht, and J. Romberg. Blind deconvolution using convex programming. *IEEE Transactions on Information Theory*, 60(3):1711–1732, 2014.
- [3] G. Aniano, B. Draine, K. Gordon, and K. Sandstrom. Common-resolution convolution kernels for space- and ground-based telescopes. *Publications of the Astronomical Society of the Pacific*, 123(908):1218, 2011.
- [4] J.-M. Azais, Y. De Castro, and F. Gamboa. Spike detection from inaccurate samplings. *Applied and Computational Harmonic Analysis*, 38(2):177–195, 2015.
- [5] T. Bendory, A. Bar-Zion, D. Adam, S. Dekel, and A. Feuer. Stable support recovery of stream of pulses with application to ultrasound imaging. *IEEE Transactions on Signal Processing*, 64(14):3750–3759.
- [6] T. Bendory, S. Dekel, and A. Feuer. Robust recovery of stream of pulses using convex optimization. *Journal of Mathematical Analysis and Applications*, 442(2):511–536, 2016.
- [7] E. Betzig, G. H. Patterson, R. Sougrat, O. W. Lindwasser, S. Olenych, J. S. Bonifacino, M. W. Davidson, J. Lippincott-Schwartz, and H. F. Hess. Imaging intracellular fluorescent proteins at nanometer resolution. *Science*, 313(5793):1642–1645, 2006.
- [8] N. Boyd, G. Schiebinger, and B. Recht. The alternating descent conditional gradient method for sparse inverse problems. *SIAM Journal on Optimization*, 27(2):616–639, 2017.
- [9] C. Boyer, Y. De Castro, and J. Salmon. Adapting to unknown noise level in sparse deconvolution. Preprint.
- [10] K. Bredies and H. K. Pikkarainen. Inverse problems in spaces of measures. *ESAIM: Control, Optimization and Calculus of Variations*, 19(1):190–218, 2013.
- [11] M. Broxton, L. Grosenick, S. Yang, N. Cohen, A. Andalman, K. Deisseroth, and M. Levoy. Wave optics theory and 3-d deconvolution for the light field microscope. *Optics express*, 21(21):25418–25439, 2013.
- [12] E. Candes and B. Recht. Exact matrix completion via convex optimization. *Communications of the ACM*, 55(6):111–119, 2012.
- [13] E. J. Candes, Y. C. Eldar, T. Strohmer, and V. Voroninski. Phase retrieval via matrix completion. *SIAM review*, 57(2):225–251, 2015.
- [14] E. J. Candès and C. Fernandez-Granda. Towards a mathematical theory of super-resolution. *Communications on Pure and Applied Mathematics*, 67(6):906–956.
- [15] E. J. Candès and C. Fernandez-Granda. Super-resolution from noisy data. *Journal of Fourier Analysis and Applications*, 19(6):1229–1254, 2013.
- [16] E. J. Candès, X. Li, Y. Ma, and J. Wright. Robust principal component analysis? *Journal of the ACM*, 58(3):11, 2011.

- [17] E. J. Candes and Y. Plan. A probabilistic and RIPless theory of compressed sensing. *Information Theory, IEEE Transactions on*, 57(11):7235–7254, 2011.
- [18] E. J. Candès, J. Romberg, and T. Tao. Robust uncertainty principles: Exact signal reconstruction from highly incomplete frequency information. *IEEE Transactions on information theory*, 52(2):489–509, 2006.
- [19] E. J. Candès and T. Tao. Decoding by linear programming. *Information Theory, IEEE Transactions on*, 51(12):4203–4215, 2005.
- [20] A. F. Carley and R. W. Joyner. The application of deconvolution methods in electron spectroscopy—a review. *Journal of Electron Spectroscopy and Related Phenomena*, 16(1):1–23, 1979.
- [21] N. Chapman and I. Barrodale. Deconvolution of marine seismic data using the l1 norm. *Geophysical Journal International*, 72(1):93–100, 1983.
- [22] J. F. Claerbout and F. Muir. Robust modeling with erratic data. *Geophysics*, 38(5):826–844, 1973.
- [23] Y. De Castro and F. Gamboa. Exact reconstruction using Beurling minimal extrapolation. *Journal of Mathematical Analysis and Applications*, 395(1):336–354.
- [24] Y. De Castro and F. Gamboa. Exact reconstruction using beurling minimal extrapolation. *Journal of Mathematical Analysis and applications*, 395(1):336–354, 2012.
- [25] B. G. R. de Prony. Essai expérimental et analytique: sur les lois de la dilatabilité de fluides élastique et sur celles de la force expansive de la vapeur de l’alkool, à différentes températures. *Journal de l’école Polytechnique*, 1(22):24–76, 1795.
- [26] H. Debye and P. Van Riel. Lp-norm deconvolution. *Geophysical Prospecting*, 38(4):381–403, 1990.
- [27] D. L. Donoho. Superresolution via sparsity constraints. *SIAM Journal on Mathematical Analysis*, 23(5):1309–1331, 1992.
- [28] D. L. Donoho. Compressed sensing. *IEEE Transactions on information theory*, 52(4):1289–1306, 2006.
- [29] B. Drachman. Two methods to deconvolve: L 1-method using simplex algorithm and l 2-method using least squares and a parameter. *IEEE transactions on antennas and propagation*, 32(3):219–225, 1984.
- [30] P. L. Dragotti, M. Vetterli, and T. Blu. Sampling moments and reconstructing signals of finite rate of innovation: Shannon meets strang–fix. *IEEE Transactions on Signal Processing*, 55(5):1741–1757, 2007.
- [31] V. Duval and G. Peyré. Exact support recovery for sparse spikes deconvolution. *Foundations of Computational Mathematics*, pages 1–41, 2015.
- [32] V. Duval and G. Peyré. Sparse regularization on thin grids i: the lasso. *Inverse Problems*, 33(5):055008, 2017.
- [33] C. Fernandez-Granda. Support detection in super-resolution. In *Proceedings of the 10th International Conference on Sampling Theory and Applications*, pages 145–148, 2013.
- [34] C. Fernandez-Granda. Super-resolution of point sources via convex programming. *Information and Inference*, 5(3):251–303, 2016.
- [35] C. Fernandez-Granda, G. Tang, X. Wang, and L. Zheng. Demixing sines and spikes: Robust spectral super-resolution in the presence of outliers. *Information and Inference*, 2017.
- [36] G. Folland. *Real Analysis: Modern Techniques and Their Applications*. Pure and Applied Mathematics: A Wiley Series of Texts, Monographs and Tracts. Wiley, 2013.
- [37] A. Gholami and M. D. Sacchi. A fast and automatic sparse deconvolution in the presence of outliers. *IEEE Transactions on Geoscience and Remote Sensing*, 50(10):4105–4116, 2012.

- [38] M. Grant and S. Boyd. CVX: Matlab software for disciplined convex programming, version 1.21. <http://cvxr.com/cvx>, Apr. 2011.
- [39] J. Haupt, W. U. Bajwa, G. Raz, and R. Nowak. Toeplitz Compressed Sensing Matrices With Applications to Sparse Channel Estimation. *IEEE Transactions Information Theory*, 56(11):5862–5875.
- [40] S. T. Hess, T. P. Girirajan, and M. D. Mason. Ultra-high resolution imaging by fluorescence photoactivation localization microscopy. *Biophysical journal*, 91(11):4258, 2006.
- [41] T. Hickey, Q. Ju, and M. H. Van Emden. Interval arithmetic: From principles to implementation. *Journal of the ACM (JACM)*, 48(5):1038–1068, 2001.
- [42] R. A. Hummel, B. Kimia, and S. W. Zucker. Deblurring gaussian blur. *Computer Vision, Graphics, and Image Processing*, 38(1):66–80, 1987.
- [43] J. A. Jensen. Deconvolution of ultrasound images. *Ultrasonic imaging*, 14(1):1–15, 1992.
- [44] J. K. Kauppinen, D. J. Moffatt, H. H. Mantsch, and D. G. Cameron. Fourier self-deconvolution: a method for resolving intrinsically overlapped bands. *Applied Spectroscopy*, 35(3):271–276, 1981.
- [45] S. Levy and P. K. Fullagar. Reconstruction of a sparse spike train from a portion of its spectrum and application to high-resolution deconvolution. *Geophysics*, 46(9):1235–1243, 1981.
- [46] Q. Li and G. Tang. Approximate support recovery of atomic line spectral estimation: A tale of resolution and precision. *arXiv preprint arXiv:1612.01459*, 2016.
- [47] Y. Li, S. Osher, and R. Tsai. Heat source identification based on constrained minimization. *Inverse Problems and Imaging*, 8(1):199–221, 2014.
- [48] S. Ling and T. Strohmer. Blind deconvolution meets blind demixing: Algorithms and performance bounds. *IEEE Transactions on Information Theory*, 2017.
- [49] S. Mallat. *A wavelet tour of signal processing*. Academic press, 1999.
- [50] J. M. Mendel. *Optimal seismic deconvolution: an estimation-based approach*. Elsevier, 2013.
- [51] A. Moitra. Super-resolution, extremal functions and the condition number of Vandermonde matrices. In *Proceedings of the 47th Annual ACM Symposium on Theory of Computing (STOC)*, 2015.
- [52] J. Murray-Bruce and P. L. Dragotti. Estimating localized sources of diffusion fields using spatiotemporal sensor measurements. *IEEE Transactions on Signal Processing*, 63(12):3018–3031.
- [53] M. S. O’Brien, A. N. Sinclair, and S. M. Kramer. Recovery of a sparse spike time series by l_1 -norm deconvolution. *IEEE Transactions on Signal Processing*, 42(12):3353–3365, 1994.
- [54] H. Pan, T. Blu, and M. Vetterli. Towards generalized fri sampling with an application to source resolution in radioastronomy. *IEEE Transactions on Signal Processing*, 65(4):821–835.
- [55] D. Pereg and I. Cohen. Seismic signal recovery based on Earth Q model. *Signal Processing*, 137:373–386, 2017.
- [56] K. G. Puschmann and F. Kneer. On super-resolution in astronomical imaging. *Astronomy and Astrophysics*, 436:373–378, 2005.
- [57] N. Rao, P. Shah, and S. Wright. Forward-backward greedy algorithms for atomic norm regularization. *IEEE Transactions on Signal Processing*, 63(21):5798–5811, 2015.
- [58] A. Repetti, M. Q. Pham, L. Duval, E. Chouzenoux, and J.-C. Pesquet. Euclid in a taxicab: Sparse blind deconvolution with smoothed $l_{1/2}$ regularization. *IEEE Signal Processing Letters*, 22(5):539–543, 2015.
- [59] N. Ricker. The form and laws of propagation of seismic wavelets. *Geophysics*, 18(1):10–40, 1953.

- [60] F. Rieke. *Spikes: exploring the neural code*. The MIT Press, 1999.
- [61] J. Romberg. Compressive sensing by random convolution. *SIAM Journal on Imaging Sciences*, 2(4):1098–1128, 2009.
- [62] L. I. Rudin, S. Osher, and E. Fatemi. Nonlinear total variation based noise removal algorithms. *Physica D: Nonlinear Phenomena*, 60(1):259–268, 1992.
- [63] F. Santosa and W. W. Symes. Linear inversion of band-limited reflection seismograms. *SIAM Journal on Scientific and Statistical Computing*, 7(4):1307–1330, 1986.
- [64] G. Schiebinger, E. Robeva, and B. Recht. Superresolution without separation. *Information and Inference*, 2017.
- [65] A. Shapiro. Semi-infinite programming, duality, discretization and optimality conditions. *Optimization*, 58(2):133–161, 2009.
- [66] R. E. Sheriff and L. P. Geldart. *Exploration seismology*. Cambridge university press, 1995.
- [67] D. Slepian. Prolate spheroidal wave functions, Fourier analysis, and uncertainty. V - The discrete case. *Bell System Technical Journal*, 57:1371–1430, 1978.
- [68] P. Stoica and R. L. Moses. *Spectral analysis of signals*. Prentice Hall, Upper Saddle River, New Jersey, 1 edition, 2005.
- [69] G. Tang, B. Bhaskar, and B. Recht. Near minimax line spectral estimation. *Information Theory, IEEE Transactions on*, 61(1):499–512, Jan 2015.
- [70] H. L. Taylor, S. C. Banks, and J. F. McCoy. Deconvolution with the l1 norm. *Geophysics*, 44(1):39–52, 1979.
- [71] J. A. Urigüen, T. Blu, and P. L. Dragotti. Fri sampling with arbitrary kernels. *IEEE Transactions on Signal Processing*, 61(21):5310–5323, 2013.
- [72] R. Vershynin. Introduction to the non-asymptotic analysis of random matrices. *arXiv preprint arXiv:1011.3027*, 2010.
- [73] M. Vetterli, P. Marziliano, and T. Blu. Sampling signals with finite rate of innovation. *IEEE transactions on Signal Processing*, 50(6):1417–1428, 2002.
- [74] J. T. Vogelstein, A. M. Packer, T. A. Machado, T. Sippy, B. Babadi, R. Yuste, and L. Paninski. Fast nonnegative deconvolution for spike train inference from population calcium imaging. *Journal of neurophysiology*, 104(6):3691–3704, 2010.
- [75] B. Zhang, J. Zerubia, and J.-C. Olivo-Marin. Gaussian approximations of fluorescence microscope point-spread function models. *Applied Optics*, 46(10):1819–1829, 2007.

Appendix

Throughout the appendix, we assume there is some compact interval $I \subset \mathbb{R}$ containing the support of the true measure μ (given in (1.2)). In problems (1.6), (2.6), and (2.15) the variable $\tilde{\mu}$ takes values in the set of finite signed Borel measures supported on I .

A Proof of Proposition 3.1: Certifying Exact Recovery

The proof of Proposition 3.1 follows standard arguments and is included for completeness (see Section A in [14] and also [24]).

Proposition 3.1. *Let $T \subseteq \mathbb{R}$ be the nonzero support of a signal μ of the form (1.2). If for any sign pattern $\rho \in \{-1, 1\}^{|T|}$ there exists a function of the form*

$$Q(t) := \sum_{i=1}^n q_i K(s_i - t) \quad (3.2)$$

satisfying

$$Q(t_j) = \rho_j, \quad \forall t_j \in T, \quad (3.3)$$

$$|Q(t)| < 1, \quad \forall t \in T^c, \quad (3.4)$$

then the unique solution to Problem (1.6) is μ .

Proof. Let ν be feasible for Problem (1.6) and define $h = \nu - \mu$. By taking the Lebesgue decomposition of h with respect to $|\mu|$ we can write

$$h = h_T + h_{T^c}, \quad (A.1)$$

where h_T is absolutely continuous with respect to $|\mu|$, and h_{T^c} is mutually orthogonal to $|\mu|$. In other words, the support of h_T is contained in T , and $h_{T^c}(T) = 0$. This allows us to write

$$h_T = \sum_{t_j \in T} b_j \delta_{t_j}, \quad (A.2)$$

for some $b \in \mathbb{R}^{|T|}$. Set $\rho := \text{sign}(b)$, where we arbitrarily choose $\rho_j = \pm 1$ if $b_j = 0$. By assumption there exists a corresponding Q interpolating ρ on T . Since μ and ν are feasible for Problem (1.6) we have $(K * h)(s_i) = 0$ for $i = 1, \dots, n$. This implies

$$\begin{aligned} 0 &= \sum_{i=1}^n q_i (K * h)(s_i) = \sum_{i=1}^n q_i \int K(s_i - t) dh(t) \\ &= \int Q(t) dh(t) = \|h_T\|_{\text{TV}} + \int Q(t) dh_{T^c}(t). \end{aligned} \quad (A.3)$$

Applying the triangle inequality, we obtain

$$\|\nu\|_{\text{TV}} = \|\mu + h_T\|_{\text{TV}} + \|h_{T^c}\|_{\text{TV}} \quad (\text{Mutual Orthogonality}) \quad (A.4)$$

$$\geq \|\mu\|_{\text{TV}} + \|h_{T^c}\|_{\text{TV}} - \|h_T\|_{\text{TV}} \quad (\text{Triangle Inequality}) \quad (A.5)$$

$$= \|\mu\|_{\text{TV}} + \|h_{T^c}\|_{\text{TV}} + \int Q(t) dh_{T^c}(t) \quad (\text{Equation A.3}) \quad (A.6)$$

$$\geq \|\mu\|_{\text{TV}} \quad (|Q(t)| \leq 1), \quad (A.7)$$

where the last inequality is strict if $\|h_{T^c}\|_{\text{TV}} > 0$ since $|Q(t)| < 1$ for $t \in T^c$. This establishes that μ is optimal for Problem (1.6), and that any other optimal solution must be supported on T . Equation (A.3) implies that any feasible solution supported on T must be equal to μ (since $\|h_T\|_{\text{TV}} = 0$), completing the proof of uniqueness. \square

B Bumps and Waves

B.1 Auxiliary Results

In this section we compile several results that will be useful in the following sections.

Lemma B.1. *For $|s| \leq 1$ we have $|(K^{\mathcal{G}})^{(i)}(s)| \leq 3$ for $i = 0, \dots, 4$. If we also have $t \geq 10$ then*

$$|(K^{\mathcal{G}})^{(i)}(s-t)| \leq 2t^4 \exp\left(-\frac{t^2}{2} + t - \frac{s^2}{2}\right), \quad (\text{B.1})$$

$$|(K^{\mathcal{R}})^{(i)}(s-t)| \leq 2t^4 \exp\left(-\frac{t^2}{2} + t - \frac{s^2}{2}\right), \quad (\text{B.2})$$

for $i = 0, \dots, 2$.

Proof. The first 4 derivatives of the Gaussian kernel are given by

$$(K^{\mathcal{G}})^{(1)}(t) = -tK^{\mathcal{G}}(t), \quad (K^{\mathcal{G}})^{(2)}(t) = (t^2 - 1)K^{\mathcal{G}}(t), \quad (\text{B.3})$$

$$(K^{\mathcal{R}})^{(1)}(t) = t(t^2 - 3)K^{\mathcal{G}}(t), \quad (K^{\mathcal{R}})^{(2)}(t) = -(t^4 - 6t^2 + 3)K^{\mathcal{G}}(t). \quad (\text{B.4})$$

If $|s| \leq 1$ then $K^{\mathcal{G}}(s) \leq 1$, so we just need to bound the polynomial factors. We have

$$|s| \leq 1, \quad (\text{B.5})$$

$$|s^2 - 1| \leq 1, \quad (\text{B.6})$$

$$|s(s^2 - 3)| \leq |s^2 - 3| \leq 3. \quad (\text{B.7})$$

For the remaining factor, note that $p(s) = s^4 - 6s^2 + 3$ has negative second derivative,

$$p^{(2)}(s) = 12s^2 - 12 \leq 0, \quad (\text{B.8})$$

so p is even and concave when $|s| \leq 1$. This implies $|p(s)| \leq p(0) = 3$.

Next assume $t \geq 10$. Since

$$K^{\mathcal{G}}(s-t) = \exp\left(-\frac{(s-t)^2}{2}\right) = \exp\left(-\frac{t^2}{2} + st - \frac{s^2}{2}\right) \leq \exp\left(-\frac{t^2}{2} + t - \frac{s^2}{2}\right), \quad (\text{B.9})$$

we again only need to bound the polynomial factors. The following bounds complete the proof:

$$|s-t| \leq 2t \leq 2t^4 \quad (\text{B.10})$$

$$|(s-t)^2 - 1| = t^2 - 2st + s^2 - 1 \leq t^2 + 2t \leq 2t^2 \leq 2t^4 \quad (\text{B.11})$$

$$|(s-t)((s-t)^2 - 3)| = t^3 - 3st^2 + 3s^2t - 3t - s^3 + 3s \leq t^3 + 3t^2 + 6t + 4 \leq 4t^3 \leq 2t^4 \quad (\text{B.12})$$

$$|(s-t)^4 - 6(s-t)^2 + 3| \leq s^4 - 4s^3t + 6s^2t^2 - 6s^2 - 4st^3 + 12st + t^4 - 6t^2 + 3 \quad (\text{B.13})$$

$$\leq t^4 + 4t^3 + 12t^2 + 16t + 10 \leq t^4 + 4t^3 + 2t^3 + t^3 + t^3 \leq 2t^4. \quad (\text{B.14})$$

□

The next lemma gives explicit formulas for the denominators of the bump and wave coefficients in Lemma 3.2. The result is obtained by a simple expansion of the expressions, so we omit the proof.

Lemma B.2. *Define*

$$D^{\mathcal{G}}(s_1, s_2) := K^{\mathcal{G}}(s_2)(K^{\mathcal{G}})^{(1)}(s_1) - (K^{\mathcal{G}})^{(1)}(s_2)K^{\mathcal{G}}(s_1), \quad (\text{B.15})$$

$$D^{\mathcal{R}}(s_1, s_2) := K^{\mathcal{R}}(s_2)(K^{\mathcal{R}})^{(1)}(s_1) - (K^{\mathcal{R}})^{(1)}(s_2)K^{\mathcal{R}}(s_1). \quad (\text{B.16})$$

Then

$$D^{\mathcal{G}}(s_1, s_2) = (s_2 - s_1) \exp\left(-\frac{s_1^2 + s_2^2}{2}\right), \quad (\text{B.17})$$

$$D^{\mathcal{R}}(s_1, s_2) = (s_2 - s_1)(3 - (s_1 - s_2)^2 + s_1^2 s_2^2) \exp\left(-\frac{s_1^2 + s_2^2}{2}\right). \quad (\text{B.18})$$

The following lemma allows us to control $D^{\mathcal{R}}$.

Lemma B.3. *Let $f : \mathbb{R}^2 \rightarrow \mathbb{R}$ be defined by $f(x, y) = 3 - (x - y)^2 + x^2 y^2$. If $\max(|x|, |y|) \leq a < 1$ then $f(x, y) \geq 3 - 4a^2 + a^4 > 0$.*

Proof. Given in Appendix B.7. □

B.2 Proof of Lemma 3.2: Existence of the Bumps and Waves

Lemma 3.2. *For a fixed kernel K , the bump B_{t_i} and wave W_{t_i} exist with coefficients given by*

$$\begin{bmatrix} b_{i,1} & w_{i,1} \\ b_{i,2} & w_{i,2} \end{bmatrix} = \frac{1}{K(\tilde{s}_{i,2} - t_i)K^{(1)}(\tilde{s}_{i,1} - t_i) - K^{(1)}(\tilde{s}_{i,2} - t_i)K(\tilde{s}_{i,1} - t_i)} \begin{bmatrix} -K^{(1)}(\tilde{s}_{i,2} - t_i) & -K(\tilde{s}_{i,2} - t_i) \\ K^{(1)}(\tilde{s}_{i,1} - t_i) & K(\tilde{s}_{i,1} - t_i) \end{bmatrix}$$

when the expression in the denominator is nonzero. The Gaussian kernel has nonzero denominator for $\tilde{s}_{i,1} \neq \tilde{s}_{i,2}$. The Ricker wavelet has nonzero denominator when $\tilde{s}_{i,1} \neq \tilde{s}_{i,2}$ and $|\tilde{s}_{i,1}|, |\tilde{s}_{i,2}| < 1$.

Proof. In matrix form, the bump and wave coefficients satisfy

$$\begin{bmatrix} K(\tilde{s}_{i,1} - t_i) & K(\tilde{s}_{i,2} - t_i) \\ -K^{(1)}(\tilde{s}_{i,1} - t_i) & -K^{(1)}(\tilde{s}_{i,2} - t_i) \end{bmatrix} \begin{bmatrix} b_{i,1} & w_{i,1} \\ b_{i,2} & w_{i,2} \end{bmatrix} = \begin{bmatrix} 1 & 0 \\ 0 & 1 \end{bmatrix}. \quad (\text{B.19})$$

We obtain the formulas in the statement by solving the system. Without loss of generality, we set $t_i = 0$. The conditions for the denominators to be non-zero then follow directly from Lemmas B.2 and B.3. □

B.3 Proof of Lemma 3.5: Symmetry of the Bumps and Waves

Lemma 3.5. *Let K be a kernel with corresponding bump B and wave W . If the kernel satisfies $K(t) = K(-t)$ for all $t \in \mathbb{R}$ then*

$$B(t, s_1, s_2) = B(-t, -s_1, -s_2) \quad \text{and} \quad W(t, s_1, s_2) = -W(-t, -s_1, -s_2), \quad (\text{3.21})$$

for all $s_1, s_2, t \in \mathbb{R}$.

Proof. By Lemma 3.2 we have

$$B(t, s_1, s_2) = \frac{-K^{(1)}(s_2)K(s_1 - t) + K^{(1)}(s_1)K(s_2 - t)}{K(s_2)K^{(1)}(s_1) - K^{(1)}(s_2)K(s_1)} \quad (\text{B.20})$$

$$= \frac{K^{(1)}(-s_2)K(-s_1 + t) - K^{(1)}(-s_1)K(-s_2 + t)}{-K(-s_2)K^{(1)}(-s_1) + K^{(1)}(-s_2)K(-s_1)} \quad (\text{B.21})$$

$$= B(-t, -s_2, -s_1) \quad (\text{B.22})$$

$$= B(-t, -s_1, -s_2) \quad (\text{B.23})$$

$$(\text{B.24})$$

since K is even and $K^{(1)}$ is odd. Similarly we have

$$W(t, s_1, s_2) = \frac{-K(s_2)K(s_1 - t) + K(s_1)K(s_2 - t)}{K(s_2)K^{(1)}(s_1) - K^{(1)}(s_2)K(s_1)} \quad (\text{B.25})$$

$$= \frac{-K(-s_2)K(-s_1 + t) + K(-s_1)K(-s_2 + t)}{-K(-s_2)K^{(1)}(-s_1) + K^{(1)}(-s_2)K(-s_1)} \quad (\text{B.26})$$

$$= -W(-t, -s_1, -s_2). \quad (\text{B.27})$$

□

B.4 Proof of Lemma 3.6: Decay of the Bumps and Waves

Lemma 3.6. *For the Gaussian and Ricker kernels we have*

$$\sum_{j=6}^{\infty} |B^{(i)}|_{\infty}^{\downarrow}((j - 1/2)\Delta) \leq \frac{10^{-12}}{\kappa(S)}, \quad \sum_{j=6}^{\infty} |W^{(i)}|_{\infty}^{\downarrow}((j - 1/2)\Delta) \leq \frac{10^{-12}}{\kappa(S)}, \quad (\text{3.27})$$

$$|B^{(i)}|_{\infty}^{\downarrow}(t) \leq \frac{10^{-12}}{\kappa(S)}, \quad |W^{(i)}|_{\infty}^{\downarrow}(t) \leq \frac{10^{-12}}{\kappa(S)}, \quad (\text{3.28})$$

for $i = 0, 1, 2$, $t \geq 10$, and $\Delta \geq 2$.

For ease of notation we denote the bump and wave coefficients by b_1, b_2, w_1 and w_2 . By the triangle inequality we have

$$\left| \frac{\partial^i}{\partial t^i} B(t, s_1, s_2) \right| \leq |b_1 K^{(i)}(s_1 - t)| + |b_2 K^{(i)}(s_2 - t)|, \quad (\text{B.28})$$

$$\left| \frac{\partial^i}{\partial t^i} W(t, s_1, s_2) \right| \leq |w_1 K^{(i)}(s_1 - t)| + |w_2 K^{(i)}(s_2 - t)|, \quad (\text{B.29})$$

for $i = 0, 1, 2$. The following lemmas bound these quantities for the Gaussian and Ricker kernels.

Lemma B.4. *Fix a sample proximity $\gamma(S, T) \leq 1$, a sample separation $\kappa(S)$, and $t \geq 10$. Then for the Gaussian kernel and $i = 0, 1, 2$ we have*

$$\left| \frac{\partial^i}{\partial t^i} B(t, s_1, s_2) \right| \leq \frac{4t^4}{\kappa(S)} \exp\left(-\frac{t^2}{2} + t\right), \quad (\text{B.30})$$

$$\left| \frac{\partial^i}{\partial t^i} W(t, s_1, s_2) \right| \leq \frac{4t^4}{\kappa(S)} \exp\left(-\frac{t^2}{2} + t\right). \quad (\text{B.31})$$

Proof. For the Gaussian kernel,

$$|b_1(K^{\mathcal{G}})^{(i)}(s_1 - t)| = \frac{|(K^{\mathcal{G}})^{(i)}(s_1 - t)(K^{\mathcal{G}})^{(1)}(s_2)|}{|D^{\mathcal{G}}(s_1, s_2)|} \quad (\text{Lemma 3.2}) \quad (\text{B.32})$$

$$\leq \frac{2t^4 \exp\left(-\frac{t^2}{2} + t - \frac{s_1^2}{2}\right) |s_2| \exp\left(-\frac{s_2^2}{2}\right)}{|s_2 - s_1| \exp\left(-\frac{s_1^2 + s_2^2}{2}\right)} \quad (\text{Lemmas B.1 and B.2}) \quad (\text{B.33})$$

$$\leq \frac{2t^4 \exp\left(-\frac{t^2}{2} + t\right)}{\kappa(S)}. \quad (\text{B.34})$$

The bound also holds for $|b_2 K^{\mathcal{G}}(s_2 - t)|$ by the same argument. For the wave,

$$|w_1(K^{\mathcal{G}})^{(i)}(s_1 - t)| = \frac{|(K^{\mathcal{G}})^{(i)}(s_1 - t)K^{\mathcal{G}}(s_2)|}{|D^{\mathcal{G}}(s_1, s_2)|} \quad (\text{Lemma 3.2}) \quad (\text{B.35})$$

$$\leq \frac{2t^4 \exp\left(-\frac{t^2}{2} + t - \frac{s_1^2}{2}\right) \exp\left(-\frac{s_2^2}{2}\right)}{|s_2 - s_1| \exp\left(-\frac{s_1^2 + s_2^2}{2}\right)} \quad (\text{Lemmas B.1 and B.2}) \quad (\text{B.36})$$

$$\leq \frac{2t^4 \exp\left(-\frac{t^2}{2} + t\right)}{\kappa(S)}. \quad (\text{B.37})$$

The same argument can be applied to $w_2(K^{\mathcal{G}})^{(i)}(s_2 - t)$. \square

Lemma B.5. *Fix a sample proximity $\gamma(S, T) \leq 0.8$, a sample separation $\kappa(S)$, and $t \geq 10$. Then for the Ricker kernel we have*

$$\left| \frac{\partial^i}{\partial t^i} B(t, s_1, s_2) \right| \leq \frac{11.3t^4}{\kappa(S)} \exp\left(-\frac{t^2}{2} + t\right), \quad (\text{B.38})$$

$$\left| \frac{\partial^i}{\partial t^i} W(t, s_1, s_2) \right| \leq \frac{4.8t^4}{\kappa(S)} \exp\left(-\frac{t^2}{2} + t\right), \quad (\text{B.39})$$

for $i = 0, 1, 2$.

Proof. We have

$$|b_1(K^{\mathcal{R}})^{(i)}(s_1 - t)| = \frac{|(K^{\mathcal{R}})^{(i)}(s_1 - t)(K^{\mathcal{R}})^{(1)}(s_2)|}{|D^{\mathcal{R}}(s_1, s_2)|} \quad (\text{Lemma 3.2})$$

$$\leq \frac{2t^4 \exp\left(-\frac{t^2}{2} + t - \frac{s_1^2}{2}\right) |s_2(s_2^2 - 3)| \exp\left(-\frac{s_2^2}{2}\right)}{|s_2 - s_1|(3 - (s_1 - s_2)^2 + s_1^2 s_2^2) \exp\left(-\frac{s_1^2 + s_2^2}{2}\right)} \quad (\text{Lemmas B.1 and B.2})$$

$$\leq \frac{4.8t^4 \exp\left(-\frac{t^2}{2} + t\right)}{\kappa(S)(3 - 4(0.8)^2 + 0.8^4)} \quad (\text{Lemma B.3}) \quad (\text{B.40})$$

$$\leq \frac{5.65t^4 \exp\left(-\frac{t^2}{2} + t\right)}{\kappa(S)}. \quad (\text{B.41})$$

The same argument applies to $|b_2 K^{\mathcal{R}}(s_2 - t)|$. For the wave,

$$\begin{aligned}
|w_1(K^{\mathcal{R}})^{(i)}(s_1 - t)| &= \frac{|(K^{\mathcal{R}})^{(i)}(s_1 - t)K^{\mathcal{R}}(s_2)|}{|D^{\mathcal{R}}(s_1, s_2)|} && \text{(Lemma 3.2)} \\
&\leq \frac{2t^4 \exp\left(-\frac{t^2}{2} + t - \frac{s_1^2}{2}\right) |s_2^2 - 1| \exp\left(-\frac{s_2^2}{2}\right)}{|s_2 - s_1|(3 - (s_1 - s_2)^2 + s_1^2 s_2^2) \exp\left(-\frac{s_1^2 + s_2^2}{2}\right)} && \text{(Lemmas B.1 and B.2)} \\
&\leq \frac{2t^4 \exp\left(-\frac{t^2}{2} + t\right)}{\kappa(S)(3 - 4(0.8)^2 + 0.8^4)} && \text{(Lemma B.3)} \quad \text{(B.42)} \\
&\leq \frac{2.4t^4 \exp\left(-\frac{t^2}{2} + t\right)}{\kappa(S)}. && \text{(B.43)}
\end{aligned}$$

The same argument applies to $|w_2(K^{\mathcal{R}})^{(i)}(s_2 - t)|$. \square

The proof is completed by combining Lemmas B.4 and B.5 with the following result, which can be applied to both the Gaussian kernel and the Ricker wavelet.

Lemma B.6. *Suppose $f(t) \leq 20t^4 \exp(-t^2/2 + t)$ for $t \geq 10$. Then*

$$\sum_{k=j}^{\infty} f(c + kd) \leq 10^{-12},$$

for any $c, d \in \mathbb{R}$ and $j \in \mathbb{Z}_{>0}$ with $d \geq 1$ and $c + jd \geq 10$.

Proof. Let $p(t) := 20t^4 \exp(-t^2/2 + t)$. For $t \geq 10$

$$p^{(1)}(t) = 80t^3 e^{-t^2/2+t} + 20t^4 e^{-t^2/2+t}(1-t) \quad \text{(B.44)}$$

$$\leq 8t^4 e^{-t^2/2+t} + 20t^4 e^{-t^2/2+t}(1-t) \quad \text{(B.45)}$$

$$= (28 - 20t)t^4 e^{-t^2/2+t} \quad \text{(B.46)}$$

$$< 0, \quad \text{(B.47)}$$

and

$$\frac{p(t)}{p(t+1)} = \frac{20t^4 \exp(-t^2/2 + t)}{20(t+1)^4 \exp(-(t+1)^2/2 + (t+1))} \quad \text{(B.48)}$$

$$= \frac{t^4}{(t+1)^4} \exp(((t+1)^2 - t^2)/2 - 1) \quad \text{(B.49)}$$

$$= \frac{t^4}{t^4 + 4t^3 + 6t^2 + 4t + 1} \exp(t - 1/2) \quad \text{(B.50)}$$

$$\geq \frac{1}{2e^{1/2}} e^t \quad \text{(B.51)}$$

$$> 2. \quad \text{(B.52)}$$

Combining these facts, we obtain a geometric-series bound, which we sum to complete the proof:

$$\sum_{k=j}^{\infty} f(c+kd) \leq \sum_{k=j}^{\infty} p(c+kd) \leq \sum_{i=10}^{\infty} p(i) \quad (\text{B.53})$$

$$\leq p(10) \sum_{i=0}^{\infty} 2^{-i} = 2p(10) \leq 10^{-12}. \quad (\text{B.54})$$

□

B.5 Proof of Lemma 3.7: Piecewise-Constant Bounds

Lemma 3.7. *Fix $\gamma(S, T)$ and $\kappa(S)$ and let $N_1 \in \mathbb{Z}_{>0}$. Partition the interval $[0, 10)$ into N_1 intervals of the form*

$$\mathcal{U}_j := \left[\frac{10(j-1)}{N_1}, \frac{10j}{N_1} \right), \quad (\text{3.29})$$

and $j = 1, \dots, N_1$. For the Gaussian and Ricker kernels, there exist functions $|\widetilde{B}^{(i)}|$, $|\widetilde{W}^{(i)}|$, $\widetilde{B}^{(i)}$, such that for all $t \in \mathcal{U}_j$ and $i = 0, 1, 2$

$$|B^{(i)}|_{\infty}(t) \leq |\widetilde{B}^{(i)}|(j), \quad (\text{3.30})$$

$$|W^{(i)}|_{\infty}(t) \leq |\widetilde{W}^{(i)}|(j), \quad (\text{3.31})$$

$$B_{\infty}^{(i)}(t) \leq \widetilde{B}^{(i)}(j). \quad (\text{3.32})$$

These bounds depend on $\gamma(S, T)$, $\kappa(S)$ and an additional parameter N_2 , satisfying $\kappa(S) > 2\gamma(S, T)/N_2$ as explained in Appendix B.5.

In this section we define piecewise-constant upper bounds for $|B^{(i)}|_{\infty}$, $|W^{(i)}|_{\infty}$, $B_{\infty}^{(i)}$ where $i = 0, 1, 2$ and $t \in [0, 10)$. We begin by partitioning the interval $[0, 10)$ into N_1 segments of the form

$$\mathcal{U}_j := \left[\frac{10(j-1)}{N_1}, \frac{10j}{N_1} \right), \quad 1 \leq j \leq N_1, \quad (\text{B.55})$$

and by dividing the interval $[-\gamma(S, T), \gamma(S, T)]$ into $2N_2$ almost disjoint segments of the form

$$\mathcal{V}_k := \left[\frac{(k-1)\gamma(S, T)}{N_2}, \frac{k\gamma(S, T)}{N_2} \right], \quad -N_2 + 1 \leq k \leq N_2. \quad (\text{B.56})$$

Next we define bounds on our functions of interest when $t \in \mathcal{U}_j$, $s_1 \in \mathcal{V}_k$ and $s_2 \in \mathcal{V}_l$

$$|b^{(i)}|_{j,k,l} \geq \sup |B^{(i)}(\mathcal{U}_j, \mathcal{V}_k, \mathcal{V}_l)|, \quad (\text{B.57})$$

$$|w^{(i)}|_{j,k,l} \geq \sup |W^{(i)}(\mathcal{U}_j, \mathcal{V}_k, \mathcal{V}_l)|, \quad (\text{B.58})$$

$$b_{j,k,l}^{(i)} \geq \sup B^{(i)}(\mathcal{U}_j, \mathcal{V}_k, \mathcal{V}_l), \quad (\text{B.59})$$

where $i = 0, 1, 2$, $1 \leq j \leq N_1$ and $-N_2 + 1 \leq k, l \leq N_2$. To be clear, $|B^{(i)}(\mathcal{U}_j, \mathcal{V}_k, \mathcal{V}_l)|$ is the image of the set $\mathcal{U}_j \times \mathcal{V}_k \times \mathcal{V}_l$ with respect to the function $|B^{(i)}|$. These bounds can be computed by interval arithmetic using the fact that the functions $B^{(i)}$ and $W^{(i)}$ can be expressed in terms of exponentials and polynomials. We provide a small description of interval arithmetic in Appendix B.6. To compute the bounds in practice, we apply the interval-arithmetic library in Mathematica, which we have found to be sufficient for our purposes. The code is available online⁶.

To define piecewise bounds that are valid on each \mathcal{U}_j , we maximize over the sets in the partition of $[-\gamma(S, T), \gamma(S, T)]^2$ which contain points that satisfy the sample-separation condition in Definition 2.2. Consider the distance between \mathcal{V}_k and \mathcal{V}_l

$$d(\mathcal{V}_k, \mathcal{V}_l) := \inf_{a \in \mathcal{V}_k, b \in \mathcal{V}_l} |a - b|. \quad (\text{B.60})$$

The following lemma implies that it is sufficient to consider the pairs $\mathcal{V}_k, \mathcal{V}_l$ such that $d(\mathcal{V}_k, \mathcal{V}_l) \geq c := \kappa(S) - 2\gamma(S, T)/N_2$.

Lemma B.7. *If $d(\mathcal{V}_k, \mathcal{V}_l) < c := \kappa(S) - 2\gamma(S, T)/N_2$ then no pair of points $s_1 \in \mathcal{V}_k, s_2 \in \mathcal{V}_l$ satisfy the sample-separation condition $|s_1 - s_2| \geq \kappa(S)$.*

Proof. Since $\mathcal{V}_k \times \mathcal{V}_l$ is compact there exist two points $\tilde{a} \in \mathcal{V}_k$ and $\tilde{b} \in \mathcal{V}_l$ such that $|\tilde{a} - \tilde{b}| = d(\mathcal{V}_k, \mathcal{V}_l)$. By the triangle inequality, for any pair of points $s_1 \in \mathcal{V}_k, s_2 \in \mathcal{V}_l$

$$|s_1 - s_2| \leq |s_1 - \tilde{a}| + |\tilde{a} - \tilde{b}| + |\tilde{b} - s_2| \quad (\text{B.61})$$

$$< \frac{2\gamma(S, T)}{N_2} + c = \kappa(S). \quad (\text{B.62})$$

□

Finally, we obtain the following bounds on $|B^{(i)}|_\infty(t)$, $|W^{(i)}|_\infty(t)$ and $B_\infty^{(i)}(t)$ for $t \in \mathcal{U}_j$ and $i = 0, 1, 2$

$$\widetilde{|B^{(i)}|}(j) := \max_{d(\mathcal{V}_k, \mathcal{V}_l) \geq c} |b^{(i)}|_{j,k,l}, \quad (\text{B.63})$$

$$\widetilde{|W^{(i)}|}(j) := \max_{d(\mathcal{V}_k, \mathcal{V}_l) \geq c} |w^{(i)}|_{j,k,l}, \quad (\text{B.64})$$

$$\widetilde{B^{(i)}}(j) := \max_{d(\mathcal{V}_k, \mathcal{V}_l) \geq c} b_{j,k,l}^{(i)}. \quad (\text{B.65})$$

These bounds are parametrized by a finite number of points and can therefore be computed explicitly as long as we fix N_1 and N_2 . Figure 28 shows, for a fixed \mathcal{U}_j , the subset of $[-\gamma(S, T), \gamma(S, T)]^2$ used to compute $\widetilde{|B^{(i)}|}(j)$, $\widetilde{|W^{(i)}|}(j)$, and $\widetilde{B^{(i)}}(j)$.

⁶http://www.cims.nyu.edu/~cfgranda/scripts/deconvolution_proof.zip

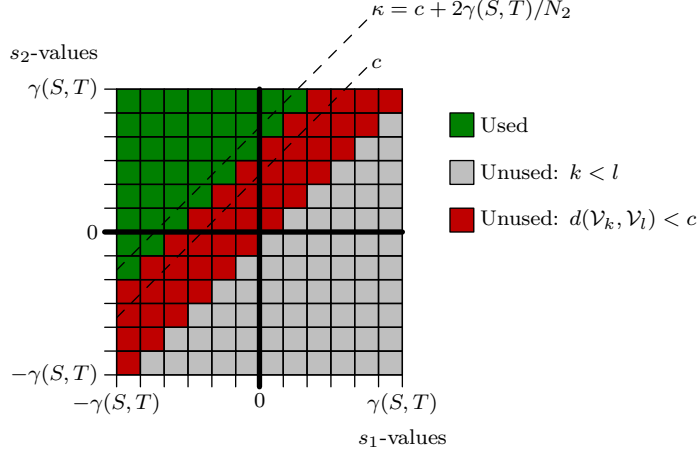


Figure 28: Squares $\mathcal{V}_k \times \mathcal{V}_l$ used to compute $\widetilde{|B|}^{(i)}(j)$, $\widetilde{|W|}^{(i)}(j)$, and $\widetilde{B}^{(i)}(j)$ for a fixed \mathcal{U}_j .

B.6 Interval Arithmetic

This section briefly describes interval arithmetic, a technique developed to handle rounding and measurement errors in numerical analysis. In this work, we apply it to derive the piecewise-constant bounds in Appendix B.5. Interval arithmetic allows us to compute an interval which contains the possible values of a function when its arguments belong to given intervals. To be precise, let $f : \mathbb{R}^n \rightarrow \mathbb{R}$ be a function that can be expressed by composing predefined functions (such as monomials or exponentials) with standard arithmetic operations. Given n intervals of the form $[a_i, b_i] \subseteq \mathbb{R}$, $1 \leq i \leq n$, the goal is to obtain an interval $[c, d] \subseteq \mathbb{R}$ such that

$$f([a_1, b_1] \times \cdots \times [a_n, b_n]) \subseteq [c, d].$$

For a set \mathcal{A} , $f(\mathcal{A})$ denotes the image of \mathcal{A} . Interval-arithmetic methods usually compute $[c, d]$ recursively by applying simple identities to obtain intervals containing the output of the functions that are composed to obtain f . The following lemma lists some of these expressions.

Lemma B.8 (Proof in [41]). *Let $f_1, f_2 : \mathbb{R}^n \rightarrow \mathbb{R}$, $\mathcal{A} \subseteq \mathbb{R}$, $f_1(\mathcal{A}) \subseteq [c_1, d_1]$ and $f_2(\mathcal{A}) \subseteq [c_2, d_2]$ for some $c_1, d_1, c_2, d_2 \in \mathbb{R}$. Then the following hold.*

1. $|f_1(\mathcal{A})| \subseteq [\max(0, c_1), \max(|c_1|, |d_1|)]$.
2. $f_1(\mathcal{A}) + f_2(\mathcal{A}) \subseteq [c_1 + c_2, d_1 + d_2]$.
3. $-f_1(\mathcal{A}) \subseteq [-d_1, -c_1]$.
4. $f_1(\mathcal{A})f_2(\mathcal{A}) \subseteq [\min(c_1d_1, c_1d_2, c_2d_1, c_2d_2), \max(c_1d_1, c_1d_2, c_2d_1, c_2d_2)]$.
5. Let $k \in \mathbb{Z}_{>0}$. If 0 is not in $[c_1, d_1]$ then $f_1(\mathcal{A})^{2k} \subseteq [\min(c_1^{2k}, d_1^{2k}), \max(c_1^{2k}, d_1^{2k})]$. If 0 is in $[c_1, d_1]$ then $f_1(\mathcal{A})^{2k} \subseteq [0, \max(c_1^{2k}, d_1^{2k})]$.
6. If $0 \notin [c_1, d_1]$, $1/f_1(\mathcal{A}) \subseteq [1/d_1, 1/c_1]$.
7. If $g : \mathbb{R} \rightarrow \mathbb{R}$ is increasing $g(f_1(\mathcal{A})) \subseteq [g(c_1), g(d_1)]$.

To conclude we illustrate how interval arithmetic works with a simple example.

Example B.9. Let

$$f(x, y) := \frac{(x - y)^2 xy}{x} \quad (\text{B.66})$$

where $x \in [1, 2]$ and $y \in [-3, 3]$. Then by Lemma B.8

$$-y \in [-3, 3], \quad x - y \in [-2, 5], \quad (x - y)^2 \in [0, 25], \quad (\text{B.67})$$

$$xy \in [-6, 6], \quad 1/x \in [1/2, 1], \quad (x - y)^2 xy \in [-150, 150], \quad (\text{B.68})$$

and $f(x, y) := \frac{(x-y)^2 xy}{x} \subseteq [-150, 150]$ for any x, y in the predefined intervals. Note that if we perform the algebraic simplification $f(x, y) = (x - y)^2 y$, the result is improved to $(x - y)^2 y \in [-75, 75]$, a tighter interval. This shows that interval arithmetic bounds are sensitive to how we express the function.

B.7 Proof of Lemma B.3

Lemma B.3. *Let $f : \mathbb{R}^2 \rightarrow \mathbb{R}$ be defined by $f(x, y) = 3 - (x - y)^2 + x^2 y^2$. If $\max(|x|, |y|) \leq a < 1$ then $f(x, y) \geq 3 - 4a^2 + a^4 > 0$.*

Proof. For fixed a , the continuous function f is restricted to a compact set, and thus must attain its minimum. We determine the critical points of f , and then show the minimum must occur on the boundary. Note that the gradient of f is given by

$$\nabla f(x, y) = (-2(x - y) + 2xy^2, 2(x - y) + 2x^2 y). \quad (\text{B.69})$$

Assume $\nabla f(x, y) = 0$ and sum the components giving

$$0 = 2xy^2 + 2x^2 y = 2xy(x + y). \quad (\text{B.70})$$

This implies $x = 0$, $y = 0$ or $x = -y$. If $x = 0$ then

$$0 = \nabla f(0, y) = (2y, -2y) \quad (\text{B.71})$$

shows $y = 0$. By symmetry, $y = 0$ implies $x = 0$. Finally, if $x = -y$ then

$$0 = \nabla f(x, -x) = (-4x + 2x^3, 4x - 2x^3) = 2x(x^2 - 2, 2 - x^2). \quad (\text{B.72})$$

Thus the critical points of f are $(0, 0)$, $(\sqrt{2}, -\sqrt{2})$, $(-\sqrt{2}, \sqrt{2})$. Restricting to $|x|, |y| \leq a < 1$, only the origin is a critical point with value $f(0, 0) = 3$. Fixing $x = a$,

$$f(a, y) = 3 - (a - y)^2 + a^2 y^2 = 3 - a^2 + (a^2 - 1)y^2 + 2ay \quad (\text{B.73})$$

is a concave quadratic in y minimized at $y = -a$. Similarly, if $x = -a$

$$f(-a, y) = 3 - (-a - y)^2 + a^2 y^2 = 3 - a^2 + (a^2 - 1)y^2 - 2ay \quad (\text{B.74})$$

is minimized at $y = a$. As f is symmetric, we have accounted for all points on the boundary, and have shown that the minimum occurs at

$$f(a, -a) = 3 - 4a^2 + a^4 = (a^2 - 3)(a^2 - 1). \quad (\text{B.75})$$

This is positive for $|a| < 1$ completing the proof. \square

C Proof of Lemma 3.10: Bounding the Q Function

Lemma 3.10. *Fix our kernel to be the Gaussian kernel or the Ricker wavelet. Assume the conditions of Lemmas 3.6 and 3.9 hold, and that there is a spike at the origin with sign $+1$. Let h denote half the distance from the origin to the spike with smallest positive location, or ∞ if no such spike exists. Then, for $0 < t \leq h$ (or $t > 0$ if $h = \infty$) and $\epsilon := 10^{-12}/\kappa(S)$,*

$$|\mathcal{B}^{(p)}(t)| \leq \|\alpha\|_\infty \left(|B^{(p)}|_\infty^\downarrow(v) + 2\epsilon + \sum_{j=1}^5 |B^{(p)}|_\infty^\downarrow(v + j\Delta(T)) + |B^{(p)}|_\infty^\downarrow(j\Delta(T) - v) \right) \quad (3.59)$$

$$|\mathcal{W}^{(p)}(t)| \leq \|\beta\|_\infty \left(|W^{(p)}|_\infty^\downarrow(v) + 2\epsilon + \sum_{j=1}^5 |W^{(p)}|_\infty^\downarrow(v + j\Delta(T)) + |W^{(p)}|_\infty^\downarrow(j\Delta(T) - v) \right), \quad (3.60)$$

for $p = 0, 1, 2$ and $v = \min(t, \Delta(T)/2)$. For $q = 1, 2$

$$\mathcal{B}^{(q)}(t) \leq \alpha_{\text{LB}} B_\infty^{(q)}(t) + \|\alpha\|_\infty \left(2\epsilon + \sum_{j=1}^5 |B^{(q)}|_\infty^\downarrow(v + j\Delta(T)) + |B^{(q)}|_\infty^\downarrow(j\Delta(T) - v) \right), \quad (3.61)$$

as long as $B_\infty^{(q)}(t) \leq 0$, where $\alpha_{\text{LB}} := 1 - \|\alpha - \rho\|_\infty \geq 0$.

Proof. Suppose the spikes are numbered so that $t_1 = 0$. We have, for $p = 0, 1, 2$,

$$|\mathcal{B}^{(p)}(t)| = \left| \alpha_1 B_1^{(p)}(t) + \sum_{t_j > 0} \alpha_j B_j^{(p)}(t) + \sum_{t_j < 0} \alpha_j B_j^{(p)}(t) \right| \quad (C.1)$$

$$\leq \|\alpha\|_\infty \left(|B^{(p)}(t, \tilde{s}_{1,1}, \tilde{s}_{1,2})| + \sum_{t_j > 0} |B^{(p)}(t - t_j, \tilde{s}_{j,1} - t_j, \tilde{s}_{j,2} - t_j)| \right) \quad (C.2)$$

$$+ \sum_{t_j < 0} |B^{(p)}(t - t_j, \tilde{s}_{j,1} - t_j, \tilde{s}_{j,2} - t_j)| \quad (C.3)$$

$$\leq \|\alpha\|_\infty \left(|B^{(p)}|_\infty^\downarrow(t) + \sum_{t_j > 0} |B^{(p)}|_\infty^\downarrow(t_j - t) + \sum_{t_j < 0} |B^{(p)}|_\infty^\downarrow(t - t_j) \right) \quad (C.4)$$

$$\leq \|\alpha\|_\infty \left(|B^{(p)}|_\infty^\downarrow(v) + \sum_{j=1}^{\infty} |B^{(p)}|_\infty^\downarrow(j\Delta(T) - v) + |B^{(p)}|_\infty^\downarrow(v + j\Delta(T)) \right) \quad (\text{Monotonicity})$$

$$\leq \|\alpha\|_\infty \left(|B^{(p)}|_\infty^\downarrow(v) + 2\epsilon + \sum_{j=1}^5 |B^{(p)}|_\infty^\downarrow(j\Delta(T) - v) + |B^{(p)}|_\infty^\downarrow(v + j\Delta(T)) \right) \quad (\text{Lemma 3.6}).$$

This establishes (3.59). The same argument applied to $|W^{(p)}|_\infty^\downarrow$ in place of $|B^{(p)}|_\infty^\downarrow$ yields (3.60).

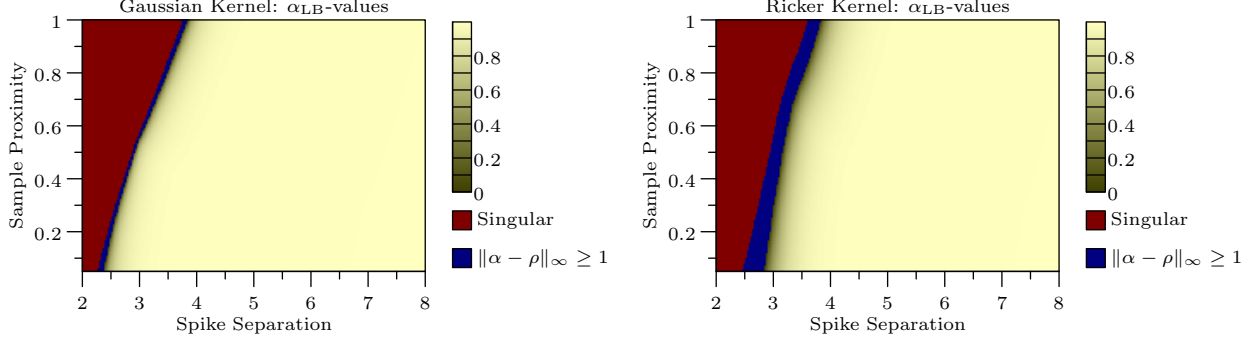


Figure 29: Lower bounds on α_{LB} for different values of the minimum separation and the sample proximity. The singular region denotes where we are unable to prove the system of interpolation equations is invertible.

For $q = 1, 2$, if in addition we assume $B_\infty^{(q)}(t) \leq 0$, then

$$\mathcal{B}^{(q)}(t) = \alpha_1 B_1^{(q)}(t) + \sum_{t_j > 0} \alpha_j B_j^{(q)}(t) + \sum_{t_j < 0} \alpha_j B_j^{(q)}(t) \quad (\text{C.5})$$

$$\leq \alpha_{\text{LB}} B^{(q)}(t, \tilde{s}_{1,1}, \tilde{s}_{1,2}) + \|\alpha\|_\infty \left(\sum_{t_j > 0} |B^{(q)}(t - t_j, \tilde{s}_{j,1} - t_j, \tilde{s}_{j,2} - t_j)| \right) \quad (\text{C.6})$$

$$+ \sum_{t_j < 0} |B^{(q)}(t - t_j, \tilde{s}_{j,1} - t_j, \tilde{s}_{j,2} - t_j)| \quad (\text{C.7})$$

$$\leq \alpha_{\text{LB}} B_\infty^{(q)}(t) + \|\alpha\|_\infty \left(\sum_{t_j > 0} |B^{(q)}|_\infty^\downarrow(t_j - t) + \sum_{t_j < 0} |B^{(q)}|_\infty^\downarrow(t - t_j) \right) \quad (\text{C.8})$$

$$\leq \alpha_{\text{LB}} B_\infty^{(q)}(t) + \|\alpha\|_\infty \left(\sum_{j=1}^{\infty} |B^{(q)}|_\infty^\downarrow(j\Delta(T) - v) + |B^{(q)}|_\infty^\downarrow(v + j\Delta(T)) \right) \quad (\text{Monotonicity})$$

$$\leq \alpha_{\text{LB}} B_\infty^{(q)}(t) + \|\alpha\|_\infty \left(2\epsilon + \sum_{j=1}^5 |B^{(q)}|_\infty^\downarrow(j\Delta(T) - v) + |B^{(q)}|_\infty^\downarrow(v + j\Delta(T)) \right) \quad (\text{Lemma 3.6}).$$

The above argument requires $\alpha_{\text{LB}} \geq 0$. In Figure 29 we apply Lemma 3.9 to compute the region where $\alpha_{\text{LB}} \geq 0$ for the Gaussian and Ricker kernels. The parameters values we use in the computation are the same as used to compute Figure 16 at the end of Section 3.4. The regions where $\alpha_{\text{LB}} \geq 0$ for the two kernels are strictly contained within the exact recovery regions stated in Theorem 2.4, as required.

□

D Duality for Problem (2.6)

Recall that I is a compact interval containing the support of μ , and that $\tilde{\mu}$ in problem (2.6) takes values in the set of finite signed Borel measures supported on I .

Lemma D.1. *Problem (2.6) is the Lagrange dual of*

$$\begin{aligned} & \text{maximize} && c^T y - \bar{\xi} \|c\|_2 \\ & \text{subject to} && \sup_{t \in I} \left| \sum_{i=1}^n c_i K(s_i - t) \right| \leq 1, \end{aligned} \tag{D.1}$$

and strong duality holds. Furthermore, optimal solutions exist for both the primal and dual problems.

Proof. For convenience, we minimize $-c^T y + \bar{\xi} \|c\|_2$ instead. The Lagrangian is given by

$$\mathcal{L}(c, \nu, \lambda) = -c^T y + \bar{\xi} \|c\|_2 + \int (C(t) - 1) d\nu(t) + \int (-C(t) - 1) d\lambda(t) \tag{D.2}$$

$$= -c^T y + \bar{\xi} \|c\|_2 + \int C(t) d(\nu - \lambda)(t) - \|\nu + \lambda\|_{\text{TV}} \tag{D.3}$$

$$= \sum_{i=1}^n c_i ((K * (\nu - \lambda))(s_i) - y_i) + \bar{\xi} \|c\|_2 - \|\nu + \lambda\|_{\text{TV}}, \tag{D.4}$$

where $C(t) := \sum_{i=1}^n c_i K(s_i - t)$ and ν, λ are finite non-negative Borel measures on I . Here the measures ν, λ act as the Lagrange multipliers (see [65]). To compute the dual function g , we minimize the Lagrangian over the primal variable, $g(\nu, \lambda) := \inf_c \mathcal{L}(c, \nu, \lambda)$. Define $v \in \mathbb{R}^n$ by $v_i := (K * (\nu - \lambda))(s_i) - y_i$. Since c occurs in an inner product with v and in an ℓ_2 -norm, we can set $c := -\alpha v / \|v\|_2$ and minimize over $\alpha \geq 0$, so that

$$\mathcal{L}(-\alpha v / \|v\|_2, \nu, \lambda) = -\alpha \|v\|_2 + \alpha \bar{\xi} - \|\nu + \lambda\|_{\text{TV}} = \alpha(\bar{\xi} - \|v\|_2) - \|\nu + \lambda\|_{\text{TV}}. \tag{D.5}$$

Unless $\|v\|_2 \leq \bar{\xi}$, the minimum is $-\infty$. Under this constraint, the minimum occurs at $\alpha := 0$, which yields the dual problem

$$\text{maximize} \quad -\|\nu + \lambda\|_{\text{TV}} \tag{D.6}$$

$$\text{subject to} \quad \sum_{i=1}^n ((K * (\nu - \lambda))(s_i) - y_i)^2 \leq \bar{\xi}. \tag{D.7}$$

Fix $\zeta := \nu - \lambda$ and let $\zeta = \zeta_+ - \zeta_-$ be the Jordan decomposition, where ζ_+, ζ_- are the positive and negative parts of ζ , respectively. Then for any feasible ζ we see that $\|\nu + \lambda\|_{\text{TV}}$ is minimized when $\nu = \zeta_+$ and $\lambda = \zeta_-$. Up to the negation we introduced for convenience, this is exactly Problem (2.6).

To prove strong duality we apply Theorem 2.3 of [65], noting that the objective is finite by weak duality, and that $c = 0$ satisfies Slater's condition. The same theorem also shows that the Problem (2.6) has a minimizing solution μ^* . To prove Problem (D.1) has a maximizing solution c^* , we

will apply Theorem 2.2 of [65] which states the following sufficient condition: there is a neighborhood \mathcal{N} of $0 \in \mathbb{R}^n$ such that for every $w \in \mathcal{N}$ there are finite Borel measures ν, λ on I satisfying

$$\inf_{c \in \mathbb{R}^n} \mathcal{L}(c, \nu, \lambda) - w^T c = -c^T(y + w) + \bar{\xi} \|c\|_2 + \int C(t) - 1 d\nu(t) + \int -C(t) - 1 d\lambda(t) > -\infty. \quad (\text{D.8})$$

This is the Lagrangian for (the minimizing version of) Problem (D.1) where y is replaced by $y + w$. Our analysis above shows that (D.8) holds for w whenever there are ν, λ satisfying

$$\sum_{i=1}^n ((K * (\nu - \lambda))(s_i) - (y_i + w_i))^2 \leq \bar{\xi}^2. \quad (\text{D.9})$$

By assumption, our noisy measurements satisfy

$$\sum_{i=1}^n ((K * \mu)(s_i) - y_i)^2 =: \beta^2 < \bar{\xi}^2. \quad (\text{D.10})$$

Letting $\mathcal{N} = \{w : \|w\|_2 < \bar{\xi} - \beta\}$ and applying the triangle inequality to (D.9) (after taking square roots) completes the proof. \square

E Proof of Lemma 2.6

Lemma 2.6. *Assume y satisfies (2.5) with $\|z\|_2 < \bar{\xi}$. If K is real analytic with $K(t) \rightarrow 0$ as $t \rightarrow \infty$ then the solution $\hat{\mu}$ to problem (2.6) is an atomic measure with finite support $\hat{T} \subseteq \mathbb{R}$ of the form*

$$\hat{\mu} = \sum_{\hat{t}_k \in \hat{T}} \hat{a}_k \delta_{\hat{t}_k}, \quad \hat{a}_1, \dots, \hat{a}_{|\hat{T}|} \in \mathbb{R}. \quad (\text{2.7})$$

Proof. By Lemma D.1, there is a minimizer μ^* for Problem (2.6) and a maximizer c^* for Problem (D.1). Then the Lagrangian (D.2) takes the form

$$\mathcal{L}(c^*, \mu_+^*, \mu_-^*) = -(c^*)^T y + \bar{\xi} \|c^*\|_2 + \int C^*(t) - 1 d\mu_+^*(t) + \int -C^*(t) - 1 d\mu_-^*(t), \quad (\text{E.1})$$

where $C^*(t) := \sum_{i=1}^m c_i^* K(s_i - t)$. Define $A \subseteq \mathbb{R}$ by

$$A = \{t \in \mathbb{R} : |C^*(t)| = 1\}. \quad (\text{E.2})$$

We first show that $A \cap I$ is finite. If not, A has a limit point. As C^* is analytic, this implies C^* is constant giving $A = \mathbb{R}$. But $\lim_{t \rightarrow -\infty} C^*(t) = 0$ by assumption, a contradiction. This proves $A \cap I$ is finite.

Applying complementary slackness, both integrals in equation (E.1) are zero. For $t \in I \setminus A$, we have $|C^*(t)| - 1 < 0$ by the feasibility of c^* and the definition of A . Thus $\mu_+^*(I \setminus A) = \mu_-^*(I \setminus A) = 0$. This shows any primal optimal solution μ^* is atomic, as required. \square

F Proofs of Auxiliary Results in Section 4

F.1 Proof of Lemma 4.1

Lemma 4.1. *Under the assumptions of Theorem 2.7, there exists a function Q of the form*

$$Q(t) := \sum_{s_i \in S} q_i K(s_i - t), \quad (4.1)$$

for some $q \in \mathbb{R}^n$ that satisfies:

1. $Q(t_j) = \text{sign}(a_j)$ for all $t_j \in T$,
2. $|Q(t)| < 1$ for all $t \in T^c$,
3. $|Q(t)| \leq 1 - C_1(t - t_j)^2$ if $|t - t_j| \leq \eta$ for some $t_j \in T$,
4. $|Q(t)| \leq 1 - C_2$ if $|t - t_j| > \eta$ for all $t_j \in T$,
5. $\|q\|_\infty \leq C_3$.

The values $\eta, C_1, C_2, C_3 > 0$ depend only on $\Delta(T)$, $\gamma(S, T)$, and $\kappa(S)$.

Proof. We consider the dual combination Q defined by equation (3.6) with coefficients adjusted to satisfy the system of equations (3.7) for $\rho := \text{sign}(a)$. By Lemmas 3.3 and 3.4, Q satisfies properties 1 and 2. To establish property 3, without loss of generality we set $t_j := 0$ and $a_j := 1$. The application of Lemma 3.11 in the proof of Lemma 3.4 shows that for each $(\Delta(T), \gamma(S, T))$ pair in Figure 6 there is a $u_1 > 0$ such that $Q^{(2)}(t) < 0$ if $t \in [-u_1, u_1]$. By Taylor's theorem

$$Q(t) \leq Q(0) + tQ'(0) + \frac{t^2}{2} \sup_{u \in [-u_1, u_1]} Q^{(2)}(u) \quad (F.1)$$

$$= 1 + \frac{ct^2}{2}, \quad (F.2)$$

for $t \in [-u_1, u_1]$ where $c := \sup_{u \in [-u_1, u_1]} Q^{(2)}(u)$ satisfies $c < 0$. This shows that property 3 holds. Similarly, the application of Lemma 3.11 in the proof of Lemma 3.4 also shows that for each $(\Delta(T), \gamma(S, T))$ pair in Figure 6 we have $|Q(t)| \leq c' < 1$ if $t \in [u_2, h]$ for a certain constant c' . Letting $C_2 = \min(1 - c', -c\eta^2/2)$ proves property 4.

For the Gaussian, by Lemmas 3.2 and B.2,

$$|b_{i,1}| = \frac{|\tilde{s}_{i,2}| \exp\left(-\frac{\tilde{s}_{i,2}^2}{2}\right)}{|\tilde{s}_{i,2} - \tilde{s}_{i,1}| \exp\left(-\frac{\tilde{s}_{i,1}^2 + \tilde{s}_{i,2}^2}{2}\right)} \leq \frac{\gamma(S, T) e^{\gamma(S, T)^2/2}}{\kappa(S)}, \quad (F.3)$$

$$|w_{i,1}| = \frac{\exp\left(-\frac{\tilde{s}_{i,2}^2}{2}\right)}{|\tilde{s}_{i,2} - \tilde{s}_{i,1}| \exp\left(-\frac{\tilde{s}_{i,1}^2 + \tilde{s}_{i,2}^2}{2}\right)} \leq \frac{e^{\gamma(S, T)^2/2}}{\kappa(S)}, \quad (F.4)$$

where we simplified notation by using $t_i = 0$. Similarly, for the Ricker,

$$|b_{i,1}| = \frac{|\tilde{s}_{i,2}(\tilde{s}_{i,2}^2 - 3)| \exp\left(-\frac{\tilde{s}_{i,2}^2}{2}\right)}{|\tilde{s}_{i,2} - \tilde{s}_{i,1}| |3 - (\tilde{s}_{i,2} - \tilde{s}_{i,1})^2 + \tilde{s}_{i,2}^2 \tilde{s}_{i,1}^2| \exp\left(-\frac{\tilde{s}_{i,1}^2 + \tilde{s}_{i,2}^2}{2}\right)} \leq \frac{D\gamma(S, T)e^{\gamma(S, T)^2/2}}{\kappa(S)}, \quad (\text{F.5})$$

$$|w_{i,1}| = \frac{|\tilde{s}_{i,2}^2 - 1| \exp\left(-\frac{\tilde{s}_{i,2}^2}{2}\right)}{|\tilde{s}_{i,2} - \tilde{s}_{i,1}| |3 - (\tilde{s}_{i,2} - \tilde{s}_{i,1})^2 + \tilde{s}_{i,2}^2 \tilde{s}_{i,1}^2| \exp\left(-\frac{\tilde{s}_{i,1}^2 + \tilde{s}_{i,2}^2}{2}\right)} \leq \frac{D'e^{\gamma(S, T)^2/2}}{\kappa(S)}, \quad (\text{F.6})$$

where $D, D' > 0$ come from the bounds on $\gamma(S, T)$ and Lemma B.3. The same bounds hold for $|b_{i,2}|$ and $|w_{i,2}|$. Combining the two bounds we obtain

$$\|q\|_\infty \leq \frac{\gamma(S, T) \|\alpha\|_\infty + \|\beta\|_\infty e^{\gamma(S, T)^2/2}}{\kappa(S)} \max(D, D'), \quad (\text{F.7})$$

which establishes property 5. Note that bounds on $\|\alpha\|_\infty$ and $\|\beta\|_\infty$ computed from $\Delta(T)$, $\gamma(S, T)$, and $\kappa(S)$ are given in Section 3.4 by applying Lemma 3.9. \square

F.2 Proof of Corollary 4.2

Corollary 4.2. *Under the assumptions of Lemma 4.1*

$$\int Q(t) d\hat{\mu}(t) \geq \|\hat{\mu}\|_{\text{TV}} - 2\|q\|_\infty \bar{\xi} \sqrt{|T|}, \quad (\text{4.3})$$

$$\int Q(t) d\hat{\mu}(t) \leq \sum_{\hat{t}_k \in \hat{T}: d(\hat{t}_k, T) \leq \eta} (1 - C_1 d(\hat{t}_k, T)^2) |\hat{a}_k| + \sum_{\hat{t}_k \in \hat{T}: d(\hat{t}_k, T) > \eta} (1 - C_2) |\hat{a}_k|. \quad (\text{4.4})$$

Proof. We have

$$\|\hat{\mu}\|_{\text{TV}} - \int Q(t) d\hat{\mu}(t) \leq \|\mu\|_{\text{TV}} - \int Q(t) d\hat{\mu}(t) = \int Q(t) d(\mu - \hat{\mu})(t), \quad (\text{F.8})$$

since μ is feasible for Problem (2.6). To prove (4.3), we bound the right hand side,

$$\int Q(t) d(\mu - \hat{\mu})(t) = \sum_{s_i \in S} q_i \int K(s_i - t) d(\mu - \hat{\mu})(t) \quad (\text{F.9})$$

$$= \sum_{s_i \in S} q_i (K * (\mu - \hat{\mu}))(s_i) \quad (\text{F.10})$$

$$\leq \|q\|_2 \sqrt{\sum_{s_i \in S} (K * (\mu - \hat{\mu}))(s_i)^2} \quad (\text{Cauchy-Schwarz}) \quad (\text{F.11})$$

$$\leq 2\bar{\xi} \|q\|_2 \quad (\text{F.12})$$

$$\leq 2\bar{\xi} \sqrt{|T|} \|q\|_\infty, \quad (\text{F.13})$$

where equation (F.12) follows from the assumption that $\hat{\mu}, \mu$ are both feasible for Problem (2.6) and the triangle inequality.

To prove (4.4), we express the quantity of interest in terms of the coefficients of $\hat{\mu}$ at the different locations

$$\int Q(t) d\hat{\mu}(t) = \sum_{\hat{t}_k \in \hat{T}} Q(\hat{t}_k) \hat{a}_k \quad (\text{F.14})$$

$$\leq \sum_{\hat{t}_k \in \hat{T}: d(\hat{t}_k, T) \leq \eta} |Q(\hat{t}_k)| |\hat{a}_k| + \sum_{\hat{t}_k \in \hat{T}: d(\hat{t}_k, T) > \eta} |Q(\hat{t}_k)| |\hat{a}_k|. \quad (\text{F.15})$$

Applying properties 3 and 4 in Lemma 4.1 and noting that $\eta < \Delta(T)/2$ completes the proof. \square

F.3 Proof of Lemma 4.3

Lemma 4.3. *Assume the conditions of Lemma 4.1. Then for any $t_j \in T$ there exists a function Q_j of the form*

$$Q_j(t) = \sum_{s_i \in S} q(j)_i K(s_i - t), \quad (\text{4.9})$$

where $q(j) \in \mathbb{R}^n$, such that:

1. $Q_j(t_j) = 1$ and $Q_j(t_l) = 0$ for $t_l \in T \setminus \{t_j\}$,
2. $|Q_j(t)| < 1$ for $t \in T^c$,
3. $|1 - Q_j(t)| \leq C'_1(t - t_j)^2$ for $|t - t_j| \leq \eta$,
4. $|Q_j(t)| \leq C'_1(t - t_l)^2$ for $|t - t_l| \leq \eta$, $l \neq j$,
5. $|Q_j(t)| \leq C'_2$ for $\min_{t_l \in T} |t - t_l| > \eta$,
6. $\|q(j)\|_\infty \leq C'_3$.

Here the values $C'_1, C'_2, C'_3 > 0$ only depend on $\Delta(T)$, $\gamma(S, T)$ and $\kappa(S)$. The constant η is the same as in Lemma 4.1.

The construction is very similar to the one presented in Section 3. We define Q_j as

$$Q_j(t) := \sum_{\tilde{s}_k \in \tilde{S}} q(j)_k K(\tilde{s}_k - t), \quad (\text{F.16})$$

where the coefficients $q(j) \in \mathbb{R}$ are chosen so that

$$\begin{aligned} Q_j(t_j) &= 1, \\ Q_j(t_l) &= 0 \quad \text{for } t_l \in T \setminus \{t_j\}, \\ Q'_j(t_i) &= 0 \quad \text{for } t_i \in T. \end{aligned} \quad (\text{F.17})$$

By Lemma 3.9 the system is invertible and if we reparametrize Q in terms of the bumps and waves defined in Section 3.2,

$$Q_j(t) = \sum_{t_i \in T} \alpha(j)_i B_{t_i}(t, \tilde{s}_{i,1}, \tilde{s}_{i,2}) + \beta(j)_i W_{t_i}(t, \tilde{s}_{i,1}, \tilde{s}_{i,2}), \quad (\text{F.18})$$

the bounds in equations (3.43) to (3.45) hold for $\|\alpha(j)\|_\infty$, $\|\alpha(j) - \rho(j)\|_\infty$ and $\|\beta(j)\|_\infty$, where $\alpha(j), \beta(j), \rho(j) \in \mathbb{R}^{|T|}$ and the entries of $\rho(j)$ are all zero except for $\rho(j)_j = \text{sign } a_j$. To control the magnitude of $Q(j)$, we decompose it as $Q_j(t) = \mathcal{B}_j(t) + \mathcal{W}_j(t)$, where

$$\mathcal{B}_j(t) := \sum_{k=1}^n \alpha(j)_k B_k(t) \quad \text{and} \quad \mathcal{W}_j(t) := \sum_{k=1}^n \beta_k W_k(t). \quad (\text{F.19})$$

These quantities can be bounded by a modified version of Lemma 3.10, which has the same proof.

Lemma F.1. *Assume the conditions of Lemmas 3.6 and 3.9 hold, and that $0 \in T$ has corresponding ρ -value $r \in \{0, 1\}$. Let h denote half the distance from the origin to the element of T with smallest positive location, or ∞ if no such element exists. Then, for $0 < t \leq h$ (or $t > 0$ if $h = \infty$) and $\epsilon := 10^{-12}/\kappa(S)$,*

$$\begin{aligned} |\mathcal{B}_j^{(p)}(t)| &\leq \|\alpha(j)\|_\infty \left(|B^{(p)}|_\infty^\downarrow(v) + 2\epsilon + \sum_{j=1}^5 |B^{(p)}|_\infty^\downarrow(v + j\Delta) + |B^{(p)}|_\infty^\downarrow(j\Delta - v) \right) \\ |\mathcal{W}_j^{(p)}(t)| &\leq \|\beta(j)\|_\infty \left(|W^{(p)}|_\infty^\downarrow(v) + 2\epsilon + \sum_{j=1}^5 |W^{(p)}|_\infty^\downarrow(v + j\Delta) + |W^{(p)}|_\infty^\downarrow(j\Delta - v) \right), \end{aligned} \quad (\text{F.20})$$

for $p = 0, 1, 2$ and $v = \min(t, \Delta(T)/2)$. Under the same conditions, if $r = 0$ we have

$$|\mathcal{B}_j^{(p)}(t)| \leq \|\alpha(j) - \rho(j)\|_\infty |B^{(p)}|_\infty^\downarrow(v) + \|\alpha(j)\|_\infty \left(2\epsilon + \sum_{j=1}^5 |B^{(p)}|_\infty^\downarrow(v + j\Delta) + |B^{(p)}|_\infty^\downarrow(j\Delta - v) \right).$$

For $q = 1, 2$

$$\mathcal{B}_j^{(q)}(t) \leq \alpha_{\text{LB}}(j) B_\infty^{(q)}(t) + \|\alpha(j)\|_\infty \left(2\epsilon + \sum_{j=1}^5 |B^{(q)}|_\infty^\downarrow(v + j\Delta) + |B^{(q)}|_\infty^\downarrow(j\Delta - v) \right), \quad (\text{F.21})$$

as long as $r = 1$, and $B_\infty^{(q)}(t) \leq 0$, where $\alpha_{\text{LB}}(j) := 1 - \|\alpha(j) - \rho(j)\|_\infty \geq 0$.

To complete the proof, we give a method for testing whether properties 2-5 are satisfied for fixed values of $\Delta(T)$, $\gamma(S, T)$, $\kappa(S)$ and the parameters N_1 and N_2 in Section 3.3. Without loss of generality we set $t_j := 0$ and restrict the analysis to $(0, h)$ for the h defined in Lemma F.1.

1. Case $r = 1$: Test whether the conditions of Lemma 3.11 hold using the same process as performed for exact recovery at the end of Section 3.5 with the bounds from Lemma F.1. Also verify that $|Q^{(2)}(t)|$ is bounded above on $[0, \eta]$.

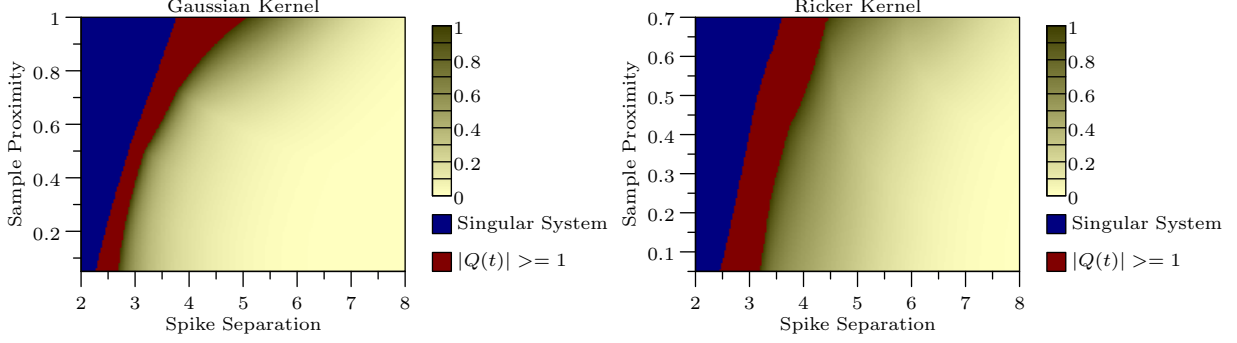


Figure 30: Bounds on $\sup_{t \in (0, h]} |Q(t)|$ when $r = 0$ for different values of the minimum separation and sample proximity.

2. Case $r = 0$: Verify that $|Q(t)| < 1$ for $t \in (0, h]$ by using the bounds on $|\mathcal{B}_j(t)|$ and $|\mathcal{W}_j(t)|$ from Lemma F.1 directly. Also verify that $|Q^{(2)}(t)|$ is bounded on $[0, \eta]$.

Case $r = 1$ above must always succeed for the region stated in Theorem 2.7, as it is the exact same calculation as performed in Section 3.5, and our bound on $|Q^{(2)}(t)|$ is always finite. In Figure 30, we compute bounds on $\sup_{t \in (0, h]} |Q(t)|$ for case $r = 0$ above. The parameter values we use in the computation are the same as used to compute Figure 16 at the end of Section 3.4. This shows that the steps above succeed for the entire region stated in Theorem 2.7.

When cases $r = 0$ and $r = 1$ above are satisfied, they yield property 2. Property 4 follows from Taylor's theorem since $|Q^{(2)}(t)|$ is bounded on $[0, \eta]$ in case $r = 0$ above. The same type of bound was used in the proof of Lemma 4.1 property 3. Property 5 follows by Lemma 3.11 for the case $r = 1$, and from Figure 30 for the case $r = 0$. To establish property 3, we apply Taylor's theorem to obtain

$$Q_j(t) \geq Q_j(0) + tQ_j^{(1)}(0) + \frac{t^2}{2} \inf_{u \in [0, \eta]} Q_j^{(2)}(u) \quad (\text{F.22})$$

$$\geq 1 - ct^2/2, \quad (\text{F.23})$$

where c is the upper bound on $|Q^{(2)}(t)|$ computed in case $r = 1$ above. By taking maxes, we can use the same coefficient C'_1 in both properties 3 and 4.

The proof of the bound on $\|q(j)\|_\infty$ is also identical to that given in Lemma 4.1. This completes the proof of Lemma 4.3.

F.4 Proof of Corollary 4.4

Corollary 4.4. *Under the conditions of Lemma 4.3*

$$\left| \int Q_j(t) d(\mu - \hat{\mu})(t) \right| \leq 2 \|q(j)\|_\infty \bar{\xi} \sqrt{|T|}, \quad (4.10)$$

$$\left| \int Q_j(t) d\hat{\mu}(t) - \sum_{\hat{t}_k \in \hat{T}: |\hat{t}_k - t_j| \leq \eta} \hat{a}_k \right| \leq C' \bar{\xi} \sqrt{|T|}, \quad (4.11)$$

for some $C' > 0$ that only depends on $\Delta(T)$, $\gamma(S, T)$, and $\kappa(S)$.

Proof. To prove (4.10) we follow the same argument as the proof of (4.3),

$$\left| \int Q_j(t) d(\mu - \hat{\mu})(t) \right| = \left| \sum_{s_i \in S} q(j)_i \int K(s_i - t) d(\mu - \hat{\mu})(t) \right| \quad (\text{F.24})$$

$$= \left| \sum_{s_i \in S} q(j)_i (K * (\mu - \hat{\mu}))(s_i) \right| \quad (\text{F.25})$$

$$\leq 2\bar{\xi} \|q(j)\|_2 \quad (\text{Cauchy-Schwarz}) \quad (\text{F.26})$$

$$\leq 2 \|q(j)\|_\infty \bar{\xi} \sqrt{|T|}. \quad (\text{F.27})$$

To prove (4.11), note that

$$\left| \int Q_j(t) d\hat{\mu}(t) - \sum_{\hat{t}_k \in \hat{T}: |\hat{t}_k - t_j| \leq \eta} \hat{a}_k \right| \quad (\text{F.28})$$

$$= \left| \sum_{\hat{t}_k \in \hat{T}: |\hat{t}_k - t_j| > \eta} \hat{a}_k Q_j(\hat{t}_k) + \sum_{\hat{t}_k \in \hat{T}: |\hat{t}_k - t_j| \leq \eta} \hat{a}_k (Q_j(\hat{t}_k) - 1) \right| \quad (\text{F.29})$$

$$= \left| \sum_{\hat{t}_k \in \hat{T}: d(\hat{t}_k, T) > \eta} \hat{a}_k Q_j(\hat{t}_k) + \sum_{\hat{t}_k \in \hat{T}: d(\hat{t}_k, T \setminus \{t_j\}) \leq \eta} \hat{a}_k Q_j(\hat{t}_k) + \sum_{\hat{t}_k \in \hat{T}: |\hat{t}_k - t_j| \leq \eta} \hat{a}_k (Q_j(\hat{t}_k) - 1) \right| \quad (\text{F.30})$$

$$\leq \sum_{\hat{t}_k \in \hat{T}: d(\hat{t}_k, T) > \eta} |\hat{a}_k| C'_2 + \sum_{\hat{t}_k \in \hat{T}: d(\hat{t}_k, T \setminus \{t_j\}) \leq \eta} |\hat{a}_k| C'_1 d(\hat{t}_k, T)^2 + \sum_{\hat{t}_k \in \hat{T}: |\hat{t}_k - t_j| \leq \eta} |\hat{a}_k| C'_1 d(\hat{t}_k, T)^2, \quad (\text{F.31})$$

by Lemma 4.3. Applying (2.10) and (2.11) completes the proof. \square

G Proof of Proposition 5.1

Our proof of Proposition 5.1 is based on the proof of Lemma 2.3 in [35].

Proposition 5.1. *Let $T \subseteq \mathbb{R}$ be the nonzero support of μ and $\mathcal{N} \subseteq S$ be the nonzero support of w . If for any sign patterns $\rho \in \{-1, 1\}^{|T|}$ and $\rho' \in \{-1, 1\}^n$ there exists a dual combination Q of the form*

$$Q(t) := \sum_{i=1}^n q_i K(s_i - t) \quad (5.1)$$

satisfying

$$Q(t_j) = \rho_j, \quad \forall t_j \in T \quad (5.2)$$

$$|Q(t)| < 1, \quad \forall t \in T^c, \quad (5.3)$$

$$q_l = \lambda \rho'_l, \quad \forall s_l \in \mathcal{N}, \quad (5.4)$$

$$|q_l| < \lambda, \quad \forall s_l \in \mathcal{N}^c, \quad (5.5)$$

then (μ, w) is the unique solution to problem (2.15). Here $\mathcal{N}^c := S \setminus \mathcal{N}$.

Proof. Let (μ', w') denote a feasible solution to Problem (2.15). Applying the Lebesgue decomposition to μ' we can write $\mu' = \mu'_T + \mu'_{T^c}$ where μ'_T is absolutely continuous with respect to $|\mu|$, and μ'_{T^c} is mutually orthogonal to $|\mu|$. Analogously, we can write $w' = w'_\mathcal{N} + w'_{\mathcal{N}^c}$, where $(w'_\mathcal{N})_i = 0$ for $s_i \notin \mathcal{N}$ and $(w'_{\mathcal{N}^c})_i = 0$ for $s_i \in \mathcal{N}$.

We first prove that if $\mu'_{T^c} = 0$ and $w'_{\mathcal{N}^c} = 0$ then $\mu = \mu'$ and $w = w'$. Let $h := \mu' - \mu$ and $g := w' - w$. This allows us to write

$$h = \sum_{t_j \in T} b_j \delta_{t_j} \quad (\text{G.1})$$

where $b \in \mathbb{R}^{|T|}$. Set $\rho = \text{sign}(b)$ and $\rho' = \text{sign}(g)$ where we choose an arbitrary value in $\{-1, 1\}$ for $\text{sign}(0)$. By assumption there exists a corresponding Q satisfying the hypotheses of Proposition 5.1 with respect to ρ, ρ' . As (μ, w) and (μ', w') are feasible, we have $(K * h)(s_i) + g_i = 0$ for $i = 1, \dots, n$. This gives

$$0 = \sum_{i=1}^n q_i ((K * h)(s_i) + g_i) = \sum_{i=1}^n q_i \int K(s_i - t) dh(t) + q^T g \quad (\text{G.2})$$

$$= \int Q(t) dh(t) + q^T g = \|h\|_{\text{TV}} + \lambda \|g\|_1, \quad (\text{G.3})$$

implying $h = 0$ and $g = 0$ and proving that $\mu = \mu'$ and $w = w'$.

Next assume that $\mu'_{T^c} \neq 0$ or $w'_{\mathcal{N}^c} \neq 0$. To finish the proof, we will show that (μ', w') is not a minimizer for Problem (2.15). Write μ as

$$\mu = \sum_{t_j \in T} a_j \delta_{t_j}, \quad (\text{G.4})$$

where $a \in \mathbb{R}^{|T|}$. Set $\rho = \text{sign}(a)$ and $\rho' = \text{sign}(w)$, where again we choose an arbitrary value in $\{-1, 1\}$ for $\text{sign}(0)$. By assumption there exists a corresponding Q satisfying the hypotheses of Proposition 5.1 with respect to ρ, ρ' . Then we have

$$\|\mu'\|_{\text{TV}} + \lambda \|w'\|_1 > \int Q(t) d\mu'(t) + q^T w' \quad (\text{G.5})$$

$$= \sum_{i=1}^n q_i ((K * \mu')(s_i) + w'_i) \quad (\text{G.6})$$

$$= \sum_{i=1}^n q_i ((K * \mu)(s_i) + w_i) \quad (\text{G.7})$$

$$= \int Q(t) d\mu(t) + q^T w \quad (\text{G.8})$$

$$= \|\mu\|_{\text{TV}} + \lambda \|w\|_1, \quad (\text{G.9})$$

where (G.5) follows from $|Q(t)| < 1$ for $t \in T^c$ and $|q_i| < \lambda$ for $s_i \in \mathcal{N}^c$. Equation (G.7) holds because (μ, w) and (μ', w') are both feasible by assumption. \square

H Proof of Lemma 2.11

Lemma 2.11. *Let w be a vector with support Ω and let μ be an arbitrary measure such that*

$$y_i = (K * \mu)(s_i) + w_i, \quad (2.19)$$

for $i = 1, \dots, n$. Assume that the pair (μ, w) is the unique solution to Problem (2.15) for the data y , and consider the data

$$y'_i = (K * \mu')(s_i) + w'_i, \quad (2.20)$$

for $i = 1, \dots, n$. Here μ' is a trimmed version of μ : it is equal to μ on a subset $T' \subseteq T$ of its support. Similarly, the support Ω' of w' satisfies $\Omega' \subseteq \Omega$. For any choice of T' and Ω' , the pair (μ', w') is the unique solution to Problem (2.15) if we set the data vector to equal y' for the same value of λ .

Proof. For any vector u and any atomic measure ν , we denote u_S and ν_S the restriction of u and ν to the subset of their support index by a set S . Let $(\hat{\mu}, \hat{w})$ be any solution to Problem (2.15) applied to y' . The pair $(\hat{\mu} + \mu_{T \setminus T'}, \hat{w} + w_{\tau \setminus \tau'})$ is feasible for Problem (2.15) applied to y since

$$(K * \hat{\mu})(s_i) + (K * \mu_{T \setminus T'})(s_i) + \hat{w}_i + (w_{\tau \setminus \tau'})_i = y'_i + (K * \mu_{T \setminus T'})(s_i) + (w_{\tau \setminus \tau'})_i \quad (\text{H.1})$$

$$\begin{aligned} &= (K * \mu')(s_i) + w'_i + (K * \mu_{T \setminus T'})(s_i) + (w_{\tau \setminus \tau'})_i \\ &= (K * \mu)(s_i) + w_i \end{aligned} \quad (\text{H.2})$$

$$= y_i, \quad (\text{H.3})$$

for $i = 1, \dots, n$. By the triangle inequality and the assumption that (μ, w) is the unique solution to Problem (2.15) applied to y , this implies

$$\|\mu\|_{\text{TV}} + \lambda \|w\|_1 < \|\hat{\mu} + \mu_{T \setminus T'}\|_{\text{TV}} + \lambda \|\hat{w} + w_{\tau \setminus \tau'}\|_1 \quad (\text{H.4})$$

$$\leq \|\hat{\mu}\|_{\text{TV}} + \|\mu_{T \setminus T'}\|_{\text{TV}} + \lambda \|\hat{w}\|_1 + \lambda \|w_{\tau \setminus \tau'}\|_1 \quad (\text{H.5})$$

unless $\hat{\mu} + \mu_{T \setminus T'} = \mu$ and $\hat{w} + w_{\tau \setminus \tau'} = w$. This implies

$$\|\mu'\|_{\text{TV}} + \lambda \|w'\|_1 = \|\mu\|_{\text{TV}} - \|\mu_{T \setminus T'}\|_{\text{TV}} + \lambda \|\hat{w}\|_1 - \lambda \|w_{\tau \setminus \tau'}\|_1 \quad (\text{H.6})$$

$$< \|\hat{\mu}\|_{\text{TV}} + \lambda \|\hat{w}\|_1, \quad (\text{H.7})$$

unless $\hat{\mu} = \mu'$ and $\hat{w} = w'$. We conclude that (μ', w') must be the unique solution to Problem (2.15) applied to y' . \square

I Proofs of Auxiliary Results in Section 5

In this section we prove the lemmas that allow us to establish exact recovery in the presence of sparse noise in Section 5. We begin by proving some bounds on the dampened noise function D which will be needed in the following sections. For notational convenience we consider $\tau \in [\tau_1, \tau_2]$ where this interval is $[0.065, 0.2375]$ for the Gaussian, and $[0.0775, 0.165]$ for the Ricker.

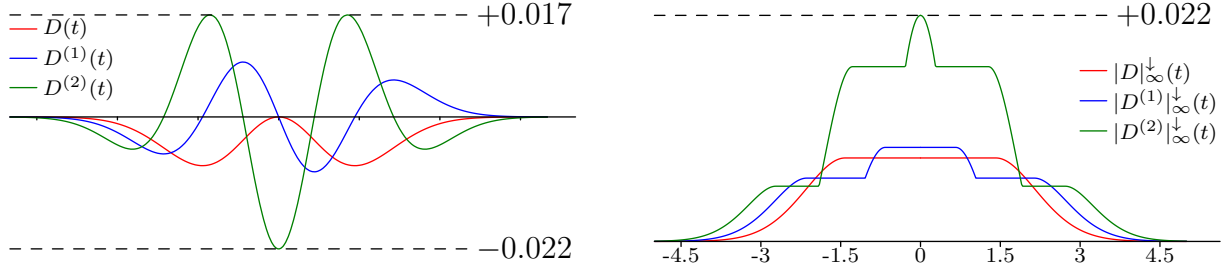


Figure 31: The left image shows the damped kernel D for the Gaussian kernel, along with its derivatives, for $\tau = .15$. On the right, we can see the corresponding monotonized bounds.

I.1 Bounds on the Damped Noise Function

For convenience, define

$$D(t) := D_0(t, 1, 1), \quad (\text{I.1})$$

and note that $D_0(t, \lambda, \rho'_i) = \lambda \rho'_i D(t)$. As in Section 3.3 where we bounded the bumps and waves, we need monotonic bounds on D and its derivatives, which we define below:

$$|D^{(j)}|_{\infty}^{\downarrow}(t) := \sup_{\substack{u \geq |t| \\ \tau \in [\tau_1, \tau_2]}} |D^{(j)}|(u), \quad (\text{I.2})$$

for $j = 0, 1, 2$. By Lemma 3.5, these functions are all even. In Figure 31 we show the derivatives of D , and their monotonized versions. The following lemmas derive bounds on D using the same techniques used to bound the bump and wave functions in Appendix B.4.

Lemma I.1. *For the Gaussian and Ricker kernels with $\tau \in [\tau_1, \tau_2]$ we have*

$$\sum_{j=6}^{\infty} |D^{(j)}|_{\infty}^{\downarrow}(j\Delta) \leq \frac{10^{-12}}{\tau_1}, \quad (\text{I.3})$$

$$|D^{(i)}|_{\infty}^{\downarrow}(t) \leq \frac{10^{-12}}{\tau_1}, \quad (\text{I.4})$$

for $i = 0, 1, 2$, $t \geq 10$, and $\Delta \geq 2$.

Proof. By Lemmas B.4 and B.5 we have

$$\left| \frac{\partial^i}{\partial t^i} B(t, s_1, s_2) \right| \leq \frac{12t^4}{\tau_1} \exp\left(-\frac{t^2}{2} + t\right), \quad (\text{I.5})$$

where the bound holds for both kernels. Note that the grid width τ can be used in place of $\kappa(S)$. Thus we have, for $t \geq 10$,

$$\left| K^{\mathcal{G}}(t) - \frac{\partial^i}{\partial t^i} B(t, s_1, s_2) \right| \leq \frac{12t^4}{\tau_1} \exp\left(-\frac{t^2}{2} + t\right) + \exp\left(-\frac{t^2}{2}\right) \quad (\text{I.6})$$

$$\leq \frac{13t^4}{\tau_1} \exp\left(-\frac{t^2}{2} + t\right), \quad (\text{I.7})$$

for the Gaussian and

$$\left| K^{\mathcal{R}}(t) - \frac{\partial^i}{\partial t^i} B(t, s_1, s_2) \right| \leq \frac{12t^4}{\tau_1} \exp\left(-\frac{t^2}{2} + t\right) + (t^2 - 1) \exp\left(-\frac{t^2}{2}\right) \quad (\text{I.8})$$

$$\leq \frac{12t^4}{\tau_1} \exp\left(-\frac{t^2}{2} + t\right) + t^4 \exp\left(-\frac{t^2}{2}\right) \quad (\text{I.9})$$

$$\leq \frac{13t^4}{\tau_1} \exp\left(-\frac{t^2}{2} + t\right), \quad (\text{I.10})$$

for the Ricker. Applying Lemma B.6 gives (I.3) and (I.4). \square

Lemma I.2. Fix $\tau \in [\tau_1, \tau_2]$ and let $N_1 \in \mathbb{Z}_{>0}$. Partition the interval $[0, 10)$ into N_1 intervals of the form

$$\mathcal{U}_j := \left[\frac{10(j-1)}{N_1}, \frac{10j}{N_1} \right], \quad (\text{I.11})$$

and $j = 1, \dots, N_1$. For the Gaussian and Ricker kernels, there exists a function $|\widetilde{D}^{(i)}|$ such that for all $t \in \mathcal{U}_j$ and $i = 0, 1, 2$

$$|D^{(i)}|_{\infty}^{\downarrow}(t) \leq |\widetilde{D}^{(i)}|(j). \quad (\text{I.12})$$

Proof. The construction here is a slight modification to the argument given in Appendix B.5. Partition $[0, 10)$ into N_1 segments of the form

$$\mathcal{U}_j := \left[\frac{10(j-1)}{N_1}, \frac{10j}{N_1} \right), \quad 1 \leq j \leq N_1, \quad (\text{I.13})$$

and define

$$|\widetilde{D}^{(i)}|(j) \geq \sup_{\substack{t \in \mathcal{U}_j \\ \tau \in [\tau_1, \tau_2]}} |D^{(i)}|(t) = \sup_{\substack{t \in \mathcal{U}_j \\ \tau \in [\tau_1, \tau_2]}} |K^{(i)}(t) - B^{(i)}(t, -\tau, \tau)|, \quad (\text{I.14})$$

for $i = 0, 1, 2$. This can be computed by interval arithmetic (see Appendix B.6). \square

Corollary I.3. Assuming the conditions and definitions in Lemmas I.1 and I.2 we have, for $i = 0, 1, 2$ and $t \in \mathcal{U}_j$

$$|D^{(i)}|_{\infty}^{\downarrow}(t) \leq \max \left(\max_{k:j \leq k \leq N_1} |\widetilde{D}^{(i)}|(k), \epsilon \right), \quad (\text{I.15})$$

where $\epsilon := 10^{-12}/\tau_1$.

I.2 Proof of Lemma 5.2: Invertibility of the Interpolation Equations

In this section, we use a variant of Lemma 3.9 to prove the interpolation equations (5.14) are invertible. We begin by reparametrizing into bumps and waves:

$$\begin{aligned} \sum_{t_j \in T} \alpha_j B_j(t_i) + \beta_j W_j(t_i) &= \psi_i, \\ \sum_{t_j \in T} \alpha_j B_j^{(1)}(t_i) + \beta_j W_j^{(1)}(t_i) &= \zeta_i, \end{aligned} \quad (\text{I.16})$$

for all $t_i \in T$ where

$$\psi_i = \rho_i - R_C(t_i), \quad (\text{I.17})$$

$$\zeta_i = -R_C^{(1)}(t_i). \quad (\text{I.18})$$

The block-matrix representation of (I.16) is:

$$\begin{bmatrix} \mathcal{B} & \mathcal{W} \\ \mathcal{B}^{(1)} & \mathcal{W}^{(1)} \end{bmatrix} \begin{bmatrix} \alpha \\ \beta \end{bmatrix} = \begin{bmatrix} \psi \\ \zeta \end{bmatrix}, \quad (\text{I.19})$$

where the different matrices are defined in (3.39).

Lemma I.4. *Suppose $\|\mathcal{I} - \mathcal{W}^{(1)}\|_\infty < 1$, and $\|\mathcal{I} - \mathcal{C}\|_\infty < 1$ where*

$$\mathcal{C} = \mathcal{B} - \mathcal{W}(\mathcal{W}^{(1)})^{-1}(\mathcal{B}^{(1)})$$

is the Schur complement of $\mathcal{W}^{(1)}$, and \mathcal{I} is the identity matrix. Then

$$\begin{bmatrix} \mathcal{B} & \mathcal{W} \\ \mathcal{B}^{(1)} & \mathcal{W}^{(1)} \end{bmatrix} \begin{bmatrix} \alpha \\ \beta \end{bmatrix} = \begin{bmatrix} \psi \\ \zeta \end{bmatrix} \quad (\text{I.20})$$

has a unique solution. Furthermore, we have

$$\|\alpha\|_\infty \leq \|\mathcal{C}^{-1}\|_\infty \left(\|\psi\|_\infty + \|\mathcal{W}\|_\infty \left\| (\mathcal{W}^{(1)})^{-1} \right\|_\infty \|\zeta\|_\infty \right), \quad (\text{I.21})$$

$$\|\beta\|_\infty \leq \left\| (\mathcal{W}^{(1)})^{-1} \right\|_\infty \left(\|\zeta\|_\infty + \left\| \mathcal{B}^{(1)} \right\|_\infty \|\alpha\|_\infty \right), \quad (\text{I.22})$$

$$\|\alpha - \psi\|_\infty \leq \|\mathcal{I} - \mathcal{C}\|_\infty \|\alpha\|_\infty + \|\mathcal{W}\|_\infty \left\| (\mathcal{W}^{(1)})^{-1} \right\|_\infty \|\zeta\|_\infty, \quad (\text{I.23})$$

where

$$\|\mathcal{I} - \mathcal{C}\|_\infty \leq \|\mathcal{I} - \mathcal{B}\|_\infty + \|\mathcal{W}\|_\infty \left\| (\mathcal{W}^{(1)})^{-1} \right\|_\infty \|\mathcal{B}^{(1)}\|_\infty, \quad (\text{I.24})$$

$$\|\mathcal{C}^{-1}\|_\infty \leq \frac{1}{1 - \|\mathcal{I} - \mathcal{C}\|_\infty}, \quad (\text{I.25})$$

$$\left\| (\mathcal{W}^{(1)})^{-1} \right\|_\infty \leq \frac{1}{1 - \|\mathcal{I} - \mathcal{W}^{(1)}\|_\infty}. \quad (\text{I.26})$$

Proof. For any matrix $A \in \mathbb{R}^{n \times n}$ such that $\|A\|_\infty < 1$ the Neumann series $\sum_{j=0}^{\infty} A^j$ converges to $(\mathcal{I} - A)^{-1}$. By the triangle inequality and the submultiplicativity of the ∞ -norm, this gives

$$\|(\mathcal{I} - A)^{-1}\|_\infty \leq \sum_{j=0}^{\infty} \|A\|_\infty^j = \frac{1}{1 - \|A\|_\infty}. \quad (\text{I.27})$$

Setting $A := \mathcal{I} - \mathcal{W}^{(1)}$ proves $\mathcal{W}^{(1)}$ is invertible, \mathcal{C} exists, and gives inequality (I.26). Setting $A := \mathcal{I} - \mathcal{C}$ proves that \mathcal{C} is invertible and gives inequality (I.25). If both $\mathcal{W}^{(1)}$ and its Schur complement \mathcal{C} are invertible, then the matrix in equation (I.20) is invertible and the system has a unique solution. Applying blockwise Gaussian elimination to the augmented system we have

$$\left[\begin{array}{cc|c} \mathcal{B} & \mathcal{W} & \psi \\ \mathcal{B}^{(1)} & \mathcal{W}^{(1)} & \zeta \end{array} \right] \implies \left[\begin{array}{cc|c} \mathcal{B} - \mathcal{W}(\mathcal{W}^{(1)})^{-1}\mathcal{B}^{(1)} & 0 & \psi - \mathcal{W}(\mathcal{W}^{(1)})^{-1}\zeta \\ & \mathcal{W}^{(1)} & \zeta \end{array} \right]. \quad (\text{I.28})$$

As a result

$$\alpha = \mathcal{C}^{-1}(\psi - \mathcal{W}(\mathcal{W}^{(1)})^{-1}\zeta), \quad (\text{I.29})$$

giving (I.21). Since $\mathcal{B}^{(1)}\alpha + \mathcal{W}^{(1)}\beta = \zeta$,

$$\beta = (\mathcal{W}^{(1)})^{-1}(\zeta - \mathcal{B}^{(1)}\alpha), \quad (\text{I.30})$$

giving (I.22). Finally, note that

$$(\mathcal{I} - \mathcal{C})\alpha = \alpha - \mathcal{C}\mathcal{C}^{-1}(\psi - \mathcal{W}(\mathcal{W}^{(1)})^{-1}\zeta). \quad (\text{I.31})$$

Rearranging gives (I.23). \square

Using $\gamma(S, T) = \kappa(S) = \tau$, the techniques of Section 3.4 apply directly to bound $\|\mathcal{B}\|_\infty$, $\|\mathcal{B}^{(1)}\|_\infty$, $\|\mathcal{W}\|_\infty$, and $\|\mathcal{W}^{(1)}\|_\infty$. This proves invertibility for $(\Delta(T), \tau)$ in the required region, as it is a subset of the $(\Delta(T), \gamma(S, T))$ region used in Theorem 2.4. To bound $\|\psi\|_\infty$ and $\|\zeta\|_\infty$ we apply the triangle inequality to obtain

$$|\psi_j| \leq 1 + \sum_{i \in \mathcal{N}} |D_{s_i}(t_j, \lambda, \rho'_i)| \quad (\text{I.32})$$

$$|\zeta_j| \leq \sum_{i \in \mathcal{N}} \left| \frac{\partial}{\partial t} D_{s_i}(t_j, \lambda, \rho'_i) \right|, \quad (\text{I.33})$$

for all $t_j \in T$. By the separation requirement on the sparse noise locations, and monotonicity we obtain the bounds

$$|\psi_j| \leq 1 + 2\lambda \sum_{i=0}^{\infty} |D|_\infty^\downarrow(i\Delta(T)), \quad (\text{I.34})$$

$$|\zeta_j| \leq 2\lambda \sum_{i=0}^{\infty} |D^{(1)}|_\infty^\downarrow(i\Delta(T)), \quad (\text{I.35})$$

for all $t_j \in T$. By Lemma I.1,

$$\|\psi\|_\infty \leq 1 + 2\lambda \left(\sum_{i=0}^5 |D|_\infty^\downarrow(i\Delta(T)) + \epsilon \right), \quad (\text{I.36})$$

$$\|\zeta\|_\infty \leq 2\lambda \left(\sum_{i=0}^5 |D^{(1)}|_\infty^\downarrow(i\Delta(T)) + \epsilon \right), \quad (\text{I.37})$$

$$(\text{I.38})$$

where $\epsilon = 10^{-12}/\tau_1$. For the Gaussian kernel with $\Delta(T) \geq 3.751$ and $\tau \in [\tau_1, \tau_2]$

$$\|\psi\|_\infty \leq 1.08732 \quad \text{and} \quad \|\zeta\|_\infty \leq 0.087317, \quad (\text{I.39})$$

whereas for the Ricker wavelet with $\Delta(T) \geq 5.056$

$$\|\psi\|_\infty \leq 1.12597 \quad \text{and} \quad \|\zeta\|_\infty \leq 0.12597, \quad (\text{I.40})$$

by Corollary I.3. Applying Lemma I.4, for the Gaussian kernel we have

$$\|\alpha\|_\infty \leq 1.09206 \quad \text{and} \quad \|\beta\|_\infty \leq 0.118824, \quad (\text{I.41})$$

and for the Ricker kernel

$$\|\alpha\|_\infty \leq 1.12633 \quad \text{and} \quad \|\beta\|_\infty \leq 0.261070. \quad (\text{I.42})$$

I.3 Proof of Lemma 5.3: Satisfying Condition (5.3)

In this section, we prove that the dual combination Q satisfies the condition $|Q(t)| < 1$ for $t \in T^c$. Without loss of generality, we restrict our attention to the region between a spike at the origin with sign +1 and an adjacent spike.

We begin by decomposing Q as the sum of three terms that account for the bumps, waves, and noise separately: $Q(t) = \mathcal{B}(t) + \mathcal{W}(t) + \mathcal{D}(t)$, where

$$\mathcal{B}(t) := \sum_{j=1}^m \alpha_j B_j(t), \quad (\text{I.43})$$

$$\mathcal{W}(t) := \sum_{j=1}^m \beta_j W_j(t), \quad (\text{I.44})$$

$$\mathcal{D}(t) := \sum_{s_i \in \mathcal{N}} D_{s_i}(t, \lambda, \rho'_i). \quad (\text{I.45})$$

Lemma 3.10 provides bounds for $|\mathcal{B}^{(p)}(t)|$, $|\mathcal{W}^{(p)}(t)|$, and $\mathcal{B}^{(q)}(t)$ for $p = 0, 1, 2$ and $q = 1, 2$. For the noise component, we have the following bounds which follow from monotonicity, Lemma I.1, and the noise separation condition:

Lemma I.5. *Fix our kernel to be the Gaussian kernel or the Ricker wavelet. Assume the conditions of Lemma I.1 hold, and that there is a spike at the origin with sign +1. Let h denote half the distance from the origin to the spike with smallest positive location, or ∞ if no such spike exists. Then, for $0 < t \leq h$ (or $t > 0$ if $h = \infty$) and $\epsilon := 10^{-12}/\tau_1$,*

$$|\mathcal{D}^{(p)}(t)| \leq 2\lambda \left(\sum_{i=0}^5 |D^{(p)}|_{\infty}^{\downarrow}(i\Delta(T)) + \epsilon \right), \quad (\text{I.46})$$

for $p = 0, 1, 2$.

Proof. By the triangle inequality and monotonicity

$$|\mathcal{D}^{(p)}(t)| \leq \sum_{i \in \mathcal{N}} |D_{s_i}^{(p)}(t, \lambda, \rho'_i)| \quad (\text{I.47})$$

$$= \lambda \sum_{i \in \mathcal{N}} |D^{(p)}(t - s_i)| \quad (\text{I.48})$$

$$= \lambda \sum_{\substack{i \in \mathcal{N} \\ t \geq s_i}} |D^{(p)}(t - s_i)| + \lambda \sum_{\substack{i \in \mathcal{N} \\ t < s_i}} |D^{(p)}(s_i - t)| \quad (\text{I.49})$$

$$\leq \lambda \sum_{i=0}^{\infty} |D^{(p)}|_{\infty}^{\downarrow}(i\Delta(T)) + \lambda \sum_{i=0}^{\infty} |D^{(p)}|_{\infty}^{\downarrow}(i\Delta(T)) \quad (\text{I.50})$$

$$\leq 2\lambda \left(\sum_{i=0}^5 |D^{(p)}|_{\infty}^{\downarrow}(i\Delta(T)) + \epsilon \right), \quad (\text{I.51})$$

where (I.50) holds due to monotonicity, and (I.51) is due to Lemma I.1. \square

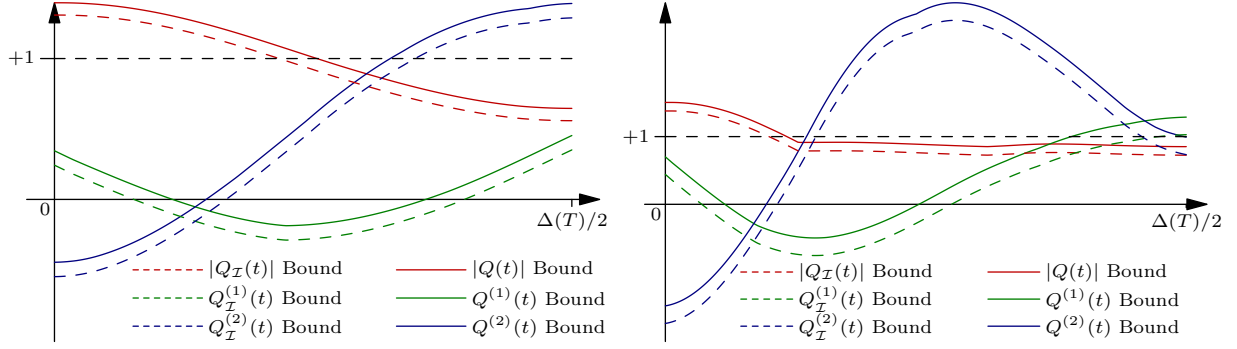


Figure 32: Upper bounds on Q , $Q^{(1)}$ and $Q^{(2)}$ for $\tau \in [\tau_1, \tau_2]$ with $\Delta(T) \geq 3.751$ for the Gaussian kernel and $\Delta(T) \geq 5.056$ for the Ricker wavelet. The difference between the dashed and undashed curves shows the contribution of the dampened noise.

We use the procedure at the end of Section 3.5 with $\gamma(S, T) = \tau_2$ to prove that $|Q(t)| < 1$ for $t \in T^c$. Figure 32 shows upper bounds on $|Q|$, $Q^{(1)}$ and $Q^{(2)}$ for $\tau \in [\tau_1, \tau_2]$ with $\Delta(T) \geq 3.751$ for the Gaussian kernel and $\Delta(T) \geq 5.056$ for the Ricker wavelet. As a result, the conditions of Lemma 3.11 are satisfied and the proof is complete.

I.4 Proof of Lemma 5.4: Satisfying Condition (5.5)

Here we prove that $|q_i| < \lambda$ for $s_i \in \mathcal{N}^c$. We begin by establishing that q_i is bounded when $s_i \in \mathcal{C}$.

Lemma I.6. *For the Gaussian and Ricker kernels, if $\tau \leq 0.6$ then $|b_1| < 1$ and $|b_2| < 1$ where*

$$B(t, -\tau, \tau) = b_1 K(-\tau - t) + b_2 K(\tau - t), \quad (\text{I.52})$$

is the bump function centered at the origin with samples at $-\tau, \tau$.

Proof. For the Gaussian kernel we have, by Lemmas 3.2 and B.2,

$$|b_1| = \frac{|(K^{\mathcal{G}})^{(1)}(\tau)|}{2\tau \exp(-\tau^2)} = \frac{\exp(\tau^2/2)}{2}, \quad (\text{I.53})$$

with the same formula for $|b_2|$. As $e^{0.6^2/2}/2 \approx 0.5986$ the result follows for the Gaussian. For the Ricker, by Lemmas 3.2 and B.2

$$|b_1| = \frac{|(K^{\mathcal{R}})^{(1)}(\tau)|}{2\tau|3 - 4\tau^2 + \tau^4| \exp(-\tau^2)} = \frac{\tau|3 - \tau^2| \exp(\tau^2/2)}{2|3 - 4\tau^2 + \tau^4|}, \quad (\text{I.54})$$

with the same formula for $|b_2|$. For $\tau \leq 0.6$

$$\frac{\tau(3 - \tau^2) \exp(\tau^2/2)}{2(3 - 4\tau^2 + \tau^4)} \leq \frac{0.6(3) \exp(0.6^2/2)}{2(3 - 4(0.6)^2)} \approx 0.6907, \quad (\text{I.55})$$

completing the proof for the Ricker wavelet. \square

If the conditions of Lemma I.6 hold then by construction $|q_i| < \lambda$ for all $i \in \mathcal{C}$. To complete the proof of Lemma 5.4, we must show that these bounds also hold for the pairs of samples closest to each spike.

For the remainder of the section, we assume there is a spike t_j at the origin with sign $+1$, and s_i, s_{i+1} are the two samples closest to the origin with $s_{i+1} = s_i + \tau$. We prove that $|q_i| < \lambda$ by showing that $|q_i| \geq \lambda$ implies $|Q(s_i)| > 1$, which contradicts Lemma 5.3. By combining Lemma I.4 and Lemma 3.2 we obtain the following result.

Lemma I.7. *Suppose s_i, s_{i+1} are the two closest samples to a spike with location $t_j = 0$. Assume the spike at the origin has sign $+1$, $\alpha_j \geq 0$, and that $s_i \leq 0 \leq s_{i+1}$. Then, under the assumptions of Lemma 5.4, we have*

$$\min(q_i, q_{i+1}) \geq -\frac{\|\beta\|_\infty e^{\tau^2/2}}{\tau} > -\lambda, \quad (\text{I.56})$$

for the Gaussian kernel and

$$\min(q_i, q_{i+1}) \geq -\frac{\|\beta\|_\infty e^{\tau^2/2}}{\tau(3-\tau^2)} > -\lambda, \quad (\text{I.57})$$

for the Ricker wavelet.

Proof. Applying Lemmas 3.2 and B.2 we have

$$b_{i,1} = \frac{s_{i+1}K^{\mathcal{G}}(s_{i+1})}{(s_{i+1} - s_i) \exp\left(-\frac{s_i^2 + s_{i+1}^2}{2}\right)}, \quad b_{i,2} = \frac{-s_i K^{\mathcal{G}}(s_i)}{(s_{i+1} - s_i) \exp\left(-\frac{s_i^2 + s_{i+1}^2}{2}\right)}, \quad (\text{I.58})$$

for the Gaussian kernel and

$$b_{i,1} = \frac{s_{i+1}(3 - s_{i+1}^2)K^{\mathcal{G}}(s_{i+1})}{(s_{i+1} - s_i)(3 - (s_i - s_{i+1})^2 + s_i^2 s_{i+1}^2) \exp\left(-\frac{s_i^2 + s_{i+1}^2}{2}\right)}, \quad (\text{I.59})$$

$$b_{i,2} = \frac{-s_i(3 - s_i^2)K^{\mathcal{G}}(s_i)}{(s_{i+1} - s_i)(3 - (s_i - s_{i+1})^2 + s_i^2 s_{i+1}^2) \exp\left(-\frac{s_i^2 + s_{i+1}^2}{2}\right)}, \quad (\text{I.60})$$

for the Ricker wavelet. Since $s_1 \leq 0 \leq s_2$ we see that both bump coefficients are non-negative for both kernels. By a similar calculation we have

$$w_{i,1} = \frac{-K^{\mathcal{G}}(s_{i+1})}{(s_{i+1} - s_i) \exp\left(-\frac{s_i^2 + s_{i+1}^2}{2}\right)}, \quad w_{i,2} = \frac{K^{\mathcal{G}}(s_i)}{(s_{i+1} - s_i) \exp\left(-\frac{s_i^2 + s_{i+1}^2}{2}\right)}, \quad (\text{I.61})$$

for the Gaussian kernel and

$$w_{i,1} = \frac{(s_{i+1}^2 - 1)K^{\mathcal{G}}(s_{i+1})}{(s_{i+1} - s_i)(3 - (s_i - s_{i+1})^2 + s_i^2 s_{i+1}^2) \exp\left(-\frac{s_i^2 + s_{i+1}^2}{2}\right)}, \quad (\text{I.62})$$

$$w_{i,2} = \frac{(1 - s_i^2)K^{\mathcal{G}}(s_i)}{(s_{i+1} - s_i)(3 - (s_i - s_{i+1})^2 + s_i^2 s_{i+1}^2) \exp\left(-\frac{s_i^2 + s_{i+1}^2}{2}\right)}, \quad (\text{I.63})$$

$$(\text{I.64})$$

for the Ricker wavelet. Thus $w_{i,1} \leq 0$ and $w_{i,2} \geq 0$ for both kernels. As $\alpha_j \geq 0$, we can lower bound $\min(q_i, q_{i+1})$ by considering the magnitudes of $w_{i,1}, w_{i,2}$. This shows

$$\min(q_i, q_{i+1}) \geq -\frac{\|\beta\|_\infty e^{\tau^2/2}}{\tau} \quad (\text{I.65})$$

for the Gaussian kernel. As $f(x) = e^{x^2/2}/x$ has $f'(x) = e^{x^2/2}(x^2 - 1)/x^2 < 0$ for $|x| < 1$ we can plug in our bound on $\|\beta\|_\infty$ and $\tau_1 = 0.065$ to obtain

$$\frac{\|\beta\|_\infty e^{\tau_1^2/2}}{\tau_1} = 1.83193 < \lambda. \quad (\text{I.66})$$

For the Ricker wavelet, the result follows from Lemma I.8, an auxiliary result that we defer to Appendix I.5. \square

To verify that $\alpha_j \geq 0$ note that

$$\alpha_j \geq \psi_j - \|\alpha - \psi\|_\infty \quad (\text{I.67})$$

$$\geq 1 - 2\lambda \left(\sum_{i=0}^5 |D|_\infty^\downarrow(i\Delta(T)) + \epsilon \right) - \|\alpha - \psi\|_\infty, \quad (\text{I.68})$$

by monotonicity and Lemma I.1, where $\epsilon := 10^{-12}/\tau_1$. This gives $\alpha_j \geq 0.907937$ for the Gaussian and $\alpha_j \geq 0.873678$ for the Ricker.

By Lemma I.7 we assume, for contradiction, that $q_i \geq \lambda$ and $q_{i+1} \geq -\frac{\|\beta\|_\infty e^{\tau^2/2}}{\tau}$. The proof with the bounds on q_i, q_{i+1} swapped is the same. Applying Lemmas I.5 and 3.10 and monotonicity, we obtain

$$Q(s_i) = q_i K(0) + q_{i+1} K(s_{i+1} - s_i) + \sum_{l \neq j} \alpha_l B_{t_l}(s_i) + \beta_l W_{t_l}(s_i) + \sum_{l \in \mathcal{N}} D_{s_l}(s_i, \lambda, \rho'_l) \quad (\text{I.69})$$

$$\begin{aligned} &\geq q_i + q_{i+1} K(\tau) \\ &\quad - 2 \left(3\epsilon + \sum_{i=1}^5 \|\alpha\|_\infty |B|_\infty^\downarrow(i\Delta(T) - \tau_2) + \|\beta\|_\infty |W|_\infty^\downarrow(i\Delta(T) - \tau_2) + \lambda \sum_{i=0}^5 |D|_\infty^\downarrow(i\Delta(T)) \right), \end{aligned} \quad (\text{I.70})$$

where $\epsilon := 10^{-12}/\tau_1$. Applying Lemma I.7 gives

$$q_{i+1} K(s_{i+1} - s_i) \geq -\frac{\|\beta\|_\infty}{\tau} \geq -\frac{\|\beta\|_\infty}{\tau_1} \quad (\text{I.71})$$

for the Gaussian and

$$q_{i+1} K(s_{i+1} - s_i) \geq -\frac{\|\beta\|_\infty}{\tau(3 - \tau^2)} \geq -\frac{\|\beta\|_\infty}{\tau_1(3 - \tau_1^2)} \quad (\text{I.72})$$

for the Ricker (differentiate $\tau(3 - \tau^2)$). If the expression on the right-hand side of (I.70) is strictly larger than 1 when $q_i = \lambda$ then we obtain $Q(s_i) > 1$ which contradicts Lemma 5.3. Computing these bounds we have $Q(s_i) \geq 1.39862$ for the Gaussian and $Q(s_i) \geq 1.19352$ for the Ricker. This contradiction implies $|q_i| < \lambda$ and completes the proof.

I.5 Lemma I.8

Lemma I.8. *Under the assumptions of Lemma I.7 we have*

$$0 \leq \frac{\|\beta\|_\infty (1 - s_{i+1}^2) K^{\mathcal{G}}(s_{i+1})}{(s_{i+1} - s_i)(3 - (s_i - s_{i+1})^2 + s_i^2 s_{i+1}^2) \exp\left(-\frac{s_i^2 + s_{i+1}^2}{2}\right)} \leq \frac{\|\beta\|_\infty e^{\tau^2/2}}{\tau(3 - \tau^2)} < \lambda, \quad (\text{I.73})$$

$$0 \leq \frac{\|\beta\|_\infty (1 - s_i^2) K^{\mathcal{G}}(s_i)}{(s_{i+1} - s_i)(3 - (s_i - s_{i+1})^2 + s_i^2 s_{i+1}^2) \exp\left(-\frac{s_i^2 + s_{i+1}^2}{2}\right)} \leq \frac{\|\beta\|_\infty e^{\tau^2/2}}{\tau(3 - \tau^2)} < \lambda, \quad (\text{I.74})$$

for the Ricker kernel with $\tau \in [\tau_1, \tau_2]$.

Proof. As $\tau_2 = 0.165$ we immediately obtain that all terms in the statement are nonnegative. We define f below so that the first inequality in (I.74) reads $0 \leq \|\beta\|_\infty f(s_i)$:

$$f(s) = \frac{(1 - s^2) \exp((s + \tau)^2/2)}{\tau(3 - \tau^2 + s^2(s + \tau)^2)}. \quad (\text{I.75})$$

Differentiating and some algebraic manipulations yield

$$f'(s) = -\frac{e^{\frac{1}{2}(s+\tau)^2} \left((s^2 - 1)^2 \tau^3 + s(3s^4 - 4s^2 + 1)\tau^2 + (3s^6 - 5s^4 + 9s^2 - 3)\tau + s(s^6 - 3s^4 + 7s^2 + 3) \right)}{\tau((s^2 + (s - 1)\tau)(s(s + \tau) + \tau) + 3)^2}. \quad (\text{I.76})$$

We will show this is always positive when $\tau \in [0.0775, 0.165]$. As the exponential and the denominator are always positive, we focus on the parenthesized term in the numerator. As $-\tau \leq s \leq 0$

$$(s^2 - 1)^2 \tau^3 \leq \tau^3 \quad (\text{I.77})$$

$$s(3s^4 - 4s^2 + 1)\tau^2 \leq 0 \quad (\text{I.78})$$

$$(3s^6 - 5s^4 + 9s^2 - 3)\tau \leq \tau(12s^2 - 3) \leq -\tau_1(3 - 12\tau_2^2) \quad (\text{I.79})$$

$$s(s^6 - 3s^4 + 7s^2 + 3) \leq s(3 - 3s^4) \leq 0. \quad (\text{I.80})$$

Noting that $\tau_2^3 - \tau_1(3 - 12\tau_2^2) \leq -0.20268$, we see that $f'(s) > 0$. This shows that $s = 0$ maximizes f . As a result,

$$f(0) = \frac{\exp(\tau^2/2)}{\tau(3 - \tau^2)} \quad (\text{I.81})$$

and

$$\frac{\|\beta\|_\infty \exp(\tau^2/2)}{\tau(3 - \tau^2)} \leq \frac{0.261070 \exp(\tau_2^2/2)}{\tau_1(3 - \tau_1^2)} \leq 1.14055 < \lambda. \quad (\text{I.82})$$

Let (a, b) be a valid pair of values for (s_i, s_{i+1}) , i.e.,

$$-\tau \leq a \leq 0 \leq b = a + \tau. \quad (\text{I.83})$$

Then $(-b, -a)$ is another valid pair. Replacing $(s_i, s_{i+1}) \rightarrow (-s_{i+1}, -s_i)$ in (I.74) gives (I.73) and completes the proof. \square